GDAŃSK UNIVERSITY OF TECHNOLOGY
FACULTY OF ELECTRONICS, TELECOMMUNICATIONS AND INFORMATICS

The author of the PhD dissertation: Natalia Leszczynska
Scientific discipline: electronics

DOCTORAL DISSERTATION

Title of PhD dissertation: Zero-Pole Approach in Microwave Passive Circuit Design

Title of PhD dissertation (in Polish): Metoda zero-biegunowa w projektowaniu pasywnych układów mikrofalowych

Supervisor *signature*	Auxiliary supervisor *signature*
Full professor Michał Mrozowski	PhD Adam Lamęcki

Gdańsk, year 2017

Contents

List of Figures

List of Tables

Symbol conventions and abbreviations

Symbol conventions

$\boldsymbol{A}$	matrix
$\boldsymbol{I}$	identity matrix
$\boldsymbol{a}$	vector
a_i	i-th element of vector **a**
a_{ij}	ij-th element of matrix **A**
a	scalar
$(\cdot)^{-1}$	matrix inverse
$(\cdot)^T$	matrix/vector transposition
$(\cdot)^H$	matrix/vector hermite transposition
$(\cdot)^\dagger$	Moore-Penrose pseudo-inverse
j	imaginary unit

General symbols

f	frequency
ω	angular frequency
s	complex frequency

S	scattering matrix
∇	gradient

Selected abbreviations

ASM	Aggressive Space Mapping
CAD	Computer-Aided Design
EM	Electromagnetic
ISM	Input Space Mapping
LTI	Linear time-invariant
MM	Manifold Mapping
OSM	Output Space Mapping
PE	Parameter extraction
SBO	Surrogate Based Optimization
SM	Space mapping
VF	Vector fitting

Chapter 1

Introduction

1.1 Background and motivation

Over the past two decades, the techniques for designing microwave components using computer-aided design (CAD) tools have developed significantly. The computer has become an indispensable device at every stage of designing circuits. Dedicated CAD techniques allow accurate analysis including the real behaviour of an analysed circuit. Appropriate use of such tools allows a better understanding the design problem. Further, proper application of computers in the design process reduces the number of time-consuming and expensive experimental steps, including those for design, fabrication, testing and tuning. This is extremely important in the case of the design and production of microwave circuits, because of the limited possibilities for changing the dimensions or manual tuning of fabricated structures [26]. Computer simulations yield well-defined values of circuit elements and allow the performance of given components to be verified before manufacturing [84]. Moreover, the cost of prototyping has been reduced by cutting the amount of labour and material used for experimental verification of prototypes.

1.1.1 Computer-aided design of microwave circuits

The design of microwave circuits with computers consists of the sequence of steps presented in Fig. 1.1. In the first step, designers choose the topology of the circuit, based on their experience. Next, the initial design is carried out. At this stage, a designer can verify the concept and consider alternative solutions. Then, structural analysis is performed using a computer equipped with appropriate software. This yields a circuit response that can be compared with requirements - the so-called design specification. If a simulated solution meets the design specification, the design process is complete and an engineering prototype can be built and tested (measured). Otherwise, computer simulations are performed in order to obtain a new design and subsequently a prototype [41].

Without CAD tools, the design process would require the construction and measurement of fabricated prototypes at each iteration, which would be time-consuming and expensive. That is, the use of computers in the design process can reduce time and costs for a design, as well as enhancing its quality.

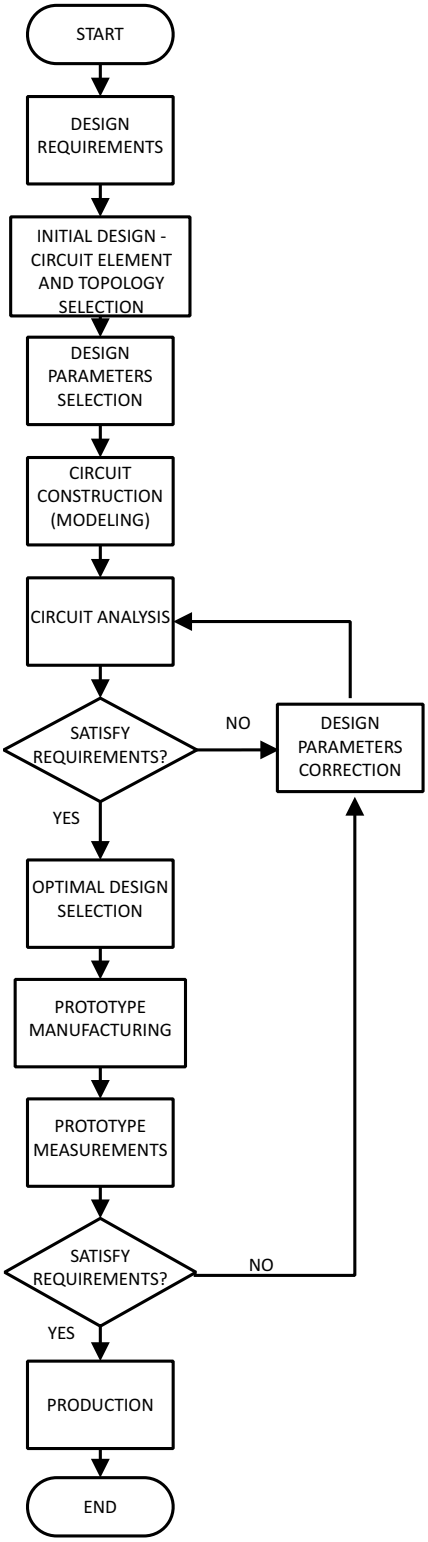

FIGURE 1.1: Flowchart of the computer aided-design process.

According to the mentioned procedure, CAD of a microwave circuit is composed of

four main steps: initial synthesis, modelling, analysis and optimisation of the circuit [77, 85]. Modelling of microwave elements consists of assigning a numerical or mathematical description to elements which approximates the behaviour of an actual component, in order that the elements can be used in circuit simulation. In the case of microwave components, the variety of elements is large. Basic building blocks of microwave passive circuits such as filters, couplers and power dividers are sections of microwave transmission lines of different types, resistors, capacitors or inductors. Transmission lines can take the form of cylindrical waveguides, or strip, microstrip and coplanar lines, and their combinations.

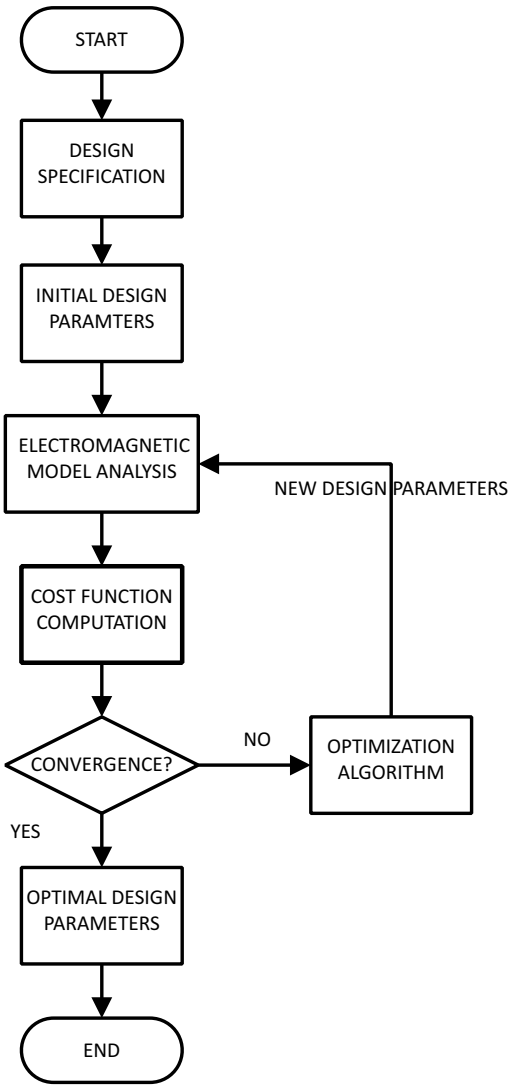

FIGURE 1.2: Flowchart of the direct optimisation process [41].

1.2 Design of microwave circuits using optimisation

The optimisation of a microwave circuit is a process of searching for the set of geometrical parameters that satisfies defined design requirements - the circuit specification. To this end, the values of the design parameters are varied and the results of the circuit analysis compared with the design requirements in order to identify which values of the parameters satisfy these requirements [11, 21, 87].

The main advantage of using optimisation methods in the microwave structure design process is their universalism. Numerical tuning takes into account all types of constraints, such as geometrical parameter restrictions, and allows us to find compromise solutions. Unfortunately, design based on optimisation techniques also has disadvantages. One of them is the complexity of the computer programs used for the design process and associated long times required for computations. In the case of microwave circuits, electromagnetic (EM) solvers are used to simulate circuit behaviour. Another disadvantage, arguably the most important potential problem, is the possibility of finding a local minimum rather than the global one.

The design procedure involving optimisation is presented in Fig. 1.2, it consists of a series of steps. First, the designer needs to determine the design specification for the desired response or responses which emerge from circuit application. In the case of linear microwave circuits, the requirements usually concern the shape of frequency responses including both amplitude and phase.

Second, unlike synthesis methods, optimisation methods only improve the properties of an assumed circuit with defined topology. This means that to start the optimisation process a designer has to prepare the initial design of the structure including the selection of topology, types of elements and initial values of geometrical dimensions. This initial design is based on simplified circuit analysis, and relies on a designer's intuition and experience. Nevertheless, it should be specified as accurately as possible, because the final solution obtained from the optimisation process may depend on the initial set of values of design parameters for the circuit considered.

In the third step, frequency responses and/or sensitivities of the circuit designed are calculated. To calculate the frequency characteristics, the structure is analysed repeatedly, using a dedicated software - full-wave simulator. After each modification of the circuit parameters made by the optimisation algorithm, a new response must be calculated. As a result, many calculations are needed, sometimes hundreds or even thousands. In addition, sensitivity analysis must be performed, to find derivatives of the minimised function.

Subsequently, the difference is calculated between the simulated response obtained from a full-wave solver and the desired characteristics; this difference is called the error function. If its value is less than the accepted value, the process stops; if not, other stopping criteria are examined.

The optimisation process stops when the goal function value or the modification of the structure dimensions saturate, that is, when in a new iteration, the goal function value or design parameter vector modification does not reach a threshold value set by the designer (for example, 0.1% of the design parameters' vector value or goal function value). Moreover, in order to limit the time taken by optimisation, the maximum number of iterations should be defined. If at least one of the stopping criteria is reached, optimisation

stops.

Otherwise, new values of the design parameters should be computed and previous steps repeated. This step is critical in design processes using optimisation methods.

1.2.1 Optimisation concept

The optimisation problem is defined as finding the global minimum of the goal function [89]:

$$C = C(\mathbf{x}) \tag{1.1}$$

where $\mathbf{x}$ is a vector of n independent variables - design parameters of an optimised circuit:

$$\mathbf{x} = [x_1, x_2, ..., x_n]^T. \tag{1.2}$$

In the initial stage of the design, elements of $\mathbf{x}$ could be values of a circuit's dimensions, while at a later stage, they could be physical dimensions of the structure, for example, the lengths of transmission lines. The goal of optimisation is to find a solution for $\mathbf{x}^*$, if it exists, which satisfies the following condition:

$$\mathbf{x}^* = \arg\min_x C(\mathbf{x}). \tag{1.3}$$

The scalar function of many variables $C(\mathbf{x})$ can be expanded around point $\mathbf{x}$ in the Taylor series. The first three terms of the expansion have the following form:

$$C(\mathbf{x} + \Delta\mathbf{x}) \simeq C(\mathbf{x}) + \nabla\mathbf{C}^T\Delta\mathbf{x} + \frac{1}{2}\nabla\mathbf{x}^T\mathbf{H}\nabla\mathbf{x} \tag{1.4}$$

where:

$$\Delta\mathbf{x} = [\Delta x_1, \Delta x_2, ..., \Delta x_n]^T \tag{1.5}$$

is a vector which consists of n increments of design variables,

$$\nabla\mathbf{C} = [\frac{\partial C}{\partial x_1}, \frac{\partial C}{\partial x_2}, ..., \frac{\partial C}{\partial x_n}]^T \tag{1.6}$$

is a vector (gradient), which consists of the derivatives of the cost function C, and $\mathbf{H}$ is a symmetric square matrix of order n of second derivatives of the goal function, called the Hessian

$$\mathbf{H} = \begin{bmatrix} \frac{\partial^2 C}{\partial x_1^2} & \frac{\partial^2 C}{\partial x_1 \partial x_2} & \cdots & \frac{\partial^2 C}{\partial x_1 \partial x_n} \\ \frac{\partial^2 C}{\partial x_2 \partial x_1} & \frac{\partial^2 C}{\partial x_2^2} & \cdots & \frac{\partial^2 C}{\partial x_2 \partial x_n} \\ \vdots & \vdots & \cdots & \vdots \\ \frac{\partial^2 C}{\partial x_n \partial x_1} & \frac{\partial^2 C}{\partial x_n \partial x_2} & \cdots & \frac{\partial^2 C}{\partial x_n^2} \end{bmatrix}.$$

The minimum conditions for the continuous function C of one parameter x are well known:

$$\frac{dC}{dx} = 0 \tag{1.7}$$

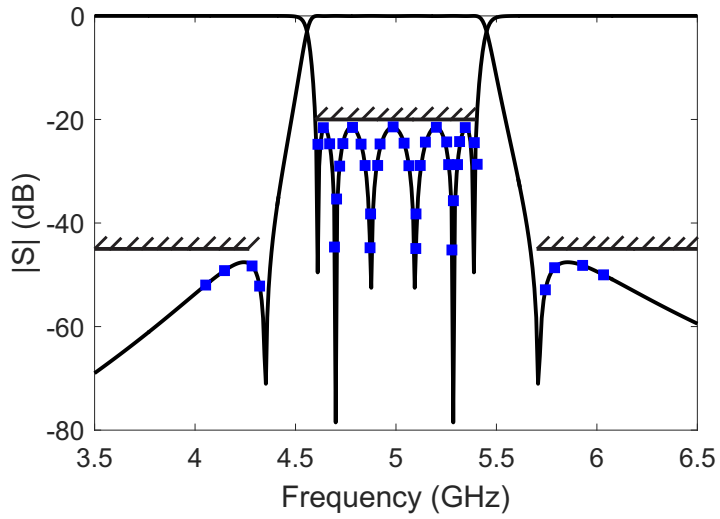

FIGURE 1.3: Circuit response with the points (blue) selected to construct the goal function and the design requirements (dashed bars).

and

$$\frac{d^2C}{dx^2} > 0 \tag{1.8}$$

For a function of many variables, Equations 1.7 and 1.8 reduce to the following form:

$$\nabla \mathbf{C}(\mathbf{x}^*) = 0 \tag{1.9}$$

and

$$\nabla \mathbf{x}^T \mathbf{H}(\mathbf{x}^*) \nabla \mathbf{x} > 0 \tag{1.10}$$

where $\mathbf{x}^*$ is the location of the global minimum of function $C(x)$. The first of these equations (1.9) means that the gradient vanishes at $\mathbf{x}^*$, while the second (1.10) indicates that at $\mathbf{x}^*$, the Hessian, is a positive definite matrix.

1.2.2 Goal function definition

The optimisation problems involved in the design of microwave circuits in the frequency domain can be formulated as searching for the values of the design parameters for which the circuit response satisfies design requirements related to its shape.

1.2.3 Goal function based on scattering parameters

The optimal design parameter values, those for which the structure response satisfies the design requirements, can be obtained by minimising a suitably defined goal function.

Usually, the frequency response obtained from simulation is compared with the desired approximated function of circuit response at certain frequency points [10, 11, 15]

$$C = \sum_{i=1}^{K} |S(f^i) - S(f^i)_{ref}|^2 \tag{1.11}$$

where $S(f^i)$ are the values of scattering parameters (the reflection or transmission coefficient or both) of the optimised structure, while $S(f^i)_{ref}$ represents the desired performance of the system at K frequency points f^i. In practice, $S(f^i)$ is often formulated as one- or two-sided specifications defining the upper and/or lower bounds for a given parameter. This is illustrated in Fig.1.3, where the dashed bars define the upper bound for the magnitude of the transmission and reflection coefficients of a bandpass filter. Such upper and lower bounds are often called a mask, and are given as a set of real numbers. In this case, one only imposes a constraint on the magnitude of the scattering parameters, and hence, the goal function becomes

$$C = \sum_{i=1}^{K} ||S(f^i)| - S_{mask}|^2. \tag{1.12}$$

In view of the variety of shapes of microwave circuit characteristics, the goal function should be specifically defined for each problem [1, 3, 14]. The key is the appropriate selection of frequency points from the characteristics. Too few frequency samples may not provide a good approximation of the circuit response. To avoid this, often as many as a few hundreds of samples are needed. This significantly increases the numerical costs and does not guarantee the convergence of the optimisation procedure.

An example of frequency point selection and a mask defining the upper bound for the goal function (1.11) are presented in Figure 1.3. The structure response is computed at the points indicated by blue squares.

1.2.4 Goal function based on response features

Another possibility is to define the cost function based on specific attributes which characterise the circuit. In [54, 64], the so-called response features are used in the goal function definition. In this method, the goal function is formulated not from the entire response of the optimised structure but rather only from selected critical features of characteristic elements [58, 66]. The goal function is then as follows [34]:

$$C = \sum_{i=1}^{M} |F_f^i - F_{ref}^i|^2 \tag{1.13}$$

where $\mathbf{F}_{ref}$ is the objective vector extracted from the specifications, while $\mathbf{F}_f$ is the vector of M response features extracted from the simulated response. In this technique, the response features usually include points corresponding to specific response levels, e.g., the return loss level in the frequency band, as well as the response frequency locations of local maxima or minima [53, 55, 56]. The feature points of the circuit's response are denoted as $F_f^i = [f^i, r^i]^T$, where f and r are the frequency and magnitude level of each point F_f.

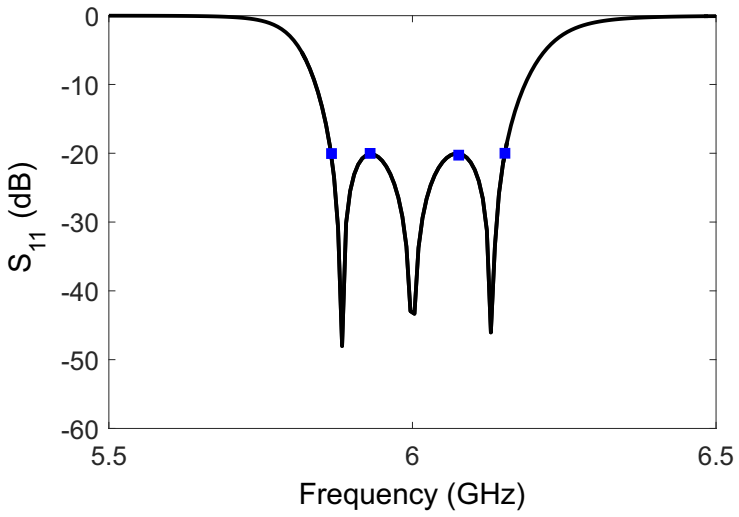

FIGURE 1.4: Microwave filter response with the response features selected to construct goal function (1.13).

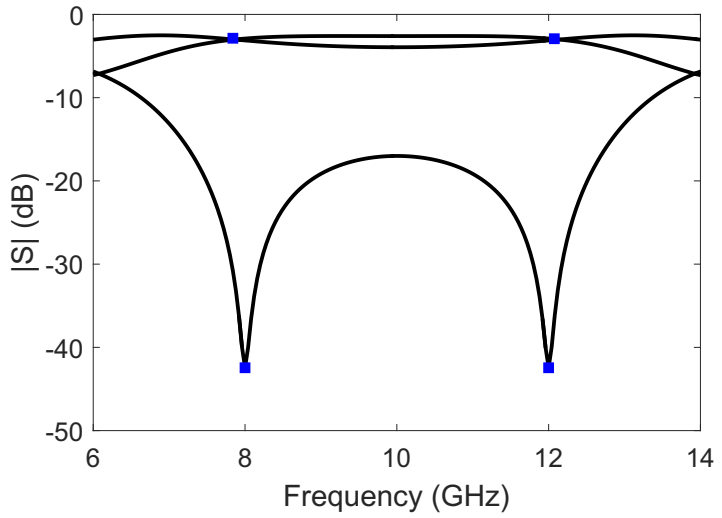

FIGURE 1.5: Microwave coupler response with the response features selected to construct goal function(1.13).

An example of a microwave bandpass filter response with selected reference features is presented in Fig.1.4. As can be seen, the response features correspond to S_{11}, a -20 dB level determining the filter bandwidth and the local maxima of the filter response. In the case of a microwave coupler response (Fig.1.5), the response features correspond to the - 3 dB level of transmission and coupled characteristics, as well as the two minima of reflection and the isolation response at the operating frequencies. The response features are less nonlinear than the scattering parameters as a function of frequency. As a result, using the response features to build the cost function speeds up the optimisation process.

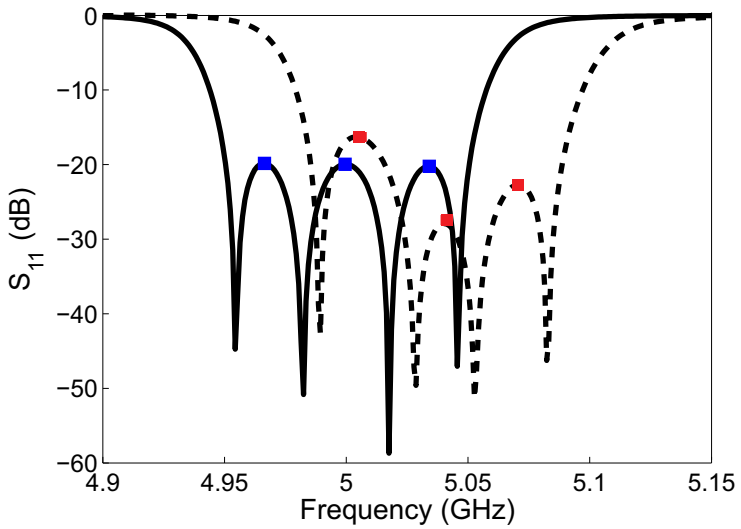

FIGURE 1.6: Microwave filter characteristics with denoted response features F_f (red) extracted from simulated response (- - -) and the reference values of the response features F_{ref} (blue) selected from desired characteristics (—).

In the optimisation process, the response features obtained from the simulated response F_f are compared with the reference ones F_{ref}. Fig. 1.6 presents the microwave filter characteristics with response features F_f extracted from the simulated response which correspond to the local maxima of the filter reflection coefficient (red points) and the reference values of response features F_{ref} which are equal to the -20 dB level of S_{11} (blue points).

However, such an approach does have shortcomings. To determine the values of response features, we need to evaluate the circuit response at many frequency points. Moreover, the feature-space methodology gives poor results when the initial solution is far from the final response [34] and when the wrong number of feature frequencies appears [92] (additional iterations needing to be performed with the goal function based on scattering parameters (1.11)). Another drawback of such a goal function definition is that only magnitude characteristics are optimised. The optimisation of phase characteristics with a goal function based on response features remains a challenge, as other authors noted in [59]. An example of the microwave filter response with the wrong number of response features obtained from the simulated response is shown in Fig.1.7.

1.2.5 Goal function based on coupling matrix elements

The definition of the cost function should be matched to the type of circuit optimised. Coupled cavity filters [22], constructed from coupled resonators, can be represented by a coupling matrix which describes interactions between resonators. As a result, for such circuits, network parameters (values of the coupling matrix) that correspond to the filter response obtained from full-wave simulation may be used [2, 18, 19, 33, 33, 37, 75] to construct the goal function instead of scattering parameters. In this approach, the scattering

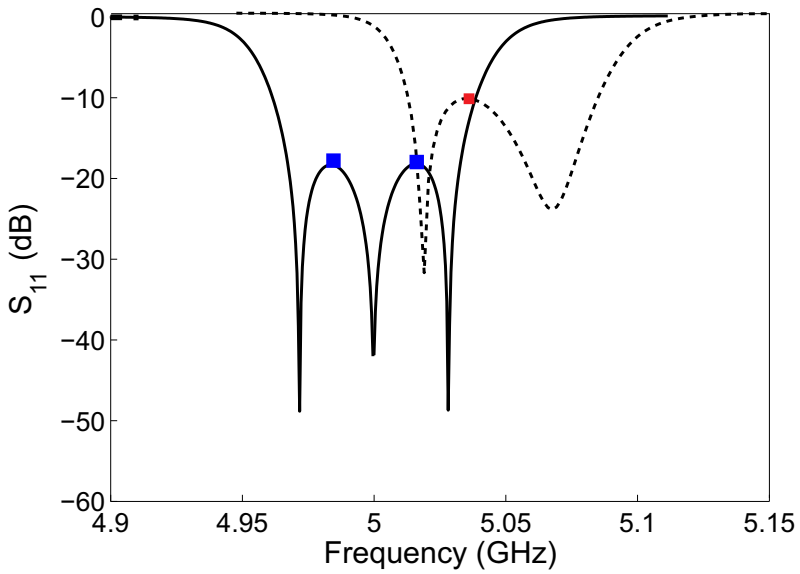

FIGURE 1.7: Microwave filter characteristics with the wrong number of response features F_f (red) extracted from the simulated response (- - -) and the reference values of response features F_{ref} (blue) selected from desired characteristics (—).

parameters computed by the full-wave solver are the input data for the procedure that finds the coupling matrix representation of the circuit's response. The reference coupling matrix is known from filter theory. In this approach, the crucial factor is the efficiency and accuracy of the procedure for identifying the coupling matrix from the simulated data.

In [75], the coupling matrix elements obtained from a rational model of simulated scattering parameters are compared with the assumed coupling scheme.

$$C = \sum_{i=1}^{N} \sum_{j=1}^{N} |m_{i,j} - m_{i,j}^{ref}|^2 \tag{1.14}$$

where $m_{i,j}$ are coupling matrix elements extracted from the simulated response, while $m_{i,j}^{ref}$ are elements of the assumed coupling matrix.

There is one drawback of such a definition of the goal function. Namely, the extraction of the coupling matrix is not always possible, in particular if the filter has dispersive elements or stray coupling.

1.2.6 Goal function based on zeros and poles of the transfer function

Recently, for microwave filter optimisation, the cost function has been defined using the zeros and poles of the filter's reflection and transmission coefficients [47, 79].

In general, the elements of the scattering matrix of microwave circuits can be represented in a form of a ratio of two polynomials [22]:

$$S_{11}(s) = \frac{F_N(s)}{E_N(s)}, \tag{1.15}$$

$$S_{21}(s) = \frac{P_{Nz}(s)}{\epsilon E_N(s)}. \tag{1.16}$$

where $P_{Nz}(s)$, $E_N(s)$ and $F_N(s)$ are complex polynomials of degree Nz and N, ϵ is a scaling factor and $s = j\omega$ is a complex frequency variable. Roots of $F_N(s)$ and $E_N(s)$ are zeros and poles of the reflection function, while roots of $P_{Nz}(s)$ are transmission zeros. S_{11} and S_{21} can be represented in the form of a rational function.

$$S_{11}(s) = \sum_{i=1}^{N} \frac{R_{11}^i}{s - p^i} \tag{1.17}$$

$$S_{21}(s) = \sum_{i=1}^{N} \frac{R_{21}^i}{s - p^i} \tag{1.18}$$

or

$$S_{11}(s) = \frac{\prod_{i=1}^{N}(s - z_{11}^i)}{\prod_{i=1}^{N}(s - p^i)}, \tag{1.19}$$

$$S_{21}(s) = \frac{\prod_{i=1}^{Nz}(s - z_{21}^i)}{\prod_{i=1}^{N}(s - p^i)} \tag{1.20}$$

where the p^i are the poles, R_{11}^i and R_{21}^i are the corresponding residues, and z_{11}^i and z_{21}^i are the zeros.

In [4, 83], goal function definition is based on the values of scattering parameters computed at certain frequency points. The optimal values of geometrical parameters of the structure considered are obtained by minimising the values of the scattering parameters at its zero $f_{z_{11}^i}$, pole $f_{z_{21}^i}$ and passband edge f_{e^i} frequency points. The goal function has the following form:

$$C = \sum_{i=1}^{N} |S_{11}(f_{z_{11}^i})|^2 + \sum_{i=1}^{Nz} |S_{21}(f_{z_{21}^i})|^2 + \sum_{i=1}^{2} (|S_{11}(f_{e^i})| - \epsilon)^2 \tag{1.21}$$

where N and Nz are numbers of zero and pole frequency points, while ϵ indicates the passband ripple. The transmission and reflection zero and passband edge frequency points are presented in Fig. 1.8

A similar approach was proposed in [44], where the goal function was formulated as:

$$C = \sum_{i=1}^{Nz} |P_{N_z}(\omega_{z_{21}^i})|^2 + \sum_{i=1}^{N} |F_N(\omega_{z_{11}^i})|^2 \tag{1.22}$$

where F_N and P_{N_z} are numerators of the filter reflection and transmission characteristics, while z_{11} and z_{21} are the zeros of the reflection and transmission functions.

Another concept involving the rational representation of filter characteristics was proposed in [47]. Instead of evaluating the frequency response over a specified frequency

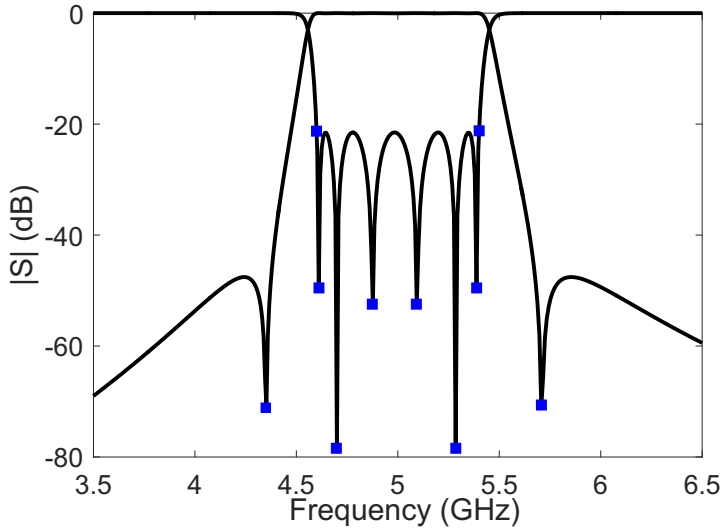

FIGURE 1.8: Circuit response with points selected to construct (1.21) goal function.

range to form the cost function, the complex zeros and poles of the rational approximation of scattering parameters are considered. The goal function definition is then based on the zeros and poles [48, 49] of a rational function model of scattering parameters. It is expressed in terms of the difference between the current locations of the zeros z_{11}^i, z_{21}^i and poles p^i of the scattering parameters obtained from the simulated response and the reference zeros $z_{11_{ref}}^i$, $z_{21_{ref}}^i$ and reference poles p_{ref}^i:

$$C = \sum_{i=1}^{N} |z_{11}^i - z_{11_{ref}}^i|^2 + \sum_{i=1}^{N_z} |z_{21}^i - z_{21_{ref}}^i|^2 + \sum_{i=1}^{N} |p^i - p_{ref}^i|^2 \tag{1.23}$$

where N is the number of zeros and poles of the reflection coefficient and N_z the number of transmission zeros. The z_{11}^i and p^i are respectively the roots of the numerator and denominator of the function S_{11} obtained from simulation and z_{21}^i are the roots of numerator of S_{21}. Fig. 1.9 presents the zeros of the reflection (x) and transmission (*) function and poles (o). The zeros and poles are extracted from a rational approximation of the scattering matrix obtained from full-wave analysis. For this, a vector-fitting procedure [35], Loewner matrix [43] or Cauchy interpolation [46] can be used. The reference locations of the zeros and poles of the scattering parameters are found analytically from a lumped element circuit or obtained from circuit synthesis [22]. Such a definition of the cost function does not need to include the phase of the optimised structure, because the phase characteristics are shaped by real or complex transmission zeros and all transmission zeros are included in the definition of the cost function. In the optimisation process, circuit geometrical parameters are modified in order that the reflection and transmission zeros and poles are positioned at the desired locations on the complex plane.

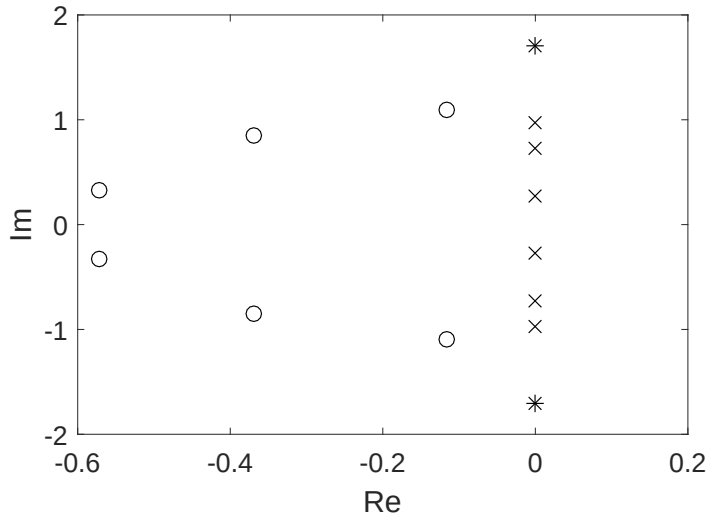

FIGURE 1.9: Circuit response with points selected to construct (1.23) goal function.

1.3 Surrogate models

Microwave optimisation techniques use various types of models. These include physically-based fine models. Fine models are analysed using EM solvers, where Maxwell's equations are numerically solved with high accuracy. Such models include all effects which occur in the physical structure, such as dispersion and radiation. As a result, the solution obtained from such models is accurate and close to the real behaviour of the analysed structure. On the other hand, EM simulations are very time-consuming and require high computational resources, and hence, design using fine models may take very long time and become a dominant cost factor, especially if numerical simulation is used in optimisation loops where a problem is solved again and again while changing the design variables. As noted above, it is challenging to perform even a single simulation based on physical principles, let alone the hundreds or thousands that are usually required for optimisation.

A second type of models are auxiliary models, so-called surrogate or coarse models which are used in the design of microwave circuits at an initial stage, to obtain a good starting point for further full-wave optimisation, and also in the optimisation loop, in place of computationally-demanding EM models. This type of model does not take into account effects such as dispersion or radiation, and hence, the solution provided is less accurate but computationally easier to calculate. Surrogate models are used to accelerate time-consuming optimisation of microwave components. Various different categories of surrogate models can be used in the design process.

One category of such models are metamodels, which are built by fitting or interpolating response data. The response data are obtained from an EM model evaluated at a certain set of sample points. The set of samples may be defined in various ways, randomly in the design space or using a space filling technique, such as Latin hypercube sampling [39, 81] where all regions of the design are treated equally. A metamodel is used in the optimisation loop instead of a full-wave model. Popular classes of such models are response

surface models [36, 76], kriging models [38, 90], artificial neural networks [24, 82, 91] and multidimensional interpolations using radial base functions [74]. One drawback of these models is that their accuracy depends on the number of training samples used to build them. In order to obtain satisfactory model accuracy, many training samples should be used.

Another category of surrogate models are circuit-based models [15, 27, 86], where an equivalent structure is composed from various circuit elements, including transmission lines, coupled lines or discontinuities. A main drawback of such models is that they can only be constructed for a limited number of predefined shapes. As a result, changes in the structure geometry are restricted to the set of available shapes.

Finally, there are discrete mesh models, which are created based on the full-wave model [72]. Such models are simulated using an EM solver but with a coarser grid (larger cell size), and as a result, a less accurate model is obtained but the simulation time is shorter. Models of this category are more accurate than metamodels or equivalent circuits but they are still quite computationally demanding.

1.3.1 Hybrid optimisation techniques using surrogate models

To reduce the time spent on computing the full-wave solution, several novel hybrid optimisation strategies [8, 20, 70] have been proposed for designing microwave structures. The main idea of these algorithms is to use a surrogate model in the modelling or optimisation instead of a computationally demanding full-wave model [73, 88]. Even though low accuracy surrogate models are exploited in the optimisation loop to solve the problem while searching, the optimal solution obtained is expected to have the accuracy of an EM model [42, 80]. In this scenario, highly-accurate models are used only for verification of the solution obtained by approximate surrogate models. In other words, the high-fidelity model is evaluated only for verification and re-calibration of the surrogate model, rather than being used directly by the optimisation algorithm. A flowchart illustrating surrogate-based optimisation (SBO) is presented in Fig. 1.10.

1.3.2 Space mapping

One of the most efficient hybrid algorithms is the space-mapping (SM) technique introduced by Bandler in [12]. In this technique, two models are used in the optimisation process, a coarse model, denoted by c, and a fine model [7, 9], denoted by f, with high and low computational costs respectively. The coarse model is not as accurate as the fine model, but it is able to solve the optimisation problem in a computationally fast way.

Space-mapping techniques combine the fast computation of a coarse model with the accuracy of a fine model. This is only possible if a link or a mapping is found between the coarse model space and fine model space. The design process is accelerated due to the limited evaluations of the computationally demanding fine model, while the coarse model and the coarse space to fine space mapping are used in the optimisation routine. In each iteration of the space-mapping method, the coarse model is optimised and one evaluation of fine model is carried out to verify the optimal solution achieved for the coarse model and refine the mapping between coarse and fine model space [5, 93].

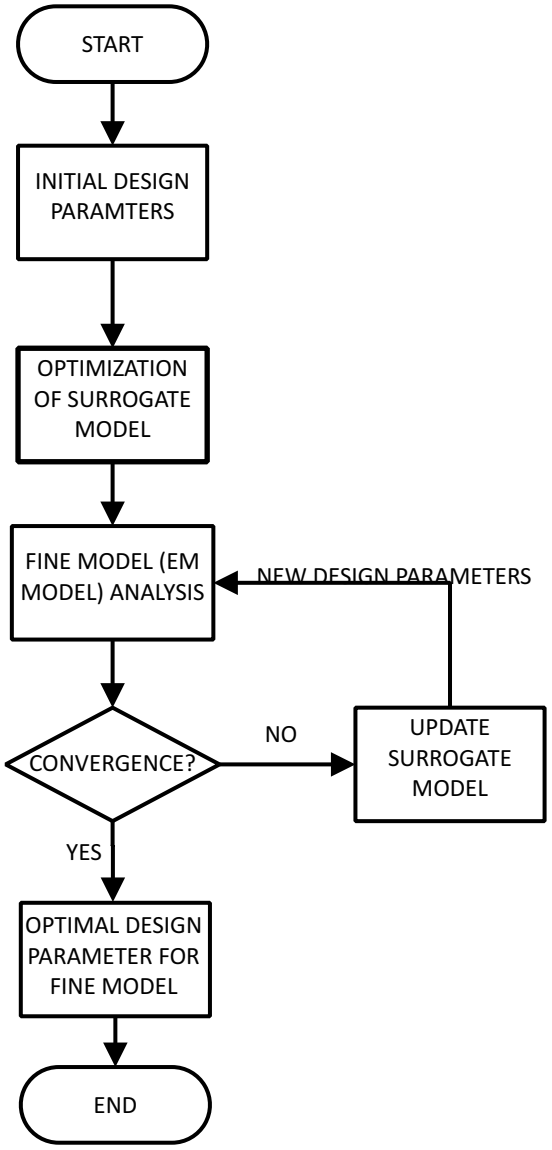

FIGURE 1.10: Flowchart of the surrogate-based optimisation process [70].

The choice of coarse model is important for the performance of the optimisation system. In particular, the coarse model is evaluated in the optimisation loop, and hence, needs to be run a large number of times. Given this, a single simulation should take much less time for the coarse model than the fine model. In an ideal situation, the total computational cost of optimisation should be determined by the fine model evaluations. That is, it only makes sense to use space mapping for optimisation when the coarse model is much less time consuming than the fine model. If, however, the coarse model is insufficiently accurate, the space-mapping algorithm may need many fine model evaluations or fail.

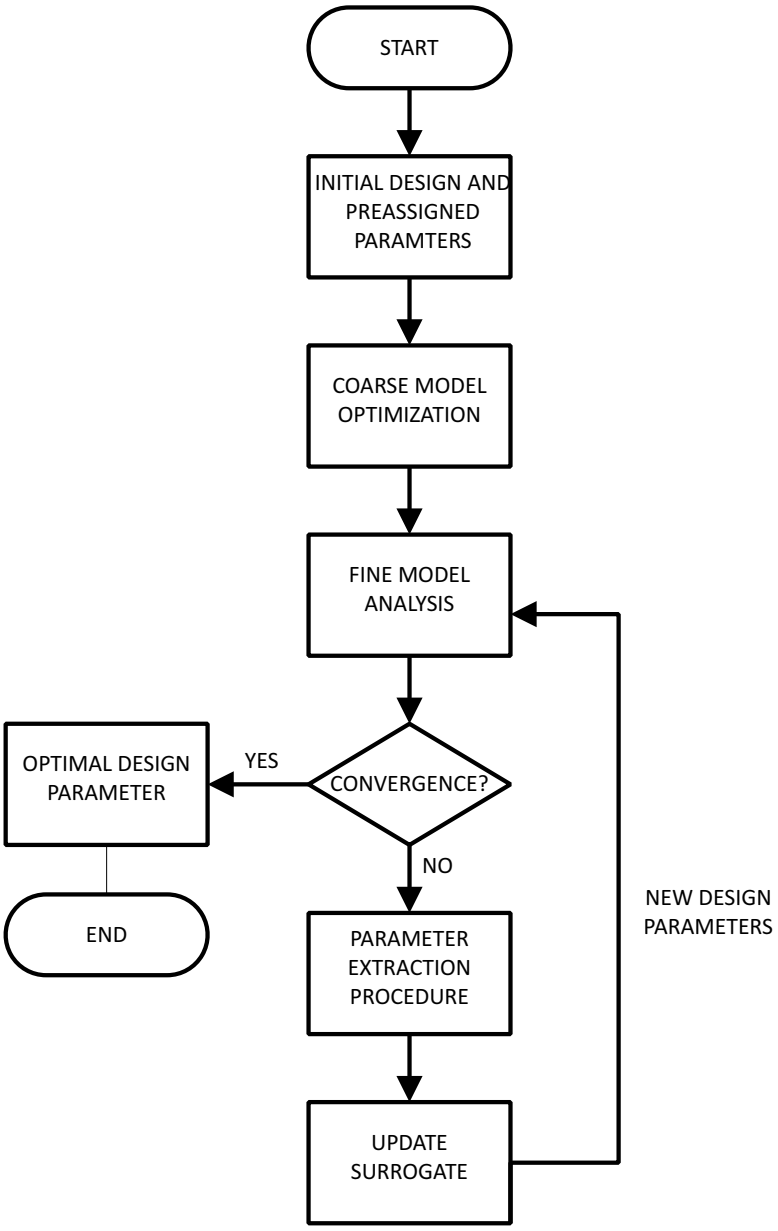

FIGURE 1.11: Flowchart of the space-mapping process [12, 41].

1.3.3 Finding the link between coarse and fine model spaces

The goal of the space-mapping algorithm is to find the vector of optimal parameters for which the circuit responses will satisfy the design requirements

$$\mathbf{x}^* = \arg\min_{\mathbf{x}} ||f(\mathbf{x}) - y|| \tag{1.24}$$

where $\mathbf{x}^*$ is a vector of optimal design variables (dimensions of the optimised structure) that satisfies the design specification, f is a fine model response (e.g., scattering parameters) and y is the desired response. To this end, a few key steps need to be carried out [7].

First, the coarse model is optimised to obtain the design specification. This optimisation may be carried out using traditional direct optimisation algorithms.

Next, the fine model is simulated for the optimal vector of design variables obtained from the coarse model optimisation. When the fine model response reaches the design specification, the optimisation procedure stops; otherwise, a mapping is established between the parameter spaces of the two models. The fine model parameter space is mapped to the coarse model design space such that the following relationship is valid

$$c(P(\mathbf{x})) = f(\mathbf{x}). \tag{1.25}$$

where c is the coarse model response and the function P is the mapping function.

The space-mapping surrogate model is defined as follows

$$s(\mathbf{x}, \mathbf{p}) = c(P(\mathbf{x})) \tag{1.26}$$

and locally approximates the fine model.
To find the mapping, suitably selected mapping parameters, so-called preassigned parameters, $\mathbf{p}$, are used. These variables are calibrated to match the surrogate response with that of the fine model. This step is called a parameter-extraction (PE) procedure and involves an optimisation process where the difference between output data coming from the calibrated surrogate model and the fine model is minimised in order to achieve the values of vector $\mathbf{p}$. The extraction is also carried out using traditional direct optimisation algorithms.

$$\mathbf{p} = \arg\min_{p} ||s(\mathbf{x}, \mathbf{p}) - f(\mathbf{x})||. \tag{1.27}$$

The space-mapping algorithm is presented in Fig. 1.11. The initial values of preassigned parameters $p^{(0)}$ are the same as corresponding parameters in the fine model or are set to zero. The initial set of design variables of the coarse model is obtained from the circuit synthesis or chosen at random with respect to the circuit topology. The initial vector of the fine model is equal to the optimal solution found with the coarse model.

1.3.4 Space mapping algorithms

There are many variants of space-mapping techniques, these reflecting the assumed relationship between the surrogate model and the fine model.

1.3.5 Aggressive space mapping

Aggressive space mapping (ASM) [6, 13] is based on quasi-Newton algorithms and has utilised Broyden updates. This variant of space mapping iteratively solves the nonlinear equation

$$g(\mathbf{x}) = P(\mathbf{x}) - \mathbf{x}_c^* \tag{1.28}$$

where $\mathbf{x}$ is the fine model design parameter vector, $\mathbf{x}_c^*$ is the optimal vector of coarse model and P is the mapping. The mapping P between two spaces is established using the following technique

$$\mathbf{x}_c = P(\mathbf{x}) \tag{1.29}$$

where $\mathbf{x}_c$ is obtained in the parameter extraction process by solving the following procedure

$$\mathbf{x}_c = \arg\min_{x_c} ||c(\mathbf{x}_c) - f(\mathbf{x})||. \tag{1.30}$$

The fine model design parameter vector $\mathbf{x}$ is updated using the following formula:

$$\mathbf{x}^{i+1} = \mathbf{x}^i + \mathbf{h}^i \tag{1.31}$$

where the correction vector $\mathbf{h}^i$ is found by solving Equation 1.32

$$\mathbf{B}^i \cdot \mathbf{h}^i = -\mathbf{g}^i \tag{1.32}$$

where matrix $\mathbf{B}^i$ is the current approximation of the Jacobian of function $\mathbf{g}$ based on all previous iterations. Initially, matrix $\mathbf{B}^0$ is set to the identity matrix and $\mathbf{x}^1 = \mathbf{x}_c^*$. During optimisation matrix, $\mathbf{B}$ is updated:

$$\mathbf{B}^{i+1} = \mathbf{B}^i + \frac{\mathbf{g}^{i+1} \cdot \mathbf{h}^{iT}}{\mathbf{h}^{iT} \cdot \mathbf{h}^i} \tag{1.33}$$

1.3.6 Input space mapping

In input space mapping (ISM) [50], the link between the spaces is expressed through a linear correlation between the coarse and the fine parameter spaces:

$$s(\mathbf{x}, \mathbf{A}, \mathbf{b}) = c(\mathbf{A} \cdot \mathbf{x} + \mathbf{b}). \tag{1.34}$$

where $\mathbf{x}$ is design parameter vector, $\mathbf{A}$ is a matrix with non-zero elements on the diagonal $\mathbf{A} = diag\{a_1, a_2, \cdots, a_n\}$ and $\mathbf{b}$ is an n $\times$ 1 vector. In the parameter extraction step, the variables that are varied are the values of $\mathbf{A}$ and $\mathbf{b}$.

1.3.7 Implicit space mapping

The implicit space-mapping [9] technique uses preassigned parameters $\mathbf{p}$ in the parameter extraction procedure, these normally being fixed in the fine model but modifiable in the coarse model. These parameters may be quantities such as the dielectric constant or substrate heights. Although in physical circuits such quantities are fixed, they can be used to match the surrogate with the high-fidelity model. The surrogate model response is defined as follows:

$$s(\mathbf{x}, \mathbf{p}) = c(\mathbf{x}, \mathbf{p}). \tag{1.35}$$

1.3.8 Frequency space mapping

In the frequency space-mapping algorithm, it is the frequency shift between the coarse and fine model that is established in the parameter extraction step [16]

$$s(\mathbf{x}, f_0, f_1) = c(\mathbf{x}, f_1 + \omega \cdot f_0) \tag{1.36}$$

where f_0 and f_1 are scalar variables initially set to 1 and 0, respectively.

1.3.9 Output space mapping

Output space mapping (OSM) [50] uses a linear correlation between coarse and fine model responses:

$$s(\mathbf{x}, \mathbf{B}, \mathbf{d}) = \mathbf{B} \cdot c(\mathbf{x}) + \mathbf{d} \tag{1.37}$$

where $\mathbf{B}$ is a matrix with non-zero elements on the diagonal, $\mathbf{B} = diag\{b_1, b_2, \cdots, b_m\}$, and $\mathbf{d}$ is an m $\times$ 1 vector. In this case, it is assumed the coarse and surrogate models have responses that are of similar shapes but slightly shifted in the frequency domain or different in amplitude.

Surrogate models can also be constructed as a combination of all the described variants. This can significantly improve the performance of the space-mapping algorithm. Properly chosen mapping can improve the performance of an optimisation system; however, the optimal selection of the mapping variant is not trivial [51].

1.3.10 Manifold mapping

Another hybrid technique is manifold mapping (MM) [28, 29], which, similar to space mapping, uses two spaces to obtain the optimal information about parameter setting in a high-fidelity model. This type of mapping does not require a parameter extraction step. Rather than correcting the misalignment in the parameter space, the technique uses a surrogate model for which the misalignment between the response spaces is corrected:

$$s^i(\mathbf{x}) = f(\mathbf{x}^i) + \mathbf{S}^i(c(\mathbf{x}) - c(\mathbf{x}^i)) \tag{1.38}$$

where s^i is surrogate model at iteration i, $\mathbf{S}^i$ is a square matrix denoted as:

$$\mathbf{S}^i = \mathbf{J}_f(\mathbf{x}^i) \cdot \mathbf{J}_c^\dagger(\mathbf{x}^i) \tag{1.39}$$

where $\mathbf{J}_f$ and $\mathbf{J}_c$ stand for the fine and coarse model response Jacobians, respectively and $(\cdot)^\dagger$ is Moore-Penrose pseudo-inverse.

This technique is based only on response correction. When the differences between the characteristics of the two models are non negligible, an additional iteration needs to be performed for direct optimisation [65] in order to reduce the difference between models. What is more, the response correction techniques like OSM and MM are used to supplement other SBO techniques where the space parameter mapping is also used to improve the algorithm [30, 40].

1.3.11 Multifidelity optimisation

A final technique that should be mentioned is a multilevel optimisation procedure [67]. In this technique, a full-wave EM model is evaluated at different levels of fidelity. The low-fidelity model may be obtained by coarsening the mesh [72] or by using different orders of the basis functions [74]. During the optimisation process, the accuracy of the low-fidelity model can be increased [69]. The initial design may be quite poor but quick to achieve. While moving closer to the optimal solution of the fine model, the coarse model accuracy should increase. This can be done by changing the mesh density. The advantage of such an approach is that there is no need to select suitable models and mapping parameters. On the other hand, a drawback of this technique is that the optimisation process may fail if there is significant misalignment between low- and high-fidelity models.

1.4 Scope, claims and goals of this work

SBO algorithms have been applied to solve many optimisation problems in the field of EM engineering [7, 50, 61], including the design of microwave filters, couplers, power dividers, impedance transformers, and antennas [5, 9, 93]. Hybrid strategies involving surrogate models have also been exploited in other fields, including electromechanical, [31, 32], aerodynamic [78], and magnetic [23, 25] problems. While space-mapping optimisation has been extensively covered in the literature, the author of this thesis believes that there is so far insufficient evidence of the suitability of this methodology for practical applications.

First of all, the SBO techniques presented in the literature have been tested on examples that involve only a few (generally less than ten) design variables [52, 56, 92], while in practice this number is usually an order of magnitude higher. Moreover, the quality of the designs is not adequately discussed. For instance, when filters are used as examples, often only the transmission coefficient S_{21} is considered in the optimisation [62, 63, 68, 71]. In practice, fulfilling the design requirements for S_{21} is not enough, since S_{11} should be considered to ensure equal-ripple behaviour of the reflection response in the frequency band of interest. What is more, in all cases found in the literature, the starting point is close to the final design [45, 60] and the problems considered are not very challenging - typically, concerning third- or fourth-order filters [9, 17, 57].

Further, in examples presented in literature, usually the goal function used in the optimisation loop is based on scattering parameters. Such traditional goal functions tend to give poor results because they have many local minima. This is easy to understand since there are infinitely many complex valued functions that have the same amplitude characteristics and different phase characteristics. Therefore, a goal function (or mapping) based on amplitude alone is not uniquely defined and the design procedure attempts to converge to some arbitrary goal (in a sense of an arbitrary phase characteristic). To overcome this problem, there is a need to develop new design strategies and test their robustness and efficiency for challenging problems with many design variables.

In this context, the main goal of this thesis is to present a new class of effective techniques to decrease the number of EM simulations needed in the design of complex microwave passive components by optimisation. In all the techniques considered in this

thesis, a goal function based on zeros and poles of a rational approximation of the scattering parameters and a hybrid approach are used to speed up the design cycle. The claims of the thesis are:

- A zero-pole goal function based on the reference zeros and poles of the rational approximation of the scattering parameters makes it possible to significantly decrease the time needed for designing linear microwave structures in comparison with the goal function based on masks and samples of the scattering parameters used in the standard approach.
- The zero-pole approach can be used in a space-mapping method, leading to a reduction in the time required for the EM simulation, while numerically tuning passive microwave structures.
- It is possible to create locally linear mapping between zeros and poles of the transfer function and the space of coarse and fine models (equivalent model and EM model respectively).

1.5 Outline of the Thesis

The thesis is organised into 8 chapters, Chapters 2 to 7 being extended versions of journal papers of the same title. The original papers that form the basis of chapters have been expanded by providing more detailed data and additional examples. An overview of the chapters is given in the following paragraphs.

Chapter 2

Chapter 2 presents an application of the zero-pole goal function for the design of pseudo-elliptic filters in an in-line topology implemented in substrate integrated waveguide (SIW) technology. A comparison with the traditional cost function is provided. Experimental validation of the method is described.

Chapter 3

In Chapter 3, a fast technique is proposed for the automated design of both amplitude and phase characteristics of microwave filters with linear phase. The first part of the chapter describes the comparison between goal function definitions based on positions of zeros and poles of filter reflection and transmission responses and the goal function based on scattering parameters. The effectiveness of the proposed zero-pole technique is illustrated with two examples.

Chapter 4

Chapter 4 presents a new space-mapping technique tailored for the CAD of microwave filters. The filter to be designed is represented by a rational filtering function, whose

zeros and poles determine the properties of the device. To quickly align the coarse and fine models and speed up the direct optimisation of the coarse model, the parameter extraction attempts to match the zeros and poles of a rational function extracted from scattering parameters, rather than frequency responses. The effectiveness and robustness of the proposed technique is illustrated with examples.

Chapter 5

In Chapter 5, a new approach to full-wave CAD of microwave filters is presented. This approach yields a method that consists of two stages and operates on the zeros and poles of the transfer function and their derivatives. The two stages make use of different models that are optimised using a low-accuracy EM solver. The design involves coarse-level optimisation at both stages, each requiring a single computation of the high-accuracy response.

Chapter 6

Surrogate modelling of the response of microwave filters is discussed in Chapter 6. Kriging is used to model the scattering parameters of a filter and the rational representation of the filter's characteristics. Surrogate models for these two variants of kriging are validated through solving a microwave filter optimisation problem. Surrogate models based on the rational representation are shown to have clear advantages over the models based on scattering parameters.

Chapter 7

The extension of the zero-pole technique to types of passive circuits other than filters is presented in Chapter 7. The reference zeros and poles for the optimised circuit are extracted from the simulated response of a device's equivalent circuit or a simplified, low-resolution numerical model. These values are compared with zeros and poles computed from the simulated response of the optimised structure.

Conclusions

This chapter summarises the research contributions of this PhD thesis. The possibilities for further improvements are also discussed.

References

[1] F. Alessandri, M. Dionigi, and R. Sorrentino. A fullwave CAD tool for waveguide components using a high speed direct optimizer. *IEEE Transactions on Microwave Theory and Techniques*, 43(9):2046–2052, Sep 1995.

[2] S. Amari, C. LeDrew, and W. Menzel. Space-mapping optimization of planar coupled-resonator microwave filters. *IEEE Transactions on Microwave Theory and Techniques*, 54(5):2153–2159, May 2006.

[3] F. Arndt, R. Beyer, J. M. Reiter, T. Sieverding, and T. Wolf. Automated design of waveguide components using hybrid mode-matching/numerical EM building-blocks in optimization-oriented CAD frameworks-state of the art and recent advances. *IEEE Transactions on Microwave Theory and Techniques*, 45(5):747–760, May 1997.

[4] W. A. Atia, K. A. Zaki, and A. E. Atia. Synthesis of general topology multiple coupled resonator filters by optimization. In *1998 IEEE MTT-S International Microwave Symposium Digest (Cat. No.98CH36192)*, volume 2, pages 821–824 vol.2, June 1998.

[5] M. Bakr, J. Bandler, M. Ismail, J. Rayas-Sanchez, and Q.-J. Zhang. Neural space-mapping optimization for EM-based design. *Microwave Theory and Techniques, IEEE Transactions on*, 48(12):2307 –2315, Dec. 2000.

[6] M. H. Bakr, J. W. Bandler, N. Georgieva, and K. Madsen. A hybrid aggressive space-mapping algorithm for EM optimization. *IEEE Transactions on Microwave Theory and Techniques*, 47(12):2440–2449, Dec 1999.

[7] J. Bandler, Q. Cheng, S. Dakroury, A. Mohamed, M. Bakr, K. Madsen, and J. Sondergaard. Space mapping: the state of the art. *Microwave Theory and Techniques, IEEE Transactions on*, 52(1):337 – 361, Jan. 2004.

[8] J. Bandler, Q. Cheng, D. Hailu, and N. Nikolova. A space-mapping design framework. *Microwave Theory and Techniques, IEEE Transactions on*, 52(11):2601 – 2610, Nov. 2004.

[9] J. Bandler, Q. Cheng, N. Nikolova, and M. Ismail. Implicit space mapping optimization exploiting preassigned parameters. *Microwave Theory and Techniques, IEEE Transactions on*, 52(1):378 – 385, Jan. 2004.

[10] J. Bandler, W. Kellermann, and K. Madsen. A superlinearly convergent minimax algorithm for microwave circuit design. In *Microwave Symposium Digest, 1985 IEEE MTT-S International*, pages 721 –724, Jun. 1985.

[11] J. W. Bandler. Optimization methods for computer-aided design. *IEEE Transactions on Microwave Theory and Techniques*, 17(8):533–552, Aug 1969.

[12] J. W. Bandler, R. M. Biernacki, S. H. Chen, P. A. Grobelny, and R. H. Hemmers. Space mapping technique for electromagnetic optimization. *IEEE Trans. Microw. Theory Tech.*, 42(12):2536 –2544, Dec. 1994.

[13] J. W. Bandler, R. M. Biernacki, S. H. Chen, R. H. Hemmers, and K. Madsen. Electromagnetic optimization exploiting aggressive space mapping. *IEEE Transactions on Microwave Theory and Techniques*, 43(12):2874–2882, Dec 1995.

[14] J. W. Bandler, R. M. Biernacki, S. H. Chen, D. G. Swanson, and S. Ye. Microstrip filter design using direct EM field simulation. *IEEE Transactions on Microwave Theory and Techniques*, 42(7):1353–1359, Jul 1994.

[15] J. W. Bandler and S. H. Chen. Circuit optimization: the state of the art. *IEEE Transactions on Microwave Theory and Techniques*, 36(2):424–443, Feb 1988.

[16] J. W. Bandler, Q. Cheng, D. H. Gebre-Mariam, K. Madsen, F. Pedersen, and J. Sondergaard. EM-based surrogate modeling and design exploiting implicit, frequency and output space mappings. In *Microwave Symposium Digest, 2003 IEEE MTT-S International*, volume 2, pages 1003–1006 vol.2, June 2003.

[17] J. W. Bandler, A. S. Mohamed, M. H. Bakr, K. Madsen, and J. Sondergaard. EM-based optimization exploiting partial space mapping and exact sensitivities. *IEEE Transactions on Microwave Theory and Techniques*, 50(12):2741–2750, Dec 2002.

[18] S. Bila, D. Baillargeat, M. Aubourg, S. Verdeyme, P. Guillon, F. Seyfert, J. Grimm, L. Baratchart, C. Zanchi, and J. Sombrin. Direct electromagnetic optimization of microwave filters. *IEEE Microwave Magazine*, 2(1):46–51, Mar 2001.

[19] S. Bila, D. Baillargeat, M. Aubourg, S. Verdeyme, F. Seyfert, L. Baratchart, C. Boichon, F. Thevenon, J. Puech, C. Zanchi, L. Lapierre, and J. Sombrin. Finite-element modeling for the design optimization of microwave filters. *IEEE Transactions on Magnetics*, 40(2):1472–1475, March 2004.

[20] S. Bila, D. Baillargeat, S. Verdeyme, and P. Guillon. Automated design of microwave devices using full EM optimization method. In *Microwave Symposium Digest, 1998 IEEE MTT-S International*, volume 3, pages 1771 –1774 vol.3, Jun. 1998.

[21] D. Calahan. *Computer aided circuits design.* McGraw-Hill, 1972.

[22] R. J. Cameron. Advanced coupling matrix synthesis techniques for microwave filters. *IEEE Transactions on Microwave Theory and Techniques*, 51(1):1–10, Jan 2003.

[23] H.-S. Choi, D.-H. Kim, I.-H. Park, and S.-Y. Hahn. A new design technique of magnetic systems using space mapping algorithm. *IEEE Transactions on Magnetics*, 37(5):3627–3630, Sep 2001.

[24] G. L. Creech, B. J. Paul, C. D. Lesniak, T. J. Jenkins, and M. C. Calcatera. Artificial neural networks for fast and accurate EM-CAD of microwave circuits. *IEEE Transactions on Microwave Theory and Techniques*, 45(5):794–802, May 1997.

[25] G. Crevecoeur, L. Dupre, and R. V. de Walle. Space mapping optimization of the magnetic circuit of electrical machines including local material degradation. *IEEE Transactions on Magnetics*, 43(6):2609–2611, June 2007.

[26] J. D. G. Swanson. First pass CAD of microstrip filters cuts development time. *Microwave & RF 95 London*, pages 8–12, 1995.

[27] B. Easter. The equivalent circuit of some microstrip discontinuities. *IEEE Transactions on Microwave Theory and Techniques*, 23(8):655–660, Aug 1975.

[28] D. Echeverria. *Multi-Level Optimization. Space Mapping And Manifold Mapping*. PhD thesis, University of Amsterdam, 2007.

[29] D. Echeverria and P. W. Hemker. Manifold mapping: a two-level optimization technique. *Computing and Visualization in Science*, 11(4):193–206, 2008.

[30] D. Echeverria, D. Lahaye, and P. W. Hemker. *Space Mapping and Defect Correction*, pages 157–176. Springer Berlin Heidelberg, Berlin, Heidelberg, 2008.

[31] L. Encica, J. Paulides, and E. Lomonova. Space mapping optimization in electromechanics: an overview of algorithms and applications. *COMPEL - The international journal for computation and mathematics in electrical and electronic engineering*, 28(5):1216–1226, 2009.

[32] P. F. Pedersen and S. Svendsen. Modeling thermally active building components using space mapping. In *Proceedings of the 7-th Symposium on Building Physics in the Nordic Countries*, pages 896–903, 2005.

[33] A. Garcia-Lamperez, S. Llorente-Romano, M. Salazar-Palma, and T. K. Sarkar. Efficient electromagnetic optimization of microwave filters and multiplexers using rational models. *IEEE Transactions on Microwave Theory and Techniques*, 52(2):508–521, Feb 2004.

[34] O. Glubokov and S. Koziel. EM-driven tuning of substrate integrated waveguide filters exploiting feature-space surrogates. In *2014 IEEE MTT-S International Microwave Symposium (IMS2014)*, pages 1–3, June 2014.

[35] B. Gustavsen and A. Semlyen. Rational approximation of frequency domain responses by vector fitting. *IEEE Transactions on Power Delivery*, 14(3):1052–1061, Jul 1999.

[36] D. M. H. Myers. *Response surface methodology: Process and Product Optimization using designed experiments*. Wiley, 1995.

[37] P. Harscher, E. Ofli, R. Vahldieck, and S. Arnari. EM-simulator based parameter extraction and optimization technique for microwave and millimeter wave filters. In *2002 IEEE MTT-S International Microwave Symposium Digest (Cat. No.02CH37278)*, volume 2, pages 1113–1116 vol.2, June 2002.

[38] G. Hawe and J. Sykulski. Considerations of accuracy and uncertainty with kriging surrogate models in single-objective electromagnetic design optimisation. *IET Science, Measurement Technology*, 1(1):37–47, January 2007.

[39] J. Helton and F. Davis. Latin hypercube sampling and the propagation of uncertainty in analyses of complex systems. *Reliability Engineering "&" System Safety*, 81(1):23 – 69, 2003.

[40] P. Hemker and D. Echeverría. A trust-region strategy for manifold-mapping optimization. *Journal of Computational Physics*, 224(1):464 – 475, 2007. Special Issue Dedicated to Professor Piet Wesseling on the occasion of his retirement from Delft University of Technology.

[41] J.-S. Hong and M. J. Lancaster. *Microstrip Filters for RF/Microwave Applications*. John Wiley.

[42] J.-S. Hong and M. J. Lancaster. Couplings of microstrip square open-loop resonators for cross-coupled planar microwave filters. *IEEE Transactions on Microwave Theory and Techniques*, 44(11):2099–2109, Nov 1996.

[43] M. Kabir and R. Khazaka. Macromodeling of distributed networks from frequency-domain data using the loewner matrix approach. *IEEE Transactions on Microwave Theory and Techniques*, 60(12):3927–3938, Dec 2012.

[44] M. Kahrizi, S. Safavi-Naeini, S. K. Chaudhuri, and R. Sabry. Computer diagnosis and tuning of rf and microwave filters using model-based parameter estimation. *IEEE Transactions on Circuits and Systems I: Fundamental Theory and Applications*, 49(9):1263–1270, Sep 2002.

[45] A. Khalatpour, R. K. Amineh, Q. S. Cheng, M. H. Bakr, N. K. Nikolova, and J. W. Bandler. Accelerating space mapping optimization with adjoint sensitivities. *IEEE Microwave and Wireless Components Letters*, 21(6):280–282, June 2011.

[46] K. Kottapalli, T. K. Sarkar, Y. Hua, E. K. Miller, and G. J. Burke. Accurate computation of wide-band response of electromagnetic systems utilizing narrow-band information. *Microwave Theory and Techniques, IEEE Transactions on*, 39(4):682–687, 1991.

[47] P. Kozakowski and M. Mrozowski. Automated CAD of coupled resonator filters. *IEEE Microw. Wireless Compon. Lett.*, 12(12):470 –472, Dec. 2002.

[48] P. Kozakowski and M. Mrozowski. New approach to fast full wave optimization of microwave filters. In *2002 32nd European Microwave Conference*, pages 1–4, Sept 2002.

[49] P. Kozakowski and M. Mrozowski. Quadratic programming approach to coupled resonator filter CAD. *IEEE Transactions on Microwave Theory and Techniques*, 54(11):3906–3913, Nov 2006.

[50] S. Koziel, J. Bandler, and K. Madsen. A space-mapping framework for engineering optimization: Theory and implementation. *Microwave Theory and Techniques, IEEE Transactions on*, 54(10):3721 –3730, Oct. 2006.

[51] S. Koziel and J. W. Bandler. Coarse and surrogate model assessment for engineering design optimization with space mapping. In *2007 IEEE/MTT-S International Microwave Symposium*, pages 107–110, June 2007.

[52] S. Koziel and J. W. Bandler. Space-mapping modelling of microwave devices using multi-fidelity electromagnetic simulations. *IET Microwaves, Antennas Propagation*, 5(3):324–333, Feb 2011.

[53] S. Koziel and J. W. Bandler. Accurate modeling of microwave structures using variable-fidelity response features. In *2015 IEEE MTT-S International Microwave Symposium*, pages 1–3, May 2015.

[54] S. Koziel and J. W. Bandler. Fast EM-driven design optimization of microwave filters using adjoint sensitivity and response features. In *IEEE MTT-S Int. Microw. Symp. Dig*, pages 1–3, May 2015.

[55] S. Koziel and J. W. Bandler. Rapid yield estimation and optimization of microwave structures exploiting feature-based statistical analysis. *IEEE Transactions on Microwave Theory and Techniques*, 63(1):107–114, Jan 2015.

[56] S. Koziel and J. W. Bandler. Reliable microwave modeling by means of variable-fidelity response features. *IEEE Transactions on Microwave Theory and Techniques*, 63(12):4247–4254, Dec 2015.

[57] S. Koziel, J. W. Bandler, and Q. S. Cheng. Constrained parameter extraction for microwave design optimisation using implicit space mapping. *IET Microwaves, Antennas Propagation*, 5(10):1156–1163, July 2011.

[58] S. Koziel, J. W. Bandler, and Q. S. Cheng. Low-cost feature-based modeling of microwave structures. In *2014 IEEE MTT-S International Microwave Symposium (IMS2014)*, pages 1–3, June 2014.

[59] S. Koziel and A. Bekasiewicz. Fast simulation-driven feature-based design optimization of compact dual-band microstrip branch-line coupler. *International Journal of RF and Microwave Computer-Aided Engineering*, 26(1):13–20, 2016.

[60] S. Koziel and A. Bekasiewicz. Rapid microwave design optimization in frequency domain using adaptive response scaling. *IEEE Transactions on Microwave Theory and Techniques*, 64(9):2749–2757, Sept 2016.

[61] S. Koziel, Q. Cheng, and J. Bandler. Space mapping. *Microwave Magazine, IEEE*, 9(6):105 –122, Dec. 2008.

[62] S. Koziel, Q. S. Cheng, and J. W. Bandler. Comparative study of space-mapping-based techniques for microwave design optimisation. *IET Microwaves, Antennas Propagation*, 6(3):361–370, February 2012.

[63] S. Koziel, Q. S. Cheng, and J. W. Bandler. Fast EM modeling exploiting shape-preserving response prediction and space mapping. *IEEE Transactions on Microwave Theory and Techniques*, 62(3):399–407, March 2014.

[64] S. Koziel, Q. S. Cheng, and J. W. Bandler. Feature-based surrogates for low-cost microwave modelling and optimisation. *IET Microwaves, Antennas Propagation*, 9(15):1706–1712, 2015.

[65] S. Koziel and D. E. Ciaurri. Reliable simulation-driven design optimization of microwave structures using manifold mapping. *Progress In Electromagnetics Research B*, 26:361–382, 2010.

[66] S. Koziel and L. Leifsson. Generalised shape-preserving response prediction for accurate modelling of microwave structures. *IET Microwaves, Antennas Propagation*, 6(12):1332–1339, September 2012.

[67] S. Koziel and S. Ogurtsov. Multi-level design optimization of microwave structures with automated model fidelity adjustment. In *Microwave Symposium Digest (IMS), 2013 IEEE MTT-S International*, pages 1–3, June 2013.

[68] S. Koziel and S. Ogurtsov. Design optimisation of antennas using electromagnetic simulations and adaptive response correction technique. *IET Microwaves, Antennas Propagation*, 8(3):180–185, February 2014.

[69] S. Koziel and S. Ogurtsov. Multilevel microwave design optimization with automated model fidelity adjustment. *International Journal of RF and Microwave Computer-Aided Engineering*, 24(3):281–288, 2014.

[70] S. Koziel and S. Ogurtsov. *Surrogate-Based Optimization*, pages 13–24. Springer International Publishing, Cham, 2014.

[71] S. Koziel, S. Ogurtsov, Q. S. Cheng, and J. W. Bandler. Rapid electromagnetic-based microwave design optimisation exploiting shape-preserving response prediction and adjoint sensitivities. *IET Microwaves, Antennas Propagation*, 8(10):775–781, July 2014.

[72] S. Koziel, S. Ogurtsova, and L. Leifssona. Simulation-driven design of antennas using coarse-discretization electromagnetic models. *Procedia Computer Science*, 4(Complete):1252–1261, 2011.

[73] A. Lamecki, P. Kozakowski, and M. Mrozowski. Efficient implementation of the Cauchy method for automated CAD-model construction. *Microwave and Wireless Components Letters, IEEE*, 13(7):268 –270, Jul. 2003.

[74] A. Lamecki, P. Kozakowski, and M. Mrozowski. CAD-model construction based on adaptive radial basis functions interpolation technique. In *15th International Conference on Microwaves, Radar and Wireless Communications*, volume 3, pages 799–802 Vol.3, May 2004.

[75] A. Lamecki, P. Kozakowski, and M. Mrozowski. Fast extraction of coupling matrix for optimization and CAD tuning problems. In *Microwave Conference, 2004. 34th European*, volume 3, pages 1385–1388, Oct 2004.

[76] J. Lee and J. Kim. Efficient global optimization of analog circuits using predictive response surface models on discretized design space. *IEEE Design Test*, 33(5):16–27, Oct 2016.

[77] J. Lee and K. Sarabandi. Synthesizing microwave resonator filters. *IEEE Microwave Magazine*, 10(1):57–65, February 2009.

[78] L. Leifsson, S. Koziel, and E. Jonsson. *Wing Aerodynamic Shape Optimization by Space Mapping*, pages 319–332. Springer International Publishing, Cham, 2014.

[79] N. Leszczynska, L. Szydlowski, and M. Mrozowski. A novel synthesis technique for microwave bandpass filters with frequency-dependent couplings. *Progress In Electromagnetics Research*, 137:35–50, 2013.

[80] G. L. Matthaei and R. J. Forse. A note concerning the use of field solvers for the design of microstrip shunt capacitances in lowpass structures. *International Journal of Microwave and Millimeter-Wave Computer-Aided Engineering*, 5(5):352–358, 1995.

[81] J.-S. Park. Optimal latin-hypercube designs for computer experiments. *Journal of Statistical Planning and Inference*, 39(1):95 – 111, 1994.

[82] J. E. Rayas-Sanchez. EM-based optimization of microwave circuits using artificial neural networks: the state-of-the-art. *IEEE Transactions on Microwave Theory and Techniques*, 52(1):420–435, Jan 2004.

[83] T. Shen, H.-T. Hsu, K. A. Zaki, A. E. Atia, and T. G. Dolan. Full-wave design of canonical waveguide filters by optimization. *IEEE Transactions on Microwave Theory and Techniques*, 51(2):504–511, Feb 2003.

[84] R. V. Snyder. Practical aspects of microwave filter development. *IEEE Microwave Magazine*, 8(2):42–54, April 2007.

[85] D. Swanson and G. Macchiarella. Microwave filter design by synthesis and optimization. *IEEE Microwave Magazine*, 8(2):55–69, April 2007.

[86] W. Tang, Y. L. Chow, and K. F. Tsang. Different microstrip line discontinuities on a single field-based equivalent circuit model. *IEE Proceedings - Microwaves, Antennas and Propagation*, 151(3):256–262, June 2004.

[87] G. C. Temes and D. A. Calahan. Computer-aided network optimization the state-of-the-art. *Proceedings of the IEEE*, 55(11):1832–1863, Nov 1967.

[88] F. Wang and Q.-J. Zhang. Knowledge-based neural models for microwave design. *Microwave Theory and Techniques, IEEE Transactions on*, 45(12):2333 –2343, Dec. 1997.

[89] S. Wrigth and J. Nocedal. *Numerical Optimization*. Springer, 1999.

[90] B. Xia, Z. Ren, and C. S. Koh. Utilizing kriging surrogate models for multi-objective robust optimization of electromagnetic devices. *IEEE Transactions on Magnetics*, 50(2):693–696, Feb 2014.

[91] A. H. Zaabab, Q.-J. Zhang, and M. Nakhla. A neural network modeling approach to circuit optimization and statistical design. *IEEE Transactions on Microwave Theory and Techniques*, 43(6):1349–1358, Jun 1995.

[92] C. Zhang, F. Feng, V.-M.-R. Gongal-Reddy, Q. J. Zhang, and J. Bandler. Cognition-driven formulation of space mapping for equal-ripple optimization of microwave filters. *IEEE Trans. Microw. Theory Tech.*, 63(7):2154–2165, July 2015.

[93] J. Zhu, J. Bandler, N. Nikolova, and S. Koziel. Antenna optimization through space mapping. *Antennas and Propagation, IEEE Transactions on*, 55(3):651 –658, Mar. 2007.

Chapter 2

Zero-pole approach to computer aided design of In-line SIW filters with transmission zeros

Based on the publication:

A. Jedrzejewski, N. Leszczynska, L. Szydlowski, M. Mrozowski, *"Zero-pole approach to computer aided design of in-line SIW filters with transmission zeros,"* published in Progress In Electromagnetics Research, Vol. 131, pp. 517-533, 2012.

This chapter presents a fast technique for the automated design of pseudo-elliptic filters in in-line topology implemented in substrate integrated waveguide (SIW) technology. The proposed method is based on an optimization routine with cost function involving zeros and poles of scattering parameters. To realize transmission zeros in in-line topology, frequency-dependent couplings were used. Such dispersive couplings were implemented as shorted stubs. The design process starts with the generation of a suitable starting point. To this end, an approximation of SIW as a rectangular waveguide is used and a fast electromagnetic solver based on mode-matching technique is utilized (μWave Wizard). The next step is the optimization process of a filter in a full-wave 3D EM simulator Ansoft HFSS. To increase the speed of convergence, a built-in derivative calculation feature was used and zeros and poles and their derivatives with respect to design parameters were extracted using the vector fitting algorithm. Experimental validation of the method is demonstrated by a third-order filter with asymmetric response and a fifth-order filter with two transmission zeros in addition to an asymmetric response. The experimental results show good agreement between the simulated and measured data.

2.1 Introduction

Coupled-resonator microwave filters are an important area of microwave engineering, a field that has been developed over many years. Constant development in this area is motivated by stringent communication system requirements concerning mainly high out-of-band rejection levels. Such requirements can be satisfied by well-established methods, e.g., by using cross-couplings between non-adjacent resonators [8–10]. Cross-couplings may introduce real or imaginary transmission zeros which improve selectivity. The design methodologies of such filters are well described in the literature [16, 24, 31]. At an initial step one finds a low-frequency prototype assuming that the couplings between resonators are frequency-independent. However, using cross-coupled resonators is not the only way the transmission zeros can be introduced. In the last decade it has been demonstrated that in-line waveguide filters may exhibit generalized Chebyshev responses if the frequency-dependent couplings are used [5, 6, 23, 33, 36]. Such couplings allow for filter implementation in in-line topologies with sharp cut-off skirts and even with an asymmetric response.

Recently a new idea for microwave filter implementation was proposed. It is based on substrate integrated waveguide (SIW), which can be easily manufactured using a standard low-cost PCB process. Filters implemented in SIW technology have many advantages and their practical realizations have been presented in a number of articles [40] - [39]. In particular, one such an advantage is the possibility of achieving a higher quality factor and better selectivity in comparison to capabilities of planar circuits. However, the implementation of cross-couplings in SIW technology is often a challenge due to the fact that in most cases the cross-coupling has to be of the opposite sign to the main coupling. This requires modification of a top or bottom (or both) metallization layer which, in turn, can produce not negligible radiation effects. It is therefore tempting to use the simplest in-line topology and increase the selectivity by using similar frequency-dependent couplings as in waveguides. Especially shorted stubs proposed in [32, 38] are particularly attractive and simple to implement in SIW. Unfortunately, unless a filter is narrowband, in which case on may use the technique proposed in [5], there is no established way of designing in-line filters with frequency-dependent couplings other than through numerical simulations and full-wave optimization.

State-of-the art of full-wave numerical solvers offer a choice of built-in optimization algorithms including simplex, gradient and genetic algorithms. However, these built-in algorithms are not very flexible in terms of the goal function definitions and may converge very slowly. As a result, the full-wave design by optimization of filters may take a very long time. To mitigate the computational cost, hybrid algorithms [14]–[37] can be applied, they use both the full-wave and analytical models. The goal of these methodologies is to shorten the design cycle by using fast but less accurate empirical model to get the information about optimal parameters setting in the electromagnetic model. In that cases the full-wave analysis is used to verify if the solution meets design specifications. The analytic model is optimized to get the satisfactory solution. If the responses of both models are not the same the algorithm reduces the differences to align the empirical model with that of the full-wave one. The success of this approach depends on the availability and the quality of the surrogate model [29, 30].

For CAD of microwave filters one may use a hybrid technique employing analytical models based a lumped element equivalent circuit. The model is very often specified in a form of a coupling matrix. This approach has been proven to be very powerful [13]–[28] but its success depends on the process of extracting the coupling matrix from electromagnetic simulations. Unfortunately, this CAD methodology cannot be applied for the filters considered in this chapter, since all coupling matrix extraction schemes assume that the coupling coefficient is frequency-independent. In our case, the frequency dependence of the coupling is essential for implementing transmission zeros in the in-line configuration.

One should note that the optimization convergence depends also on the set starting point and cost function. In microwave CAD of passive devices one usually uses goal functions based on the scattering parameters evaluated at many [7, 12] or at a few frequency points [34]. Such goal functions, often specified in the form of a frequency mask, compare the desired level of S parameters in a prescribed frequency range with that obtained from the simulation.

For microwave filters with transmission zeros it is more beneficial to choose the frequency points in that goal function definition in such a way that S_{11} and S_{21} are evaluated only at band edges as well as at the transmission and reflection zeros [4, 11, 35]. Although, this approach has originally been used for filter prototype synthesis, it is also useful for full-wave optimization as simulations have to carried out at a very few frequency points, which results in shorter design cycle.

In [25] a new optimization technique, designed for CAD of microwave filters was proposed. In this method, the location zeros and poles of the reflection characteristics, rather than the values of S-parameters, are used to construct the goal function. It has been shown [27] that for this new type of goal functions, filters can be designed even if the initial design is very bad.

In this chapter we use the zero-pole approach proposed in [25] as a fast way of designing in-line SIW filters with transmission zeros using numerical full-wave optimization. The method allows for the realization of SIW filters with arbitrarily located transmission zeros. Each transmission zero is generated by a frequency-dependent coupling which is implemented by a stub. This stub is also responsible for the generation of the direct coupling between adjacent resonators. The optimization process is carried out on two levels: the starting point is generated using a rectangular waveguide model, and the final design is obtained by tuning the response in a 3D FEM solver. The design procedure is illustrated by two examples involving three and five-pole generalized Chebyshev filters.

2.2 Design Procedure

2.2.1 Preliminary Relations

For the general Chebyshev approximation of filters composed of N coupled resonators the transfer function $S_{21}(\omega)$ [22] is defined as

$$|S_{21}(\omega)| = \frac{1}{1 + \epsilon^2 F_N^2(\omega)} \tag{2.1}$$

where ϵ is a ripple constant related to the passband return loss, $F_N(s)$ represents a filtering function and ω is a real frequency variable. The filtering function can by defined as a rational function [26, 27], that is

$$F_N(s) = \frac{R_N(s)}{P_{Nz}(s)} \tag{2.2}$$

where $s = j\omega$ is a complex frequency variable. Transmission and reflection functions of any two-port filtering structure composed of a series of N coupled resonators may be expressed also as a polynomial [15]

$$S_{11}(s) = \frac{R_N(s)}{E_N(s)} \tag{2.3}$$

$$S_{21}(s) = \frac{P_{Nz}(s)}{\epsilon E_N(s)} \tag{2.4}$$

where $P_{Nz}(s)$, $R_N(s)$ and $E_N(s)$ are complex polynomials. S_{11} and S_{21} share the common denominator $E_N(s)$ which is of the Nth degree with N being the degree of filtering function. The polynomial $R_N(s)$ is also of the Nth degree and polynomial $P_{Nz}(s)$, which contains the transfer function transmission zeros, is of degree N_z where N_z is a number of finite-position transmission zeros. The roots of $E_N(s)$ and $R_N(s)$ correspond to the filter's reflections/transmission poles and reflection zeros, respectively.

Assume that P_i are roots of the denominator, Z_i are roots of the numerator of an ideal transfer function and R_i are the roots of the numerator of the reflection function. The cost function for design of microwave filters [25–27] is defined as follows

$$C = \sum_{i=1}^{M} |Z_i' - Z_i|^2 + \sum_{i=1}^{N} |P_i' - P_i|^2 + \sum_{i=1}^{N} |R_i' - R_i|^2 \tag{2.5}$$

where N is the number of poles and zeros of polynomials $R_N(s)$ and $E_N(s)$, and M is the number of prescribed transmission zeros. Z_i' and P_i' are the zeros and poles of the rational function approximation of S_{21} and R_i' are the zeros of the numerator of the rational function interpolating S_{11} for the filter being optimized.

To determine the position of Z_i', P_i' and R_i' from the transmission and reflection characteristics calculated by the full-wave analysis, we interpolate S_{11} and S_{21} using the vector fitting [21] procedure. In our technique the values of S_{11} and S_{21} are evaluated at a few frequency points, this guarantees good approximation of transmission and reflection functions, and is not time consuming. The minimum number of points which have to be provided is equal to 2N + 1, where N is the order of the filter.

2.2.2 Algorithm

The designing process starts with generation of a suitable starting point. To do this an SIW was initially modeled as a rectangular waveguide, and the whole filter was designed using this model, using the cost function presented in the previous section. We applied μWave Wizard [3] software, which is a very fast tool based on the mode-matching analysis. Moreover, this software has several built-in tools which facilitate the design of filters. For

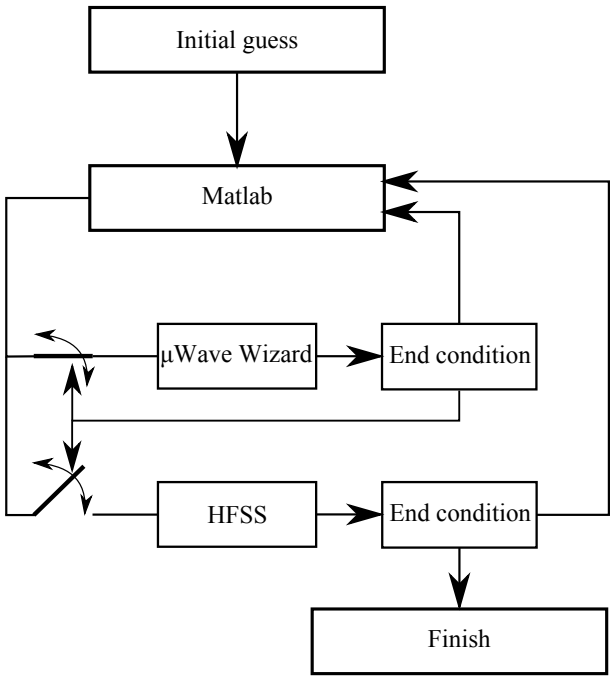

FIGURE 2.1: The optimization process.

generalized Chebyshev filters a fast optimizer based on the zero-pole approach [25] is provided as an add-on tool. The starting point for design of an in-line waveguide model with stubs was chosen at random within the range of possible dimensions for a given filter. The final solution obtained from μWaveWizard optimizer yields the initial values for a proper optimization of our target SIW structure.

Using this starting point, the SIW filter was optimized using a gradient-based Quadratic Programming method, available in the Matlab Optimization toolbox [2]. Full-wave simulations were carried-out in Ansoft HFSS v.13 [1]. We took the advantage of the fact that this electromagnetic solver has built-in tools for the calculation of first derivatives. This feature was used to compute the gradient of the cost function proposed in the previous section. At each optimization step the structure was analysed at 2N+1 frequency points in the desired passband, where the N is the order of the filter.

In the optimization procedure both μWaveWizard (for generating the starting point) and HFSS were invoked from the Matlab environment. As a result, the optimization procedure is fully automated. The tuning process is depicted in Fig. 2.1. It should be emphasized that the generation of the starting point using a waveguide model with initial dimensions selected at random takes much less time than one simulation in 3D EM simulator so it will not be considered.

2.3 Experimental verification

To verify the method outlined in the previous section two bandpass filters have been designed. Both filters have been fabricated on a Taconic RF-35 substrate which has a

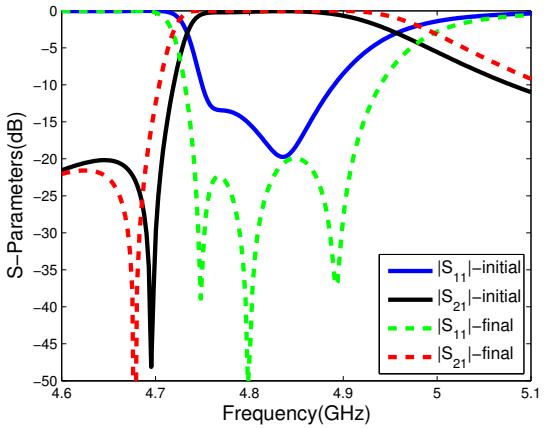

FIGURE 2.2: Scattering parameters for the initial dimensions (x_{str} in Table 2.1) and final dimensions (x_{opt} in Table 2.1) of a 3-pole generalized Chebyshev in-line SIW filter with one transmission zero.

relative dielectric constant equal to 3.5 and thickness of 0.762 mm. A standard low cost PCB process was used to manufacture both circuits. All metallized vias have the same diameter equal to 1 mm and spacing between their centres is equal to 1.5 mm.

2.3.1 Third order in-line SIW filter with one transmission zero

The first example is an in-line third order filter centred at $f_0 = 4.825$ GHz with the bandwidth equal to 150 MHz. The filter has 20 dB return loss and one transmission zero placed on the lower side of the passband at f_z=4.678 GHz. The filter consists of three directly connected resonator cavities with a frequency-dependent coupling placed between the first and second resonator. The dispersive coupling is implemented via a shorted stub and controls both the proper value of the coupling coefficient at the midband frequency and the position of the transmission zero.

The initial filter response is depicted in Fig. 2.2. It can be observed that the return

TABLE 2.1: Results of the optimization of a third order in-line SIW filter with one transmission zero (the starting point is denoted by x_{str} and is given in the second and fifth column, the final dimensions, denoted as x_{opt} are given in the third and sixth column).

x	x_{str}	x_{opt}	x	x_{str}	x_{opt}
L_1	4.903	4.495	w_1	11.807	13.889
L_2	26.574	28.371	w_2	7.478	9.733
L_3	6.418	6.011	w_3	7.478	9.733
L_4	19.780	20.859	w_4	10.807	12.955
tap_l	11.869	12.550	tap_w	5.150	4.700

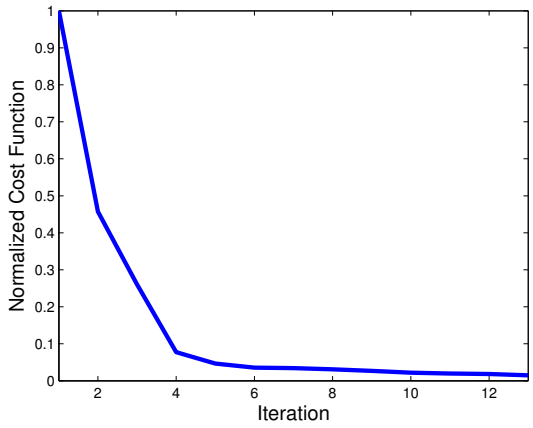

FIGURE 2.3: Convergence of the optimization routine for a 3-pole generalized Chebyshev filter with one transmission zero.

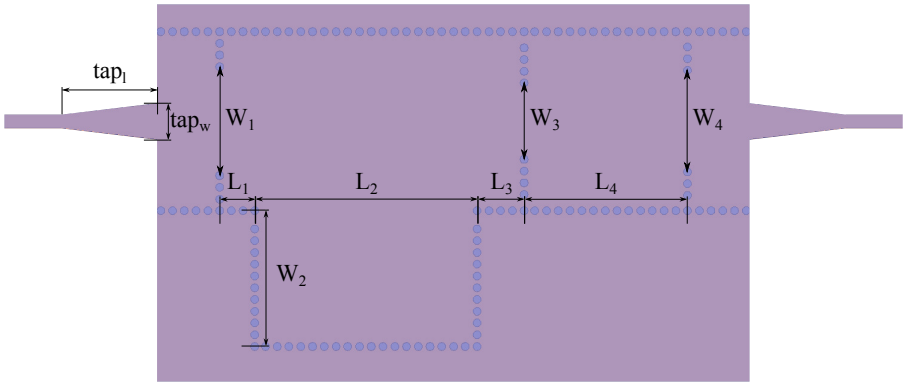

FIGURE 2.4: Layout of an in-line 3-pole generalized Chebyshev filter with one transmission zero using SIW technology. Cavity and coupling dimensions are measured from centre to centre of vias.

loss has been degraded to the level of 13 dB in the worst case. Additionally, it can be seen that the transmission zero has been moved up by 16.5 MHz in comparison with the desired position. However, such initially dimensioned SIW component, obtained using zero-pole optimization of a rectangular waveguide model is a good starting point for further tuning with a 3D FEM solver.

For a full-wave tuning step ten independent variables were chosen for the zero-pole optimization routine. To obtain the results satisfying specifications, only thirteen iterations were needed. The final filter characteristics and convergence profile are presented in Fig. 2.2 and Fig. 2.3, respectively. The set of initial values x_{str} and the final solutions x_{opt} are presented in Table 2.1 (all dimensions in millimetres).

The layout of the proposed filter is shown in Fig. 2.4. At a first sight it looks as if the filter consisted of two resonators. In fact, the left-hand side of the filter (a SIW

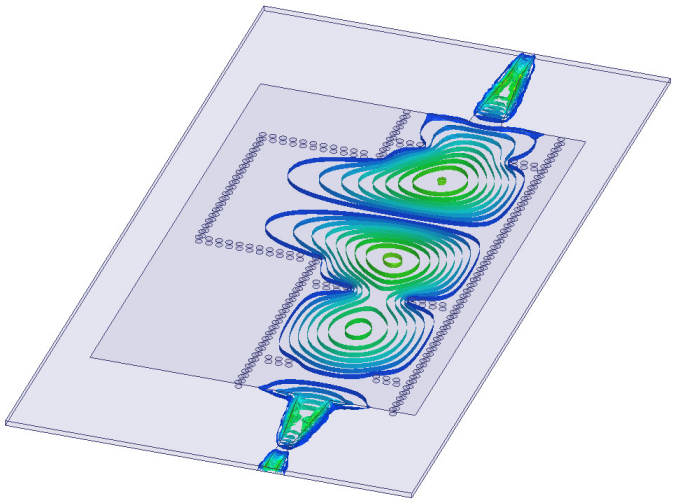

FIGURE 2.5: Electric field distribution of an in-line 3-pole generalized Chebyshev filter with one transmission zero using SIW technology at centre frequency.

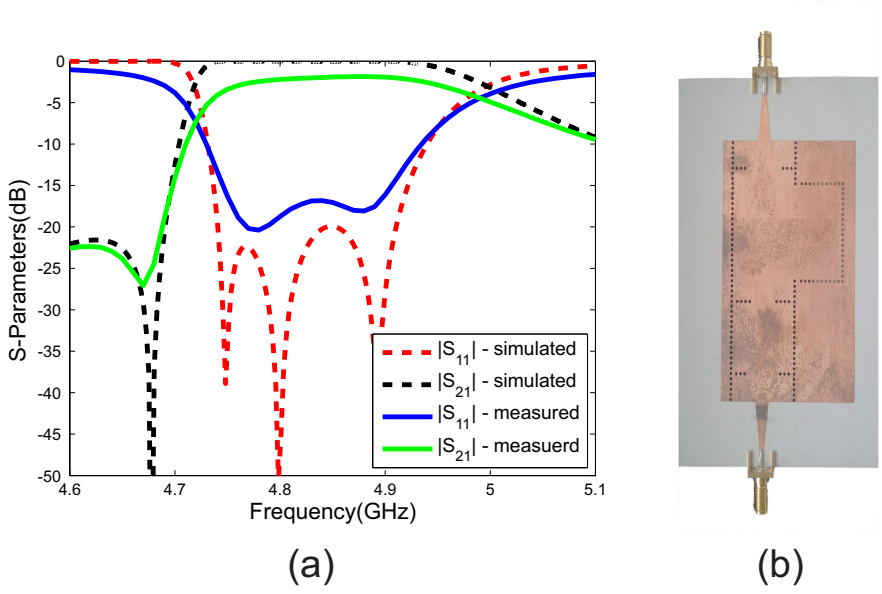

FIGURE 2.6: a) Measured (solid) and simulated (dashed) response of the a 3% FBW 3-pole generalized Chebyshev in-line SIW filter with one transmission zero, b) photo of the fabricated filter.

section with a stub) consists of two cavities which are produced by loading the long SIW waveguide section with the impedance of the stub (approximately in a mid-point between irises w_1 and w_3). To prove this, the E-field distribution at the centre frequency is presented in Fig. 2.5. Three resonances, similar to the ones which can be expected in the in-line filter are clearly visible. The comparison between the measured component and the ideal characteristics are presented in Fig. 2.6. As can be seen, the filter return loss performance has been degraded to approximately 17 dB, which is still a satisfactory

result. The filter band has been slightly narrowed. All mentioned effects are mainly caused by fabrication errors which lead to detuning of the resonators. The transmission zero is placed at the desired frequency, which ensures the assumed out-of-band rejection level. The filter insertion loss (IL) is at the 2.3 dB level. Such value of IL is the effect of losses included in the dielectric substrate and finite conductivity of the top and bottom metallization layers as well as low quality of via holes metallization. All these elements strongly influence unloaded quality factors of the resonators. Nevertheless, the measured characteristics are acceptable.

2.3.2 Fifth order in-line SIW filter with two transmission zeros

The second example is an in-line fifth order filter centred at f_0 =4.95 GHz with the bandwidth equal to 300 MHz. The filter has a 20 dB return loss level and two transmission zeros located at the lower and upper sides of the passband at f_{z1} = 4.7 GHz and f_{z2} = 5.14 GHz. The filter consists of five directly connected resonant cavities with frequency-dependent couplings placed between the first and second resonator, and the fourth and fifth. Similarly as in previous case the dispersive couplings were implemented as shorted stubs.

The initial filter response, obtained by optimizing a waveguide model, is shown in Fig. 2.7. It can be observed that the filter bandwidth, as well as the return loss level, are different from the assumed values. The return loss level has been degraded to the level of 2 dB in the worst case. The transmission zero placed on the upper side of the passband has moved up by about 30 MHz. The second transmission zero has been shifted up by 10 MHz.

In this example fifteen independent variables were chosen for the optimization routine. To achieve characteristics satisfying the specifications twenty nine iterations were needed. The design is completely automated and takes about 6 hours of a CPU time on a work-

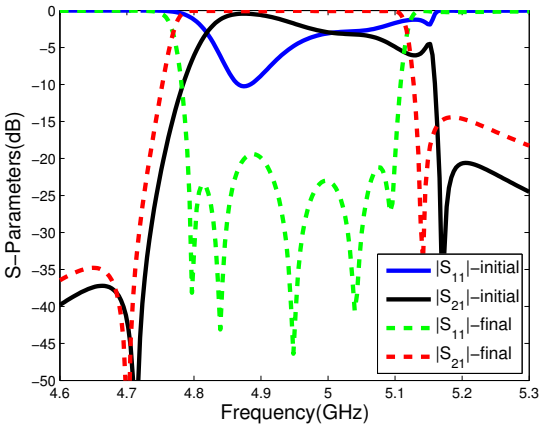

FIGURE 2.7: Scattering parameters for the initial dimensions (x_{str} in Table 2.2) and final dimensions (x_{opt} in Table 2.2) of a 5-pole generalized Chebyshev in-line SIW filter with two transmission zeros.

TABLE 2.2: Result of the optimization for the fifth order in-line SIW filter with two transmission zeros (the starting point is denoted by x_{str} and is given in the second and fifth column, the final dimensions, denoted as x_{opt} are given in the third and sixth column).

x	x_{str}	x_{opt}	x	x_{str}	x_{opt}
L_1	9.162	9.536	w_1	14.838	15.795
L_2	20.174	18.049	w_2	19.585	30.089
L_3	13.293	15.196	w_3	9.645	10.173
L_4	20.866	21.514	w_4	9.390	9.782
L_5	2.382	3.071	w_5	16.344	16.605
L_6	31.828	30.525	w_6	14.403	14.993
L_7	1.802	1.301			
tap_w	5.150	5.150	tap_l	11.869	11.869

station. In the near future this time will be further significantly reduced by applying an in-house 3D FEM solver with GPU accelaration [17–20]. The final filter characteristics and convergence profile are presented in Fig. 2.7 and Fig. 2.12, respectively. The set of starting values x_{str} and the final solutions x_{opt} are presented in Table 2.2 (all dimensions in millimetres). The layout of the proposed filter is shown in Fig. 2.8. The field distribution shown in Fig. 2.9 clearly shows five electrical resonators generating five poles which clearly demonstrates that stubs load long sections in the middle and act as zero-generating elements.

Fig. 2.10 presents a comparison between the measured and simulated scattering parameters of the fabricated filter. As can be seen, the filter return loss performance has been degraded to approximately 15 dB and the filter passband has been narrowed by 40 MHz. Nevertheless, the return loss performance is still acceptable. Both transmission

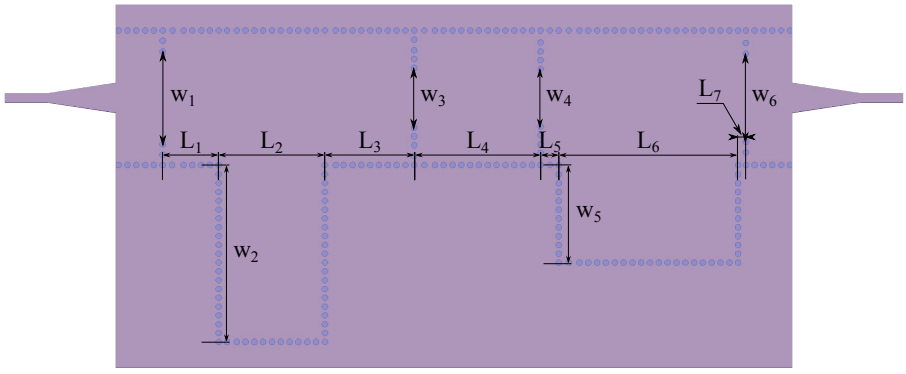

FIGURE 2.8: Layout of an in-line 5-pole generalized Chebyshev filter with one transmission zeros using SIW technology. Cavity and coupling dimensions are measured from centre to centre of vias.

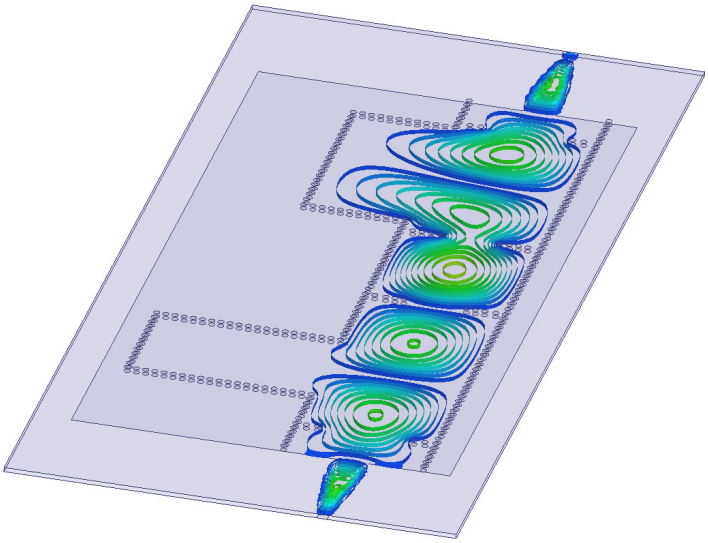

FIGURE 2.9: Electric field distribution in an in-line 5-pole generalized Chebyshev filter with two transmission zeros using SIW technology at centre frequency.

zeros are clearly observed on the left and right sides of the passband. Each of them has been moved down by about 30 MHz from their designed frequencies. The filter in-band insertion loss level is approximately equal to 2.3 dB. As in a previous example, it is caused by the dielectric losses and poor metallization of via-holes.

As can be seen, measurements of both filters are in relatively good agreement with

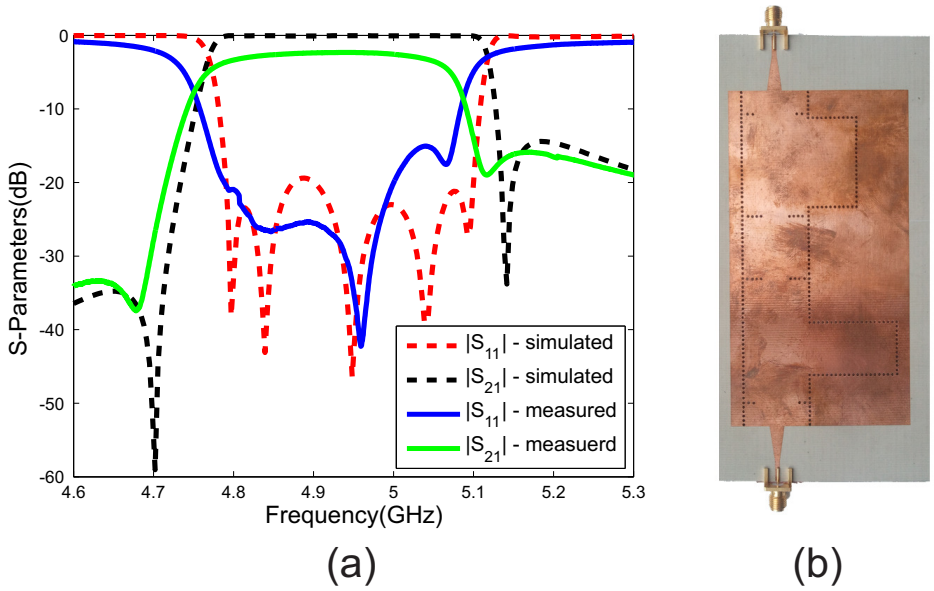

FIGURE 2.10: a) Measured (solid) and simulated (dashed) response of a 6% FBW in-line 5-pole SIW filter with two transmission zeros, b) photo of the fabricated filter.

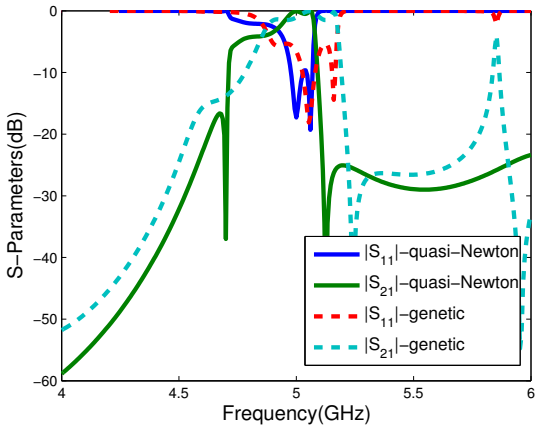

FIGURE 2.11: Final solutions delivered by the quasi-Newton (solid) and genetic (dashed) algorithm of a 6% FBW in-line 5-pole SIW filter with two transmission zeros.

the simulated results. In both examples the insertion loss level is around 2.3 dB which is mainly produced through low quality of the fabrication process. Nevertheless, the presented examples validate the proposed design algorithm.

For comparison, a built-in optimizer available in HFSS was tested to optimize the same filter. From a few available algorithms the quasi-Newton and genetic algorithms were chosen. Three different cost functions were tested with these algorithms.

In the simplest and most common case the cost function was declared as a frequency mask 1.12. For specific frequency ranges the conditions for the reflection and transmission parameters were assumed, e.g. in the passband the reflection coefficient should achieve level less than or equal to -20 dB. The convergence of the quasi-Newton algorithm is

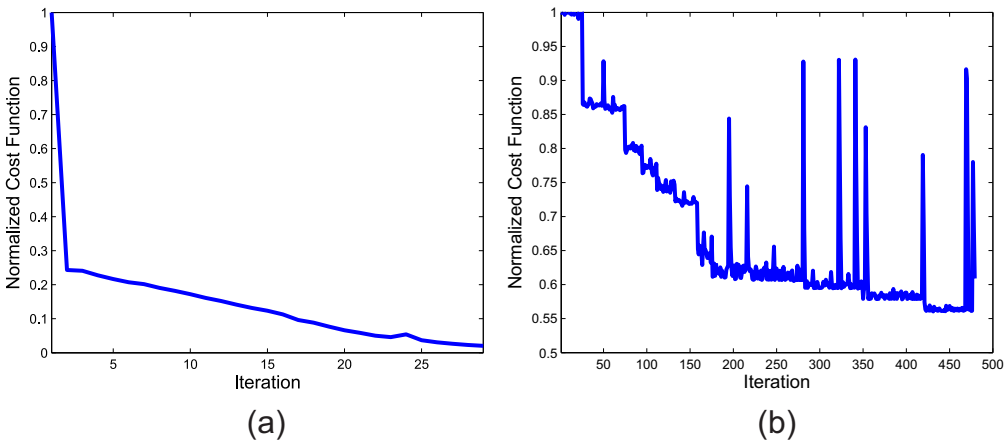

FIGURE 2.12: Convergence of the optimization routine for a 5-pole in-line SIW filter with two transmission zeros (a) zero-pole cost function, b) quasi-Newton using a traditional cost function available in HFSS).

presented in Fig. 2.12. After about 200 iterations stagnation can be observed.

2.4 Conclusions

Computer aided design of pseudo-elliptic in-line SIW bandpass filters with frequency-dependent couplings based on the zero-pole optimization technique has been presented. The application of the proposed procedure was demonstrated through the design of a new type in-line substrate integrated waveguide (SIW) filters with arbitrary placed transmission zeros. The initial dimensions of the designed structures were obtained using μWave Wizard, a full-wave simulator designed for the optimization of microwave structures. The HFSS software was subsequently applied to achieve the final response of the filters. Both tools have been integrated via Matlab software, in which the zero-pole extraction and optimization method were implemented. The numerical tests showed that to design the 3rd and 5th order filters fewer than twenty and thirty iterations were required, respectively. The comparison with traditional goal function based of frequency mask have been shown. Measured characteristics of the presented examples validate both the concept of new pseudo-elliptic in-line SIW filters and the proposed design procedure.

Acknowledgment

This work has been carried out within the framework of the COST IC0803 RFCSET project and supported by the Polish Ministry of Science and Higher Education under Contract COST IC0803 618/N-COST/09/2010.

References

[1] High Frequency Structure Simulator (HFSS).

[2] Matlab.

[3] μWave Wizard.

[4] S. Amari. Synthesis of cross-coupled resonator filters using an analytical gradient-based optimization technique. *IEEE Transactions on Microwave Theory and Techniques*, 48(9):1559–1564, Sep 2000.

[5] S. Amari and J. Bornemann. Using frequency-dependent coupling to generate finite attenuation poles in direct-coupled resonator bandpass filters. *IEEE Microwave and Guided Wave Letters*, 9(10):404–406, Oct 1999.

[6] S. Amari, J. Bornemann, W. Menzel, and F. Alessandri. Diplexer design using pre-synthesized waveguide filters with strongly dispersive inverters. In *Microwave Symposium Digest, 2001 IEEE MTT-S International*, volume 3, pages 1627–1630 vol.3, May 2001.

[7] F. Arndt, J. Brandt, V. Catina, J. Ritter, I. Rullhusen, J. Dauelsberg, U. Hilgefort, and W. Wessel. Fast CAD and optimization of waveguide components and aperture antennas by hybrid MM/FE/MoM/FD methods-state-of-the-art and recent advances. *IEEE Transactions on Microwave Theory and Techniques*, 52(1):292–305, Jan 2004.

[8] A. Atia, A. Williams, and R. Newcomb. Narrow-band multiple-coupled cavity synthesis. *IEEE Transactions on Circuits and Systems*, 21(5):649–655, Sep 1974.

[9] A. E. Atia and A. E. Williams. New type of waveguide bandpass filters for satellite transponders. *COMSAT Technical Review*, 1(1):21–43, 1971.

[10] A. E. Atia and A. E. Williams. Narrow-bandpass waveguide filters. *IEEE Transactions on Microwave Theory and Techniques*, 20(4):258–265, Apr 1972.

[11] W. A. Atia, K. A. Zaki, and A. E. Atia. Synthesis of general topology multiple coupled resonator filters by optimization. In *Microwave Symposium Digest, 1998 IEEE MTT-S International*, volume 2, pages 821–824 vol.2, June 1998.

[12] J. W. Bandler, R. M. Biernacki, S. H. Chen, D. G. Swanson, and S. Ye. Microstrip filter design using direct em field simulation. *IEEE Transactions on Microwave Theory and Techniques*, 42(7):1353–1359, Jul 1994.

[13] S. Bila, D. Baillargeat, M. Aubourg, S. Verdeyme, P. Guillon, F. Seyfert, J. Grimm, L. Baratchart, C. Zanchi, and J. Sombrin. Direct electromagnetic optimization of microwave filters. *IEEE Microwave Magazine*, 2(1):46–51, Mar 2001.

[14] S. Bila, D. Baillargeat, S. Verdeyme, and P. Guillon. Automated design of microwave devices using full EM optimization method. In *Microwave Symposium Digest, 1998 IEEE MTT-S International*, volume 3, pages 1771–1774 vol.3, June 1998.

[15] R. J. Cameron. General coupling matrix synthesis methods for chebyshev filtering functions. *IEEE Transactions on Microwave Theory and Techniques*, 47(4):433–442, Apr 1999.

[16] R. J. Cameron. Advanced coupling matrix synthesis techniques for microwave filters. *IEEE Transactions on Microwave Theory and Techniques*, 51(1):1–10, Jan 2003.

[17] A. Dziekonski, A. Lamecki, and M. Mrozowski. GPU acceleration of multilevel solvers for analysis of microwave components with finite element method. *IEEE Microwave and Wireless Components Letters*, 21(1):1–3, Jan 2011.

[18] A. Dziekonski, A. Lamecki, and M. Mrozowski. A memory efficient and fast sparse matrix vector product on a GPU. *Progress In Electromagnetics Research*, 116:49–63, 2011.

[19] A. Dziekonski, A. Lamecki, and M. Mrozowski. Tuning a hybrid GPU-CPU V-cycle multilevel preconditioner for solving large real and complex systems of FEM equations. *IEEE Antennas and Wireless Propagation Letters*, 10:619–622, 2011.

[20] A. Dziekonski, P. Sypek, A. Lamecki, and M. Mrozowski. Finite element matrix generation on a GPU. *Progress In Electromagnetics Research*, 128:249–265, 2012.

[21] B. Gustavsen and A. Semlyen. Rational approximation of frequency domain responses by vector fitting. *IEEE Transactions on Power Delivery*, 14(3):1052–1061, Jul 1999.

[22] M. L. J-S. Hong. *Microstrip Filters for RF/Microwave Application*. John Wiley and Sons, 2001.

[23] P. Kozakowski, A. Lamecki, M. Mongiardo, M. Mrozowski, and C. Tomassoni. Computer-aided design of in-line resonator filters with multiple elliptical apertures. In *Microwave Symposium Digest, 2004 IEEE MTT-S International*, volume 2, pages 611–614 Vol.2, June 2004.

[24] P. Kozakowski, A. Lamecki, P. Sypek, and M. Mrozowski. Eigenvalue approach to synthesis of prototype filters with source/load coupling. *IEEE Microwave and Wireless Components Letters*, 15(2):98–100, Feb 2005.

[25] P. Kozakowski and M. Mrozowski. Automated CAD of coupled resonator filters. *IEEE Microwave and Wireless Components Letters*, 12(12):470–472, Dec 2002.

[26] P. Kozakowski and M. Mrozowski. Automated synthesis of coupled resonator filters with a given topology. In *Microwaves, Radar and Wireless Communications, 2002. MIKON-2002. 14th International Conference on*, volume 2, pages 373–376 vol.2, 2002.

[27] P. Kozakowski and M. Mrozowski. New approach to fast full wave optimization of microwave filters. In *Microwave Conference, 2002. 32nd European*, pages 1–4, Sept 2002.

[28] P. Kozakowski and M. Mrozowski. Quadratic programming approach to coupled resonator filter CAD. *IEEE Transactions on Microwave Theory and Techniques*, 54(11):3906–3913, Nov 2006.

[29] S. Koziel and J. W. Bandler. Coarse and surrogate model assessment for engineering design optimization with space mapping. In *2007 IEEE/MTT-S International Microwave Symposium*, pages 107–110, June 2007.

[30] S. Koziel and J. W. Bandler. Space-mapping optimization with adaptive surrogate model. *IEEE Transactions on Microwave Theory and Techniques*, 55(3):541–547, March 2007.

[31] A. Lamecki, P. Kozakowski, and M. Mrozowski. Fast synthesis of coupled-resonator filters. *IEEE Microwave and Wireless Components Letters*, 14(4):174–176, April 2004.

[32] R. Liu, Q. Wang, and H. Li. Post waveguide filters with compact shorting stubs. In *Circuits and Systems for Communications, 2008. ICCSC 2008. 4th IEEE International Conference on*, pages 323–325, May 2008.

[33] U. Rosenberg, S. Amari, and F. Seyfert. Pseudo-elliptic direct-coupled resonator filters based on transmission-zero-generating irises. In *Microwave Conference (EuMC), 2010 European*, pages 962–965, Sept 2010.

[34] T. Shen, H.-T. Hsu, K. A. Zaki, A. E. Atia, and T. G. Dolan. Full-wave design of canonical waveguide filters by optimization. *IEEE Transactions on Microwave Theory and Techniques*, 51(2):504–511, Feb 2003.

[35] H. L. Thal. Design of microwave filters with arbitrary responses. *International Journal of Microwave and Millimeter-Wave Computer-Aided Engineering*, 7(3):208–221, 1997.

[36] F. M. Vanin, E. J. Wollack, K. Zaki, and D. Schmitt. Polarization-preserving quadruple-ridge waveguide filter and four-fold symmetric transformer. In *2006 IEEE MTT-S International Microwave Symposium Digest*, pages 127–130, June 2006.

[37] F. Wang and Q.-J. Zhang. Knowledge-based neural models for microwave design. *IEEE Transactions on Microwave Theory and Techniques*, 45(12):2333–2343, Dec 1997.

[38] D. Zelenchuk and V. Fusco. Low insertion loss substrate integrated waveguide quasi-elliptic filters for V-band wireless personal area network applications. *IET Microwaves, Antennas Propagation*, 5(8):921–927, June 2011.

[39] X. Zhang, Z. Yu, and J. Xu. Novel band-pass substrate integrated waveguide (SIW) filter based on complementary split ring resonators (CSRRS). *Progress In Electromagnetics Research*, 72:39–46, 2007.

[40] Z. Zhang, Y. Fan, Y. Cheng, and Y. Zhang. A compact multilayer dual-mode substrate integrated circular cavity (SICC) filter for X-band application. *Progress In Electromagnetics Research*, 122:453–465, 2012.

Chapter 3

Automated Design of Linear Phase Filters

Based on the publication:

N. Leszczynska, L. Szydlowski, M. Mrozowski, *"Automated Design of Linear Phase Filters,"* published in proceedings of Microwaves, Radar, and Wireless Communication (MIKON), 2014 20th International Conference on, pp. 1-4, 2014.

This chapter presents a fast technique for an automated design of microwave filters with linear phase. The proposed method exploits the cost function defined using the location of complex zeros and poles of the filter's transfer and reflection function. The effectiveness of the proposed technique is presented with two illustrative examples.

3.1 Introduction

Microwave filters used in satellites and terrestrial communication systems have to satisfy severe requirements concerning mainly high out-of-band rejection, low insertion loss and/or equalized group delay. Synthesis techniques [10] are used to design microwave filters, however they can yield only an approximate solution which needs subsequent numerical tuning to meet design specification. Final designs can only be obtained through an optimization process involving full-wave simulators.

Optimization can involve various cost functions. The standard cost functions are functions based on the scattering parameters computed at many frequency points [3, 4]. When the filter to be designed has to show a flat group delay response, the cost function is modified to include the terms responsible for a linear phase. Since the full-wave electromagnetic simulation is the most time-consuming step in the process of the filter design, the challenge is to reduce the number of required electromagnetic simulations.

Recently we have proposed a cost function based on the zeros and poles [9] of a rational function model of scattering parameters. This function is suitable for all types

of pseudoelliptic responses including linear phase filters. An additional advantage is that the number of frequency points at which the structure is evaluated can be very low, as a very efficient vector fitting [6] or Cauchy interpolation [8] algorithms can be used to extract zeros and poles from very sparsely sampled frequency characteristics. Moreover, the technique seems to be immune to the choice of the starting point for the optimization and consequently it allows one to find the filter parameters without any prior synthesis. In fact, the starting point for the optimization can be vary far from the optimal solution, and yet the number of iterations required by the optimization procedure to converge is very small. The proposed method was tested on two illustrative examples of bandpass filters with linear phase that confirmed the effectiveness and robustness of the proposed approach.

3.2 Theory

Typically, the cost functions for the direct optimization are based on scattering parameters [3, 4]. In the standard approach used in computed aided design, the goal function is defined by comparing the elements of the scattering parameters computed at a number of arbitrarily selected frequency points with the desired response. For the filters with equalized group delay the goal function consist of three components: the reflection and transmission characteristics and the phase of the transmission characteristics of the filter:

$$E = \sum_{i=1}^{A} |S'_{11}(i) - S_{11}(i)|^2 + \sum_{i=1}^{A} |S'_{21}(i) - S_{21}(i)|^2 + \sum_{i=1}^{A} |phase(S'_{21})(i) - phase(S_{21})(i)|^2 \tag{3.1}$$

where the S_{11}, S_{21} and $phase(S_{21})$ are the desired filter response at A frequency points and S'_{11}, S'_{21} and $phase(S'_{21})$ are the parameters obtained from simulation. One drawback of the above goal function is that the number of frequency points (A) may be large, often as many as a few hundred points are required. As a result, the full-wave design-by-optimization of microwave structures may take a very long time. For complex problems, this type of approach may be completely impractical. Moreover, the optimization process often fails to converge if the starting solution is far from the design specification.

In our approach, we use, for optimization of linear phase filters, a cost function based on the zeros and poles of rational functions approximating the scattering parameters. This definition of the cost function, combined with a gradient based optimization technique, was proposed in [9] and has been shown to give very good results in filter design [7, 9] but its performance for linear phase filters has not been examined so far. The filter design is based on the direct analysis of the locations of zeros and poles in the filter's transfer and reflection function. Broadly speaking, the goal function employed in the optimization process is expressed in terms of the difference between the current locations of the zeros Z'_i, P'_i and poles R'_i of the scattering parameters obtained from the simulated response, and the reference zeros Z_i, R_i and reference poles P_i:

$$C = \sum_{i=1}^{M} |Z_i' - Z_i|^2 + \sum_{i=1}^{N} |P_i' - P_i|^2 + \sum_{i=1}^{N} |R_i' - R_i|^2 \tag{3.2}$$

where N is the number of poles and zeros of the ideal reflection function, and M is the number of prescribed transmission zeros. To determine the position of Z_i', P_i', and R_i' from the transmission and reflection characteristics calculated by the full-wave analysis, we interpolate S_{11} and S_{21} using the vector-fitting [6] procedure or Cauchy interpolation [8]. The reference location of the zeros and poles of the scattering parameters are found analytically from a lumped element model [5]. Such definition of cost function does not need to include phase of filter because the phase characteristic is shaped by real or complex transmission zeros and all transmission zeros are included in the definition of cost function. The filter is simulated only at $2N + 1$ frequency points in the frequency band, where N is the filter order. This significantly reduces the time taken up by electromagnetic simulation, and consequently decreases the duration of the optimization process.

3.3 Results

To illustrate the validity of the concept outlined in the previous section two linear phase bandpass filters were designed using both the goal function based on locations of zeros and poles of filter's transfer and reflection characteristics (3.2) and the traditional goal function given by (3.1). Both filters were optimized using a gradient based Quadratic Programing method, available in Matlab [1] environment, using either the cost function (3.1) or a zero-pole goal function (3.2). The starting point for both filters were chosen arbitrarily within the range of possible dimension for given topology.

3.3.1 Fourth-Order Waveguide Linear Phase Filter

The first example is fourth-order linear phase filter centered at $f_0 = 5$ GHz with the bandwidth equal to 100 MHz. The filter has a 20 dB return loss level and a pair of real transmission zeros introduced to ensure linear phase (their locations are $1.55 + \mathrm{j}5 \cdot 10^9$ and

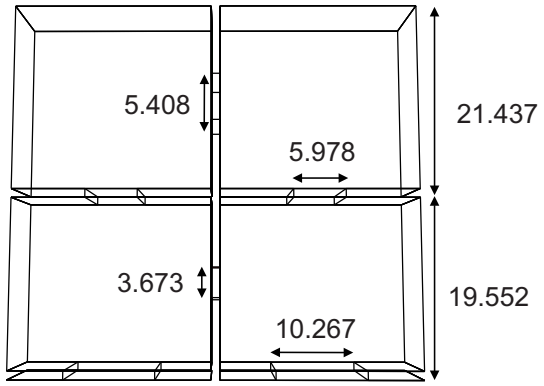

FIGURE 3.1: Fourth-order filter with linear phase with imposed dimensions (units: mm).

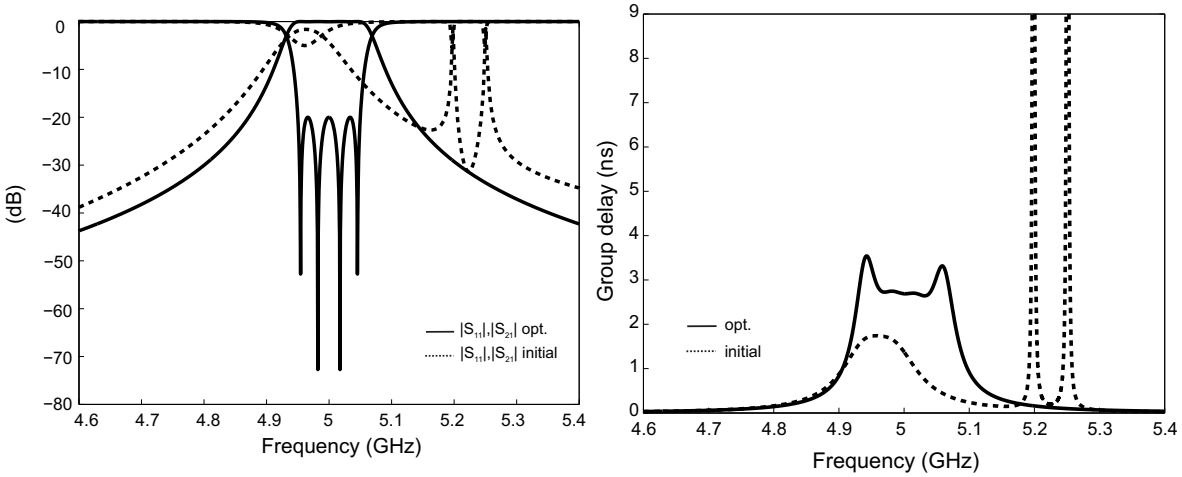

(a) Result of the optimization for the fourth-order filter.

(b) Group delay response of the fourth-order filter.

FIGURE 3.2: Dashed line - random starting point, solid line - after optimization.

-1.55 - j5$\cdot 10^9$). The filter is composed of four rectangular cavities loaded with a dielectric, and involves three direct couplings and one cross coupling between the first and fourth cavity – see Fig. 3.1. Making the cross and one direct coupling dispersive gives additional design flexibility. The dielectric constant is equal 3.47. The filter was simulated in the μWave Wizard [2] software, which is a very fast tool based on mode-matching analysis. In the optimization procedure μWave Wizard was invoked from the Matlab environment.

The starting point for this filter was chosen at random. At each iteration the structure was analysed at 7 frequency points in the passband and a few frequency points outside the passband for zero-pole optimization. During traditional optimization the filter was analysed at 25 frequency points spread evenly between 4.8 and 5.4 GHz. Six variables

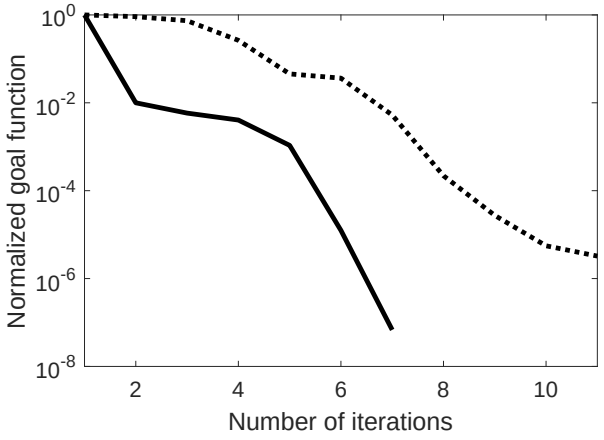

FIGURE 3.3: Convergence of the optimization routine for a fourth-order filter. Dashed line - classical goal function, solid line - zero-pole goal function.

were optimized simultaneously. The characteristics for the starting point are presented in Fig. 3.2a. It can be observed that the response does not meet the design specification and is far from the typical filter characteristic. To obtain results that satisfy the requirements 11 iterations of the cost function (3.1) and 7 iterations of our zero-pole algorithm were needed. The transmission zeros meet the desired specification (Fig. 3.2b). It is clearly seen that both cost functions give convergence to the correct characteristics, however the zero-pole goal function is slightly faster (Fig. 3.3). Both cost function are presented in the same measure in order to be able to compare both curves. The zero-pole goal function values were recalculated to the classical goal function measure.

3.3.2 Waveguide Linear Phase Filter With Frequency-Dependent Couplings

The second example is more challenging, it is a fifth-order filter with frequency-dependent couplings and linear phase proposed in [11]. This filter consists of a triplet (with one strongly dispersive cross-coupling) that is further directly connected (also via dispersive couplings) to two resonators placed at the input and output – Fig. 3.4. Due to the dispersive couplings, the circuit provides four transmission zeros - a complex pair and two imaginary ones. The proposed filter was centered at f_0=9.98 GHz with a fractional bandwidth of 320 MHz. The positions of the imaginary transmission zeros were f_{z1}= 9.66 GHz and f_{z2}=10.3 GHz. The complex zeros are located at 1.5+j9.98 $\cdot$ 10^9 and -1.5+j9.98 $\cdot$ 10^9. The filter was designed with our in-house 3D FEM solver, during the optimization process it was invoked from Matlab.

Again the starting point for this filter was chosen within the range of possible dimension for given topology. At each iteration the structure was analysed at 11 frequency points in the passband for zero-pole goal function and a few frequency points outside the passband. Using the cost function (3.1) the filter was analysed at 50 frequency points spread evenly between 9.5 and 10.5 GHz. Fifteen variables were optimized simultaneously. Fig. 3.5a presents the initial filter response, as can be seen it is far from the desired

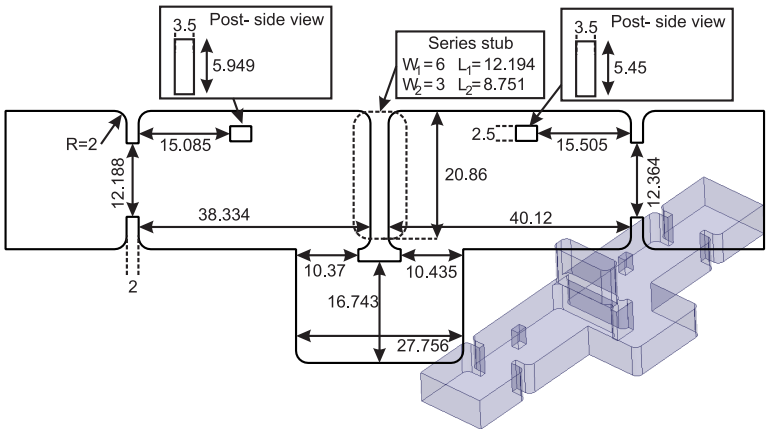

FIGURE 3.4: Top view of the fifth-order filter layout with imposed dimensions (units: mm). Perspective view shown in the inset. [11]

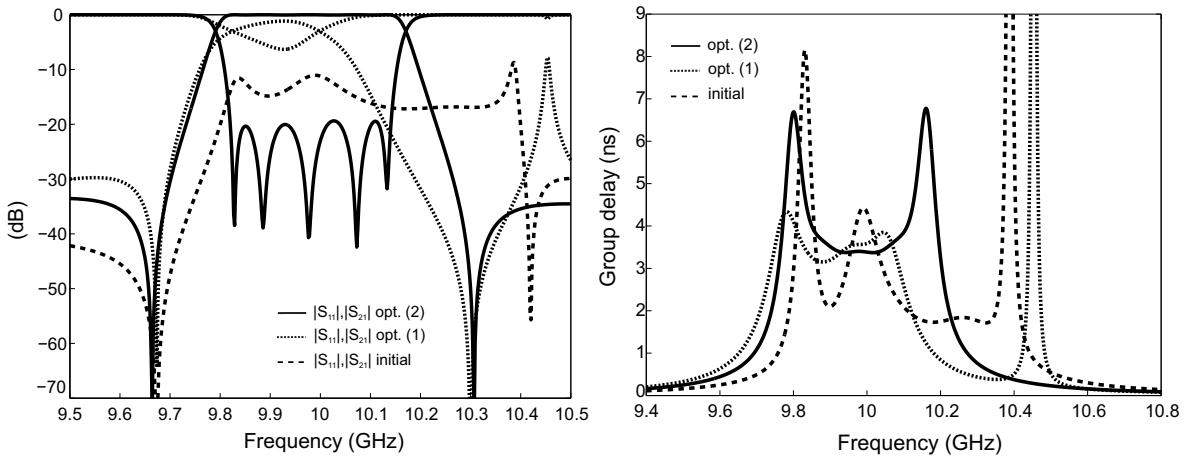

(a) Initial and final solutions of filter.

(b) Group delay responses.

FIGURE 3.5: Result of the optimization for the fifth-order filter. Dashed line - random starting point, solid line - after optimization using (3.2), dotted line - after optimizatiom using (3.1).

one, the reflection characteristic is totally degraded. Despite this poor starting point just ten iterations of our zero-pole algorithm were needed to obtain satisfactory result. The complex pair of transmission zeros meets the desired specification, as can be seen from the flat group-delay characteristics in the passband (Fig. 3.5b). Unlike zero-pole optimization, the optimization process using cost function (3.1) algorithm failed to converge in 37 iterations - Fig. 3.6. Fig. 3.5a shows the final filter response for both cost functions. Since the traditional optimization was unsuccessful, we decided to repeat the test beginning from a starting point that was very close to the desired response. In this case both simulations converged. The zero-pole goal function convergence was very fast, only 5 iterations were needed to obtain a satisfactory result. The algorithm involving goal

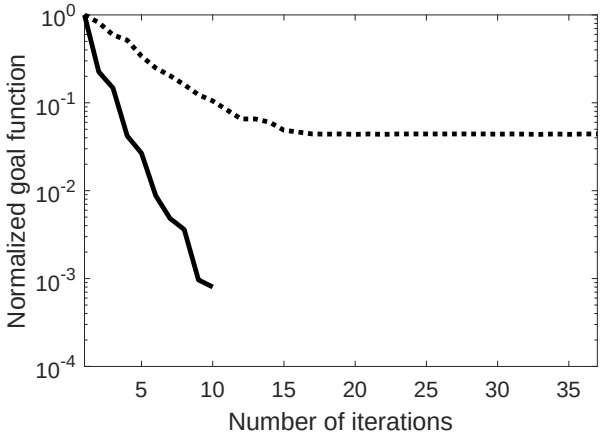

FIGURE 3.6: Convergence of the optimization routine for a fifth-order filter for the first starting point. Dashed line - classical goal function, solid line - zero-pole goal function.

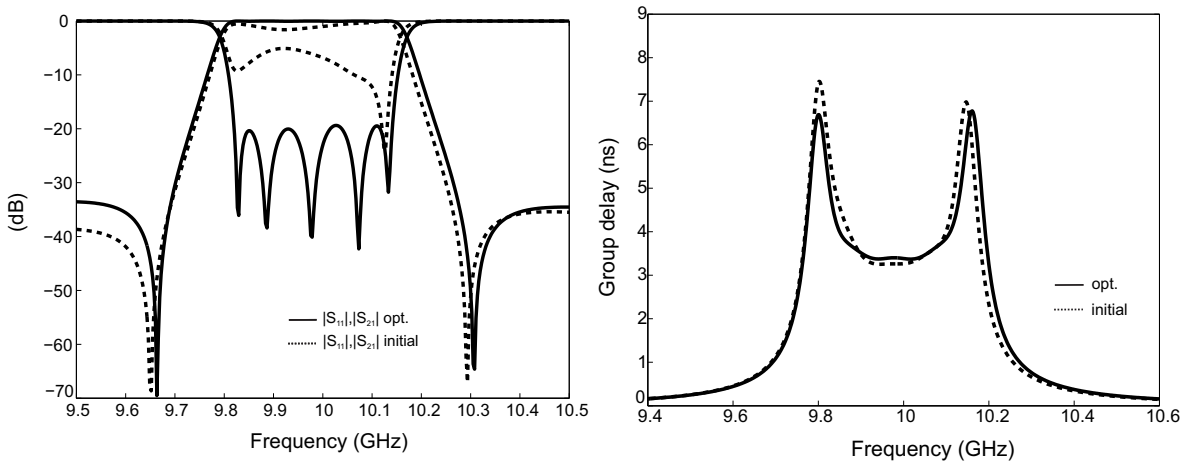

(a) Initial and final solutions of filter.

(b) Group delay responses.

FIGURE 3.7: Result of the optimization for the fifth-order filter. Dashed line - starting point (obtained by perturbing the final solution), solid line - after optimization.

function (3.1) converged as well, but needed as many as 18 iterations - Fig. 3.8. Results for both methods are presented in Fig. 3.7a and Fig. 3.7b.

The filter was fabricated, the comparison between the optimization results and measurement data for scattering parameters and group delay are presented in Fig. 3.9a and Fig. 3.9b, respectively. It is clearly seen that cost function (3.2) converges to correct characteristics regardless of the starting point. In contrast to this, the cost function (3.1) converges to correct characteristics only when the starting point is close to the reference response.

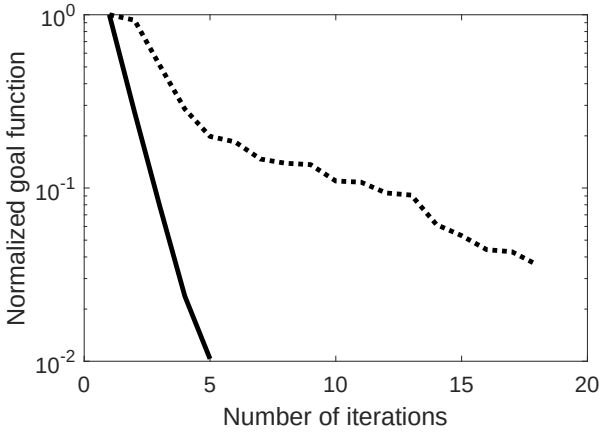

FIGURE 3.8: Convergence of the optimization routine for a fifth-order filter for the second starting point. Dashed line - classical goal function, solid line - zero-pole goal function.

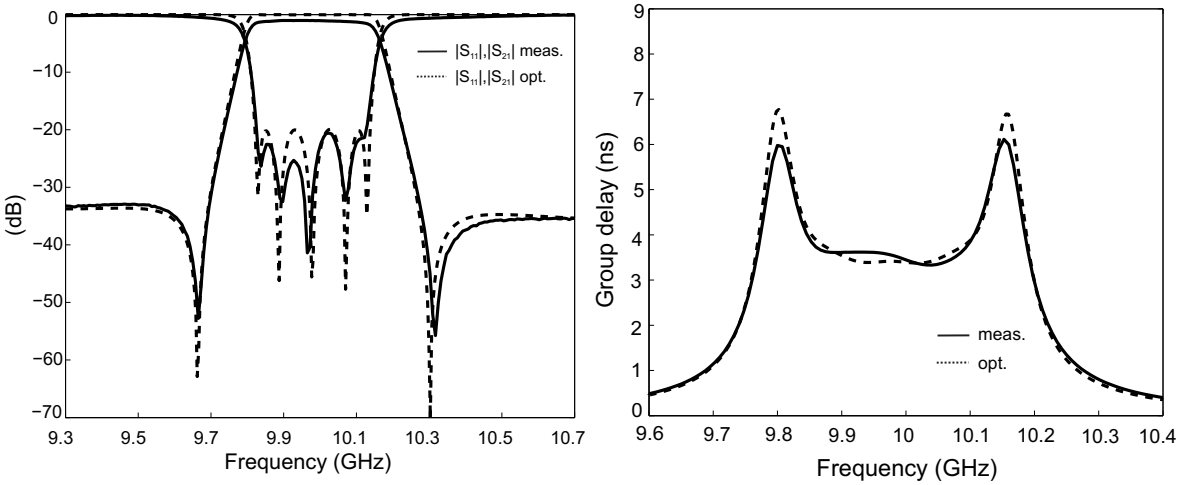

(a) The optimization and measurement characteristics.

(b) The optimization and measurement characteristics of group delay.

FIGURE 3.9: The optimization and measurement characteristics of group delay of fifth-order filter [11].

3.4 Conclusion

In this chapter we presented the concept for the fast design and optimization of microwave filters with linear phase using the zero-pole cost function. The efficiency of the proposed technique has been demonstrated through the design of two microwave bandpass filters with linear phase. The presented optimization algorithm involving a goal function based on zeros an poles of transfer and reflection characteristics converges faster than numerical tuning with a cost function based on scattering parameters.

Acknowledgment

This work was supported by the National Science Centre under contract DEC-2011/01/B/ST7/06634.

References

[1] Matlab.

[2] μWave Wizard.

[3] F. Arndt, R. Beyer, J. Reiter, T. Sieverding, and T. Wolf. Automated design of waveguide components using hybrid mode-matching/numerical EM building-blocks in optimization-oriented CAD frameworks-state of the art and recent advances. *Microwave Theory and Techniques, IEEE Transactions on*, 45(5):747–760, May 1997.

[4] J. Bandler, R. Biernacki, S. H. Chen, J. Swanson, D.G., and S. Ye. Microstrip filter design using direct EM field simulation. *Microwave Theory and Techniques, IEEE Transactions on*, 42(7):1353–1359, Jul 1994.

[5] R. Cameron. Advanced coupling matrix synthesis techniques for microwave filters. *Microwave Theory and Techniques, IEEE Transactions on*, 51(1):1 – 10, Jan. 2003.

[6] B. Gustavsen and A. Semlyen. Rational approximation of frequency domain responses by vector fitting. *Power Delivery, IEEE Transactions on*, 14(3):1052 –1061, Jul. 1999.

[7] A. Jedrzejewski, N. Leszczynska, L. Szydlowski, and M. Mrozowski. Zero-pole approach to computer aided design of in-line SIW filters with transmission zeros. *Progress In Electromagnetics Research*, 131:517 – 533, Sep. 2012.

[8] K. Kottapalli, T. K. Sarkar, Y. Hua, E. K. Miller, and G. J. Burke. Accurate computation of wide-band response of electromagnetic systems utilizing narrow-band information. *Microwave Theory and Techniques, IEEE Transactions on*, 39(4):682–687, 1991.

[9] P. Kozakowski and M. Mrozowski. Automated CAD of coupled resonator filters. *Microwave and Wireless Components Letters, IEEE*, 12(12):470 –472, Dec. 2002.

[10] A. Lamecki, P. Kozakowski, and M. Mrozowski. Fast synthesis of coupled-resonator filters. *Microwave and Wireless Components Letters, IEEE*, 14(4):174 – 176, April 2004.

[11] L. Szydlowski and M. Mrozowski. A self-equalized waveguide filter with frequency-dependent (resonant) couplings. *IEEE Microwave and Wireless Components Letters*, 24(11):769–771, Nov 2014.

Chapter 4

Zero-Pole Space Mapping for CAD of Filters

Based on the publications:

N. Leszczynska, L. Szydlowski, M. Mrozowski, *"Zero-Pole Space Mapping for CAD of Filters,"* published in IEEE Microwave and Wireless Components Letters, Vol. 24, No. 9, pp. 581 - 583, 2014.

N. Leszczynska, M.Klinkosz, M. Mrozowski, *"Substrate-Integrated Waveguide (SIW) Filter Design Using Space Mapping,"* published in proceedings of 2016 21st International Conference on Microwave, Radar and Wireless Communications (MIKON), pp. 1-4, 2016.

In this chapter, we propose a new space-mapping technique tailored to the CAD of microwave filters. The goal of space mapping is to achieve a satisfactory design with the minimal number of fine model evaluations. In our approach, the filter is represented by a rational function. To quickly align the coarse and fine models, and to speed up the direct optimization of the coarse model, we propose matching the zeros and poles of a rational function extracted from scattering parameters, rather than the frequency responses.

4.1 Introduction

Microwave filters have been the subject of intense research for many years, and they play a major role in satellite and terrestrial communication systems. The design of such filters often demands an optimization process [2, 4, 10] based on electromagnetic solvers, which require large computational resources and are CPU-intensive. As a result, the full-wave design-by-optimization of filters may take a very long time. For complex problems, this type of approach may be impractical.

Over the past few years, several novel hybrid optimization strategies [4, 11] have become popular for designing microwave structures. The main idea of these algorithms is to use an empirical surrogate model in the optimization loop, rather than attacking the problem using direct optimization involving a full-wave simulator.

One of the most efficient hybrid algorithms is the space-mapping (SM) technique introduced by Bandler in [1]. In this technique, two different optimization spaces, coarse and fine, are used. Space mapping combines a fast but low-fidelity coarse model with a slow but accurate fine model in order to accelerate the optimization process.

In this chapter, we propose a new variant of space mapping, tailored to the design of microwave filters. Typically, in microwave CAD, the cost functions for the direct optimization of the coarse model and parameter-extraction process are based on scattering parameters. The idea is to compare and minimize the differences between the elements of the scattering matrix computed using the simulator and the desired reference response, at a number of arbitrarily selected frequency points.

One drawback of this approach is that the number of frequency points may be large. Such a goal function can make the optimization process too long, especially if the convergence is not very good. In our method, for the direct optimization of the coarse model and the parameter-extraction procedure, a cost function based on the zeros and poles [10] of a rational function model of the scattering parameters is applied.

This definition of the cost function, combined with a gradient optimization technique, was proposed in [10], and has been shown to give very good results in direct filter optimization using a commercial FEM solver [8], dimensional synthesis of filters [15] and in coupling matrix synthesis [14]. It is based on the direct analysis of the locations of the zeros and poles in the filter transfer and reflection function. For this reason, quasi-elliptic filters can be handled in the same way as all-pole filters. To date, however, the zero-pole approach has not been used in the space-mapping framework. For instance, the synthesis employed in [15] involved two steps: the synthesis of a circuit model and the extraction of individual resonators and couplings using HFSS to simulate elementary segments of the filter. The synthesis resulted in a response that was close to the final response, and which could quickly be tuned in directly in a FEM solver using the zero-pole goal function. Similarly, all zero-pole computations in [8] were carried out using a full wave commercial FEM solver.

In the this chapter we propose to use the zero-pole matching concept at both levels of space mapping: for coarse model optimization and for aligning the coarse and fine model responses. This allows us to further decrease the computational time as the zeros and poles of the fine model can be extracted from full wave simulations performed at a very low number of points. The zero-pole goal function implicitly performs frequency-space mapping, and allows excellent matching between models and a faster direct optimization due to very good convergence properties [8]. The proposed method has been tested on five illustrative examples, detailed below, which have confirmed the effectiveness and robustness of the proposed approach.

4.2 Theory

The space-mapping methodology has been well-documented in the literature [1, 4, 5, 12]. However, it is necessary to first recall the basics of this method and to introduce terminology. The design objective is to calculate an optimal solution for the fine model, without going to direct optimization. To achieve the design goal with as few evaluations of the fine model as possible, the space-mapping technique involves four major steps [5]. In the kth iteration, firstly the coarse model is optimized to obtain the desired specifications,

$$x_f^{k+1} = \arg\min_{x_f} U(R_s(x_f, x_p^k)) \tag{4.1}$$

where U is a suitable goal function, x_f is the design-parameter vector, and the x_p are the model variables [12]. The R_s is the response of the SM surrogate model. The second step is the fine-model computation, carried out using an electromagnetic simulator. The third step is the parameter-extraction procedure, which is the most crucial step in the optimization process:

$$x_p^k = \arg\min_{x_p} ||(R_f(x_f^k) - R_s(x_f^k, x_p))||. \tag{4.2}$$

In this step, the model parameters x_p are calibrated to match the surrogate-model response R_s to that of the fine model R_f. The variables represented by x_p are not considered design parameters, but are used in the parameter-extraction procedure to align the response of the coarse model with that of the fine model. Next, the surrogate model is re-optimized to better predict a fine model solution. The algorithm stops when a satisfactory solution for the fine model is found.

In our approach, which we call zero-pole (Z-P) space mapping, we propose to use a goal function based on the zeros and poles of rational functions approximating the scattering parameters. This will be applied in the case of both the parameter extraction and the coarse-model optimization. Broadly speaking, the goal function used for parameter extraction and coarse-model optimization, is expressed in terms of the difference between the current locations of the zeros Z_i' (S_{21}), R_i' (S_{11}) and poles P_i' of the scattering parameters obtained from the simulated response, and the reference zeros Z_i, R_i and reference poles P_i:

$$C = \sum_{i=1}^{M} |Z_i' - Z_i|^2 + \sum_{i=1}^{N} |P_i' - P_i|^2 + \sum_{i=1}^{N} |R_i' - R_i|^2 \tag{4.3}$$

where N is the number of poles and zeros of the ideal reflection function, and M is the number of prescribed transmission zeros. To determine the positions of Z_i', R_i', and P_i' from the transmission and reflection characteristics calculated by the full-wave analysis, we interpolate S_{11} and S_{21} using the Cauchy method [9] or the vector-fitting [7] procedure. The extracted zeros and poles are paired with the reference values. To find the right pairs, the combination that minimizes the value of each term in eq. (4.3) is sought. This strategy is simple to implement and effective.

For the direct optimization of the coarse model, the reference location of the zeros and poles of the scattering parameters are found analytically from [6]. The design variables

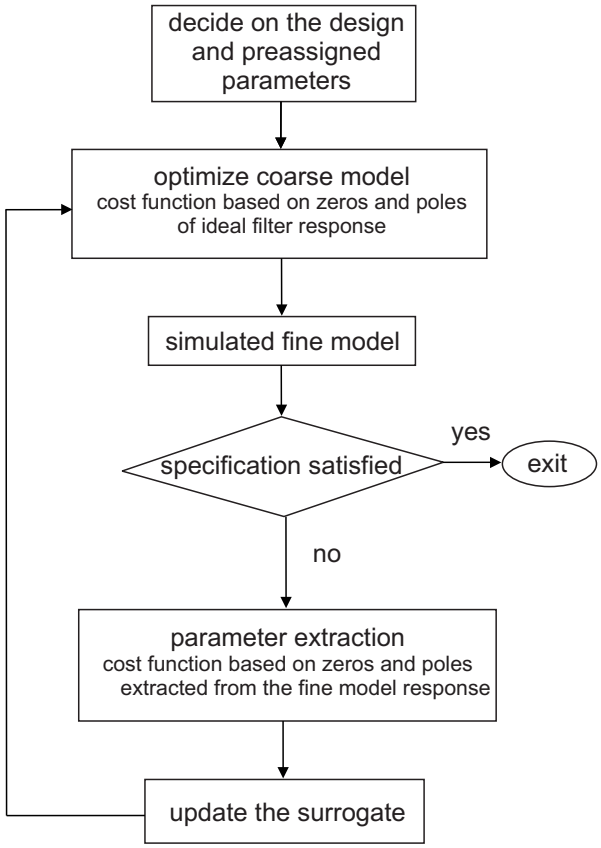

FIGURE 4.1: Flowchart for zero-pole space-mapping optimization.

of the coarse model are varied until the cost function (4.3) reaches the desired minimum. The fine model is simulated at only $2N + 1$ frequency points. This significantly reduces the time taken by the electromagnetic model simulation, and consequently decreases the duration of the optimization process[1].

In the parameter-extraction procedure, model parameters are calibrated to match the surrogate response with that of the fine model. In this case, the zeros and poles are extracted from the fine-model response, (S_{11}) and (S_{21}), and are taken as the reference zeros and poles in the parameter-extraction process. The model parameters are varied until the zeros and poles of the coarse model match those of the fine model. The design process is presented in Fig. 4.1.

4.3 Results

4.3.1 High-Temperature Superconductor Quarter-Wave Parallel Coupled-Line Microstrip Filter

To illustrate the application of the proposed space-mapping method, five bandpass filters were designed. The first example, commonly used for space-mapping tests, is a parallel-coupled microstrip filter [3–5, 12]. We have applied the proposed design method, and then compared our results with those obtained by implicit space-mapping optimization on the same problem [3].

The filter is centered at $f_0 = 4.033$ GHz, with the bandwidth equal to 50 MHz and the return loss level equal to 15 dB. The physical structure of the fine and coarse model are the same as in [3–5, 12], the models were simulated in Momentum and Agilent ADS, respectively Fig. 4.2. The design parameters are the lengths of the coupled lines and spacings between them $x_f = [l_1\ l_2\ l_3\ s_1\ s_2\ s_3]^T$. The substrate heights and relative constant of the coupling sections are used as model (preassigned) parameters. The starting point for the design is was chosen at random.

The design begins with coarse model optimization. When this optimization converges, the response is evaluated with a fine model. We call this response the initial design: it satisfies the design specification in the coarse space, but not in the fine model space.

The coarse model optimized solution and fine model evaluation at coarse optimal design is depicted in Fig. 4.3a. As can be seen, this is not too far from the final solution, as the ADS models used in the coarse space are of sufficiently high quality with respect to the full wave simulations. Consequently, to obtain results that satisfy the specifications,

[1]The extraction of zeros and poles in the fine model may be in error if all the frequency points are located far from the desired passband This may happen if the quality of the coarse model is poor and the mismatch between the coarse and fine model spaces is large. The evaluation of the fine and coarse model at a few extra points resolves the problem.

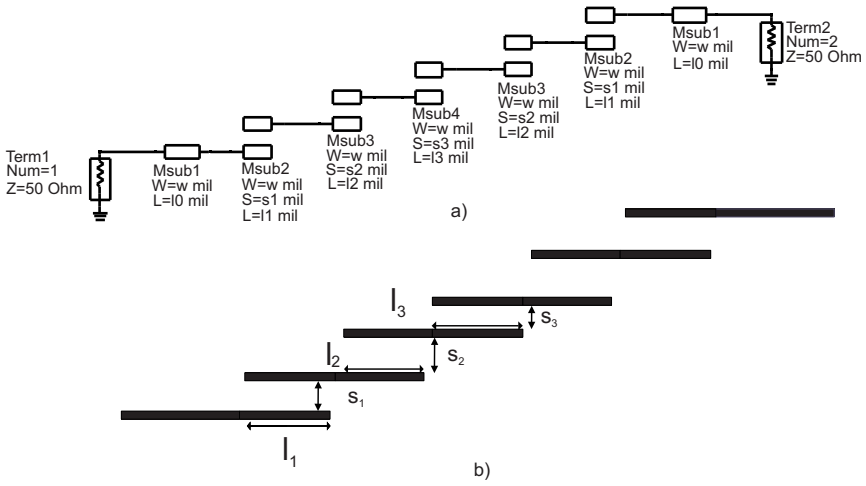

FIGURE 4.2: High-temperature superconductor filter – a) coarse model, b) fine model.

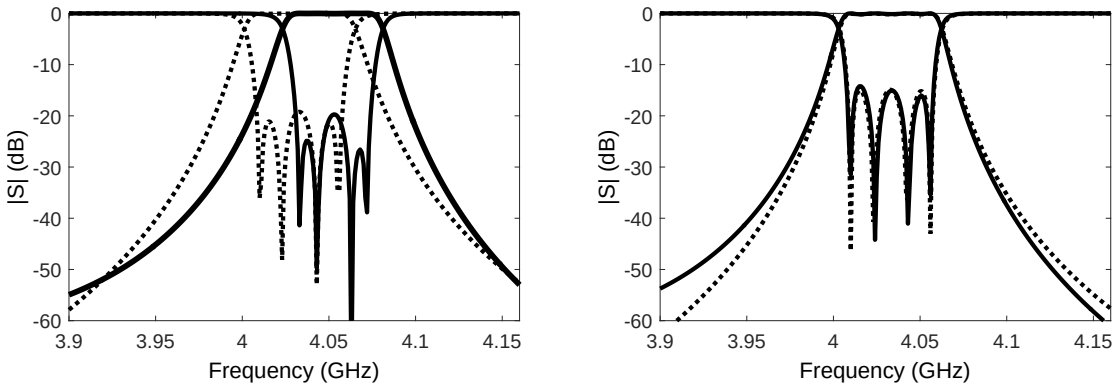

(a) Initial solution. (b) Final solution.

FIGURE 4.3: Responses of the coarse (- - -) and fine (—) models of parallel-coupled filter.

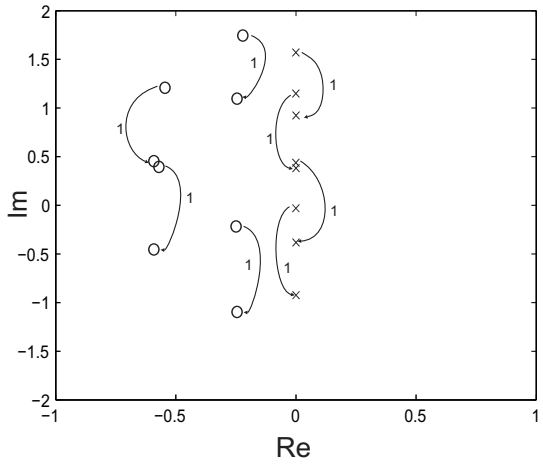

FIGURE 4.4: Location of the zeros (x) of S_{11} and poles (o) of S_{11} and S_{21} (in the low-pass prototype domain) of high-temperature superconductor filter through optimization process.

only one iteration of the proposed Z-P space-mapping algorithm was needed Fig. 4.3b, this is a better result than that reported in [3], where a classical approach based on matching frequency responses was employed. In that case, two iterations were required, the fine simulations also had to be carried out at many frequency points. The final solution is $l_1 = 190.62$, $l_2 = 187.84$, $l_3 = 190.44$, $s_1 = 22.72$, $s_2 = 90.12$, $s_3 = 105.52$ (dimensions in mil).

A snapshot of the location[2] of the zeros (x) and poles (o) of S_{11} for the fine model at the beginning of the procedure and after the first iteration is presented in Fig. 4.4. Curved lines with arrows show the direction of movement.

[2]Zeros and poles are plotted for the low-pass prototype domain.

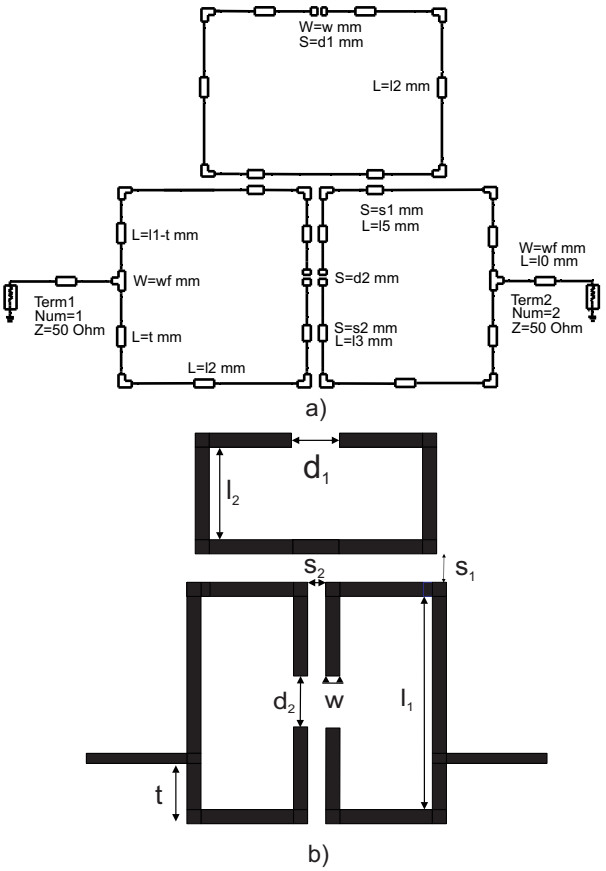

FIGURE 4.5: Open-loop bandpass filter – a) coarse model, b) fine model.

4.3.2 Open-Loop Bandpass Filter with Single Transmission Zero

The second example is an open-loop bandpass filter in a triplet configuration. The filter is centered at $f_0 = 950$ MHz with the bandwidth equal to 40 MHz, and has a 20 dB return loss. The transmission zero is located on the upper side of the passband at $f_z = 992$ MHz. The filter is composed of three directly coupled open-loop resonators and one cross coupling between the first and the third resonator. The design parameters are the lengths of resonators, spacings between them, the positions of the feed lines, and the width of the resonators. The surrogate model contains eight design variables $x_f = [l_1\ l_2\ d_1\ d_2\ s_1\ s_2\ t\ w]^T$.

The physical structure of the filter is shown in Fig. 4.5. As in the case of previous example, this filter was implemented in Agilent Momentum. The coarse model was implemented in Agilent ADS. The filter is optimized using the input space-mapping algorithm. The length and width of feed lines were set to 10 mm and 1 mm, respectively. The dielectric constant was equal to 10.8, and the substrate height was 1.27 millimeters. As in the previous example, both ADS and Momentum were invoked from the Matlab tool.

The set of initial values $x_c^* = [19.4195\ 8.5028\ 1.6929\ 1.2088\ 0.9920\ 1.7328\ 3.6000\ 1.6413]^T$. The initial filter response is depicted in Fig. 4.6a. It can be observed that the return loss level has been degraded to 12 dB in the worst case. However, it can be seen that the

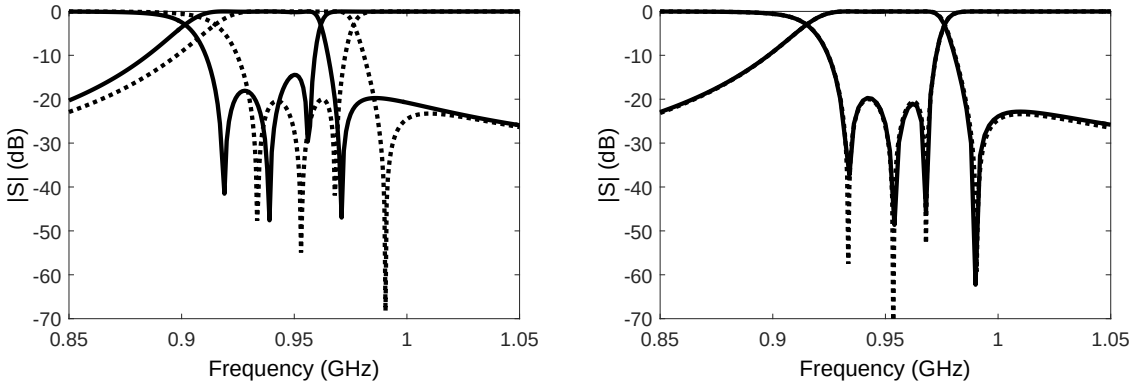

(a) Initial solution of open-loop filter. (b) Final solution of open-loop filter.

FIGURE 4.6: Responses of the coarse (- - -) and fine (—) models of open-loop filter.

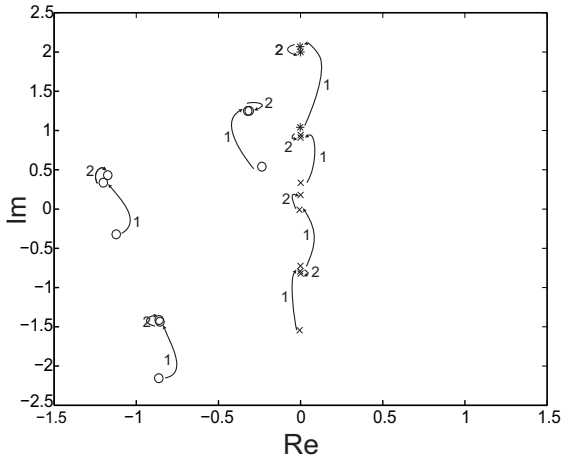

FIGURE 4.7: Locations of the zeros S_{11} (x) and of S_{21} (*), and of poles of S_{11} and S_{21} (o) (in the low-pass prototype domain) of the open-loop filter through optimization process.

transmission zero has been moved down by 20 MHz in comparison with the desired position. The fine-model passband has been narrowed, and the center frequency has moved down. To obtain results that satisfy the specifications, only two iterations of the proposed zero-pole space-mapping algorithm were needed. The final filter characteristics are presented in Fig. 4.6b. The changes in the location of the zeros of S_{11} (x), and S_{21} (*) and of poles (o) of the filter are presented in Fig. 4.7. The set of the final solutions $x_f^* = [19.3046\ 8.3578\ 1.5153\ 1.3460\ 0.9386\ 1.9135\ 3.5233\ 1.5733]^T$ (in millimeters).

4.3.3 Fifth-Order Substrate-Integrated Waveguide (SIW) Filter

The third example was an all-pole filter that involved only six design parameters. More challenging are the filters with transmission zeros and many design variables. The second example is a fifth-order inline bandpass SIW filter with two imaginary transmission zeros

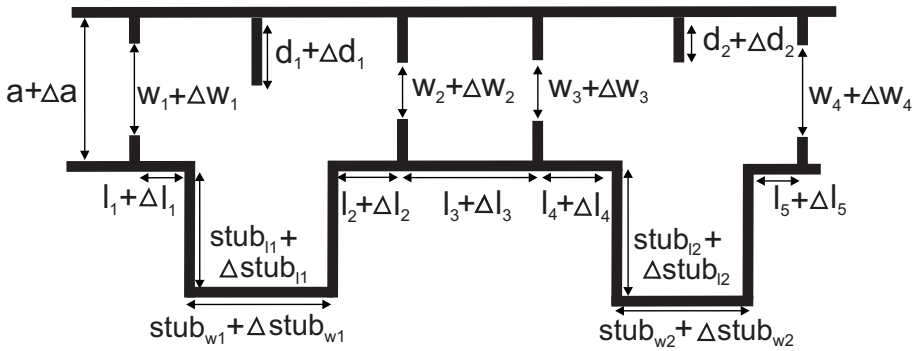

FIGURE 4.8: Coarse model of fifth-order inline SIW filter

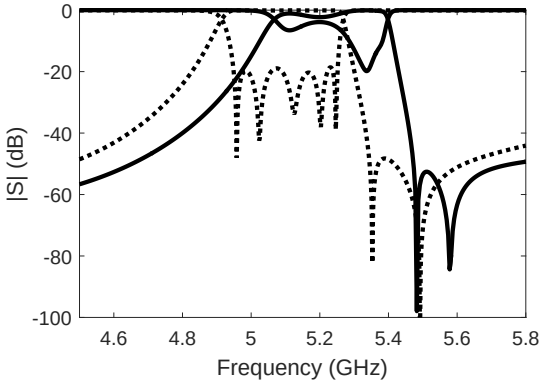

(a) Initial design (fine model response - solid line (—) evaluated at optimal coarse model solution - dashed line (- - -)) of fifth-order SIW filter

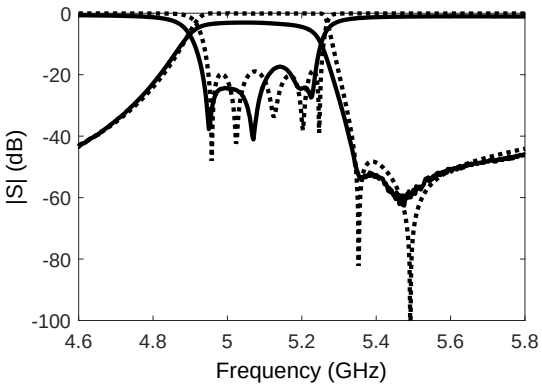

(b) Measured (solid line (—)) and final fine model characteristics (dashed line ((- - -))) of fifth-order SIW filter

FIGURE 4.9: Responses of fifth-order SIW filter.

[15]. The filter is centered at f_0=5.1 GHz, with bandwidth equal to 300 MHz, the return loss level equal to 20 dB and two transmission zeros at 5.35 GHz and 5.49 GHz. In [15], this filter was synthesized using the frequency-dependent coupling-matrix. Here we use the space-mapping approach to design this filter without any prior circuit or dimensional synthesis.

The starting point for the Z-P space-mapping design is chosen at random, and the response is far from the desired one. The filter is optimized using the Z-P algorithm applied to the input, aggressive and the implicit space-mapping technique. This filter design involves up to 15 design variables—namely, the lengths and widths of the filter. The model parameters in the implicit space mapping are the shifts in the design variables, denoted by Δ at Fig. 4.8.

The coarse model (rectangular waveguide - see Fig. 4.8) and fine model were simulated in μWave Wizard and HFSS v.13, respectively. The coarse model optimization yields the initial design (the final coarse design evaluated in the fine model framework) shown by the

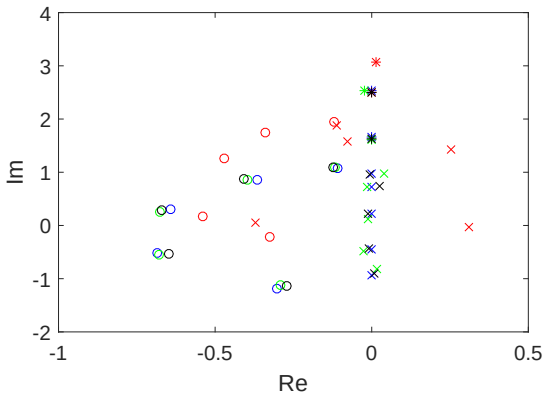

FIGURE 4.10: Locations of the zeros of S_{11} (x) and S_{21} (*), and of poles (o) of S_{11} and S_{21} (in the low-pass prototype domain), of the fifth-order SIW filter through the optimization process

solid line in Fig. 4.9a. In this case, the mismatch between the initial design and the final response is larger than in the previous example. Nevertheless, to obtain the final design, only three (for the input space mapping) or five (for the implicit and aggressive space mapping) iterations of our zero-pole space-mapping algorithm were needed. Locations of the zeros of S_{11} (x) and S_{21} (*), and of poles (o) of S_{11} and S_{21} (in the low-pass prototype domain), of the fifth-order SIW filter through the optimization process are presented in Fig. 4.10. Positions of zeros and poles are denoted by red, green, black and blue color for first, second, third and fourth iteration, respectively.

The final solution is $l_1 = 8.08$, $l_2 = 11.22$, $l_3 = 20.44$, $l_4 = 12.00$, $l_5 = 8.31$, $w_1 = 13.94$, $w_2 = 8.81$, $w_3 = 9.05$, $w_4 = 14.32$, $stub_{l1} = 19.98$, $stub_{l2} = 21.15$, $stub_{w1} = 21.15$, $stub_{w2} = 19.67$, $d_1 = 10.81$, $d_2 = 6.77$ (dimensions in millimeters). The final filter characteristics are presented in Fig. 4.9b, together with the measurements of the fabricated device. The Z-P space-mapping algorithm was also verified on cross-coupled filters involving complex transmission zeros and cross-coupled filters with resonant source-load connection [14]. In all cases, very good convergence was observed and the simulations of the fine model were performed on few frequency points.

4.3.4 Substrate-Integrated Waveguide (SIW) Filter with Linear Phase

The fourth example is a planar four-order linear phase filter centered at $f_0 = 5$ GHz with the bandwidth equal to 100 MHz. The filter has a 20 dB return loss and a pair of real transmission zeros introduced to ensure linear phase. The filter is composed of four side-by-side horizontally oriented SIW cavities, and involves three direct couplings and one cross coupling between the first and fourth SIW cavity – see fig. 4.11. The coarse model of the SIW filter was modeled as a rectangular waveguide in the *mu*Wave Wizard software, which is a very fast tool based on mode-matching analysis. The fine model was simulated in HFSS v.13 workspace. The design parameters are the lengths of the resonators and the iris widths $x_f = [l_1\ l_2\ w_{12}\ w_{23}\ w_{14}\ w_s]^T$ (mm). The substrate

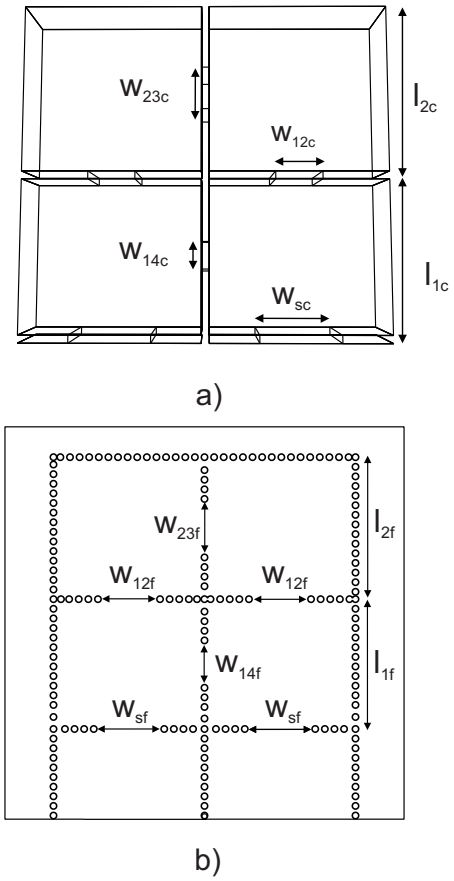

FIGURE 4.11: Substrate-integrated waveguide (SIW) filter with linear phase – a) coarse model, b) fine model.

parameters are the dielectric constant, equal to 3.47, and the height, equal to 0.737 millimeters. In the optimization procedure, both μWave Wizard and HFSS were invoked from with the Matlab environment.

The initial filter response is presented in Fig. 4.12a. It can be observed that the return loss level has been degraded to 16 dB in the worst case. The center frequency has moved up by about 41 MHz. The locations of the transmission zeros have changed: they have moved up as can be observed in the group delay response, Fig. 4.12b.To obtain results that satisfy the requirements, only two iterations of our zero-pole space-mapping algorithm were needed.

The final filter characteristics are presented in Fig. 4.13a. The transmission zeros meet the desired specification (Fig. 4.13b). The final solutions $x_f^* = [19.9442\ 21.7965\ 5.9876\ 5.3257\ 3.6070\ 10.2595]^T$ (all dimensions in millimeters). The evolution of the zeros of S_{11} (x) and S_{21} (*) and the poles (o) of the fine model through the iterations of space-mapping is shown in Fig. 4.14. In this example, we obtained satisfactory results using the input space-mapping algorithm with zero-pole goal function in the surrogate-model optimization and parameter-extraction process. The fine-model simulations were carried out in each iteration only at 9 frequency points.

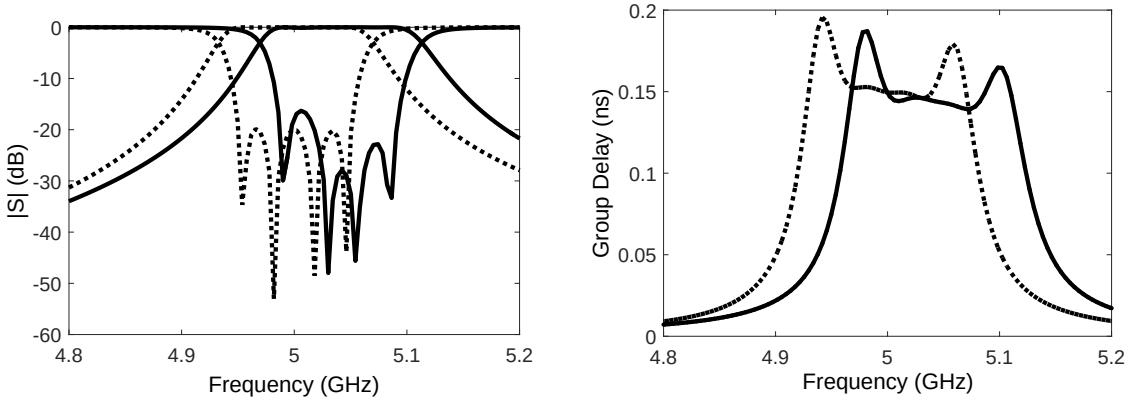

(a) Initial solution of SIW filter.

(b) Initial group delay of SIW filter.

FIGURE 4.12: Responses of the coarse (- - -) and fine (—) models of the SIW filter with linear phase.

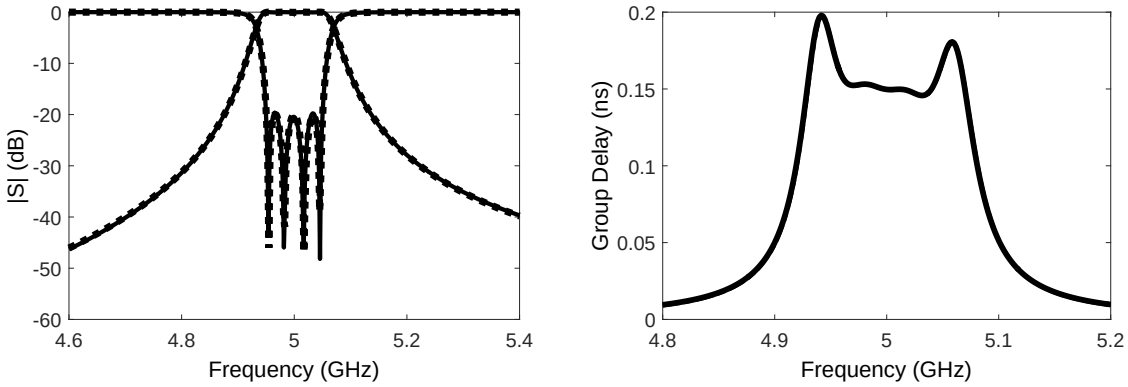

(a) Final solution of SIW filter with linear phase.

(b) Final group delay responses of SIW filter with linear phase.

FIGURE 4.13: Responses of the fine (—) and coarse (- - -) model for the final solution of the SIW filter with linear phase.

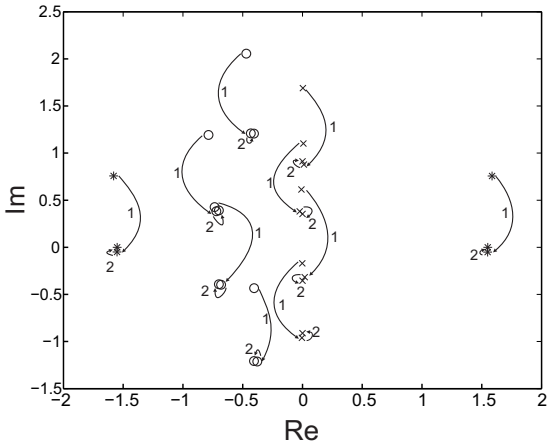

FIGURE 4.14: Locations of the zeros of S_{11} (x) and S_{21} (*), and of poles (o) of S_{11} and S_{21} (in the low-pass prototype domain), of the SIW filter with linear phase through the optimization process.

4.3.5 Ninth order combline filter

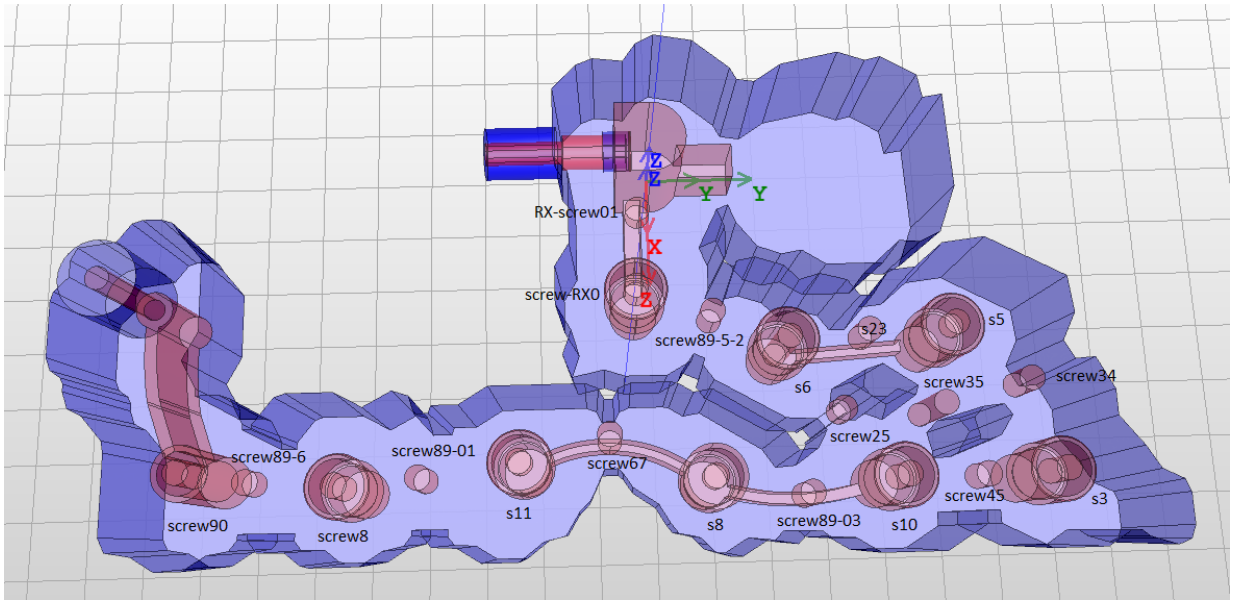

FIGURE 4.15: Ninth order combline filter – a) coarse model, b) fine model.

The last example is a combline ninth-order filter centered at $f_0 = 1.7475$ GHz with the bandwidth equal to 75 MHz. In terms of complexity and the number of design variables, the filter is far more challenging than the examples published in any literature known to the author of this thesis and related to space mapping technique. The filter has 23 dB return loss and two transmission zeros located at 1.8 GHz and 1.84 GHz which improve the selectivity of the transfer function. The filter was simulated with an InventSIM FEM solver [13], the structure is presented at Fig. 4.15. The solver employs higher-

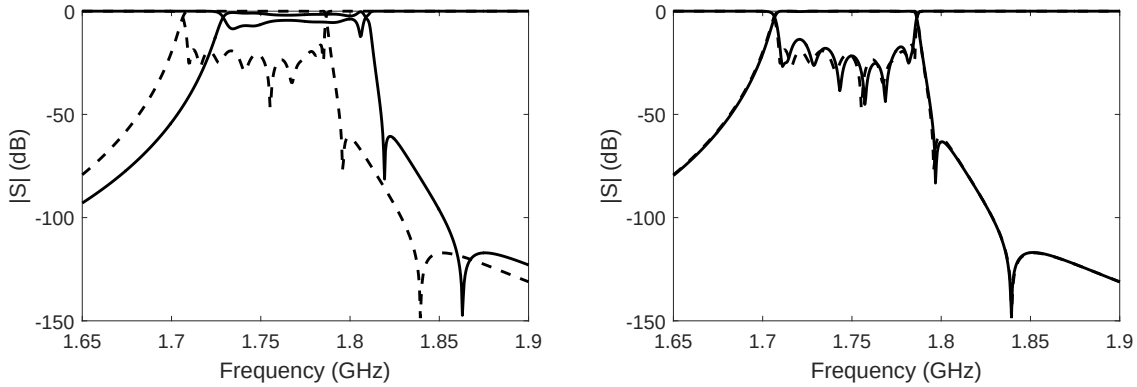

(a) Initial solution of combline filter. (b) Final solution of combline filter.

FIGURE 4.16: Responses of the coarse (- - -) and fine (—) models of the combline filter.

order curvilinear finite elements and fast frequency sweep. In this case, the coarse model response is computed with the first-order basis functions and coarse mesh settings, while the fine model is computed utilizing the second-order basis functions and dense mesh. The size of the problem (in terms of the number of degrees of freedoam in FEM matrices) is equals to 335110 and 2303526 for the coarse and fine model, respectively. This example consist of as many as 20 optimization parameters which are heights of tuning screws $x_f = [RX - screw01,\ screw - RX0,\ s3,\ s5,\ s6,\ screw89 - 01,\ screw89 - 03,\ screw89 - 5 - 2,\ screw25,\ screw35,\ screw67,\ screw8,\ screw45,\ s8,\ s10,\ s11,\ screw23,\ screw34,\ screw89 - 6,\ screw90]^T$ (mm). In this example, input zero-pole space mapping is used in the optimization procedure.

The initial filter response is presented in Fig. 4.16a. The response of the fine model at the starting point is far from the design specification, as can be seen the characteristics are shifted in frequency. Moreover, the positions of transmission zeros have moved as well. The return loss level has been degraded. Five evaluations of fine model were needed to reach the final solution Fig. 4.16b. This is equal to only four zero-pole space mapping iterations. The final solutions $x_f^* = [-7.105\ -8.245\ -7.682\ -7.922\ -9.305\ -9.457\ -9.909\ -11.465\ -6.604\ -12.000\ -12.421\ -6.676\ -9.800\ -9.514\ -9.183\ -9.443\ -10.505\ -11.744\ -9.113\ -9.991]^T$ (all dimensions in millimeters).

4.4 Summary

In this chapter, we have presented a concept for the fast design and optimization of microwave filters using a new variant of the space-mapping technique which involves a zero-pole goal function in direct optimization of a coarse model and a parameter-extraction procedure. The efficiency of this approach has been demonstrated through the design of bandpass filters. In all cases, a final design was obtained after few iterations, which is equivalent to up to five electromagnetic simulations of the respective structures. Moreover,very few frequency points were used in each fine-model simulations. We have shown that the combination of space-mapping technique and the efficient zero-pole cost function

yields excellent results in microwave filter design even for very challenging structures such as the ninth-order combline filter considered as a last example in this chapter.

Acknowledgment

This work was supported by the Polish National Science Centre under contract UMO-2012/07/B/ST7/01241.

References

[1] J. W. Bandler, R. M. Biernacki, S. H. Chen, P. A. Grobelny, and R. H. Hemmers. Space mapping technique for electromagnetic optimization. *IEEE Trans. Microw. Theory Tech.*, 42(12):2536 –2544, Dec. 1994.

[2] J. W. Bandler and S. H. Chen. Circuit optimization: the state of the art. *IEEE Trans. Microw. Theory Tech.*, 36(2):424 –443, Feb. 1988.

[3] J. W. Bandler and Q. S. Cheng. New developments in space mapping CAD technology. *in China-Japan Joint Microwave Conference*, pages 1 – 4, 2006.

[4] J. W. Bandler, Q. S. Cheng, S. A. Dakroury, A. S. Mohamed, M. H. Bakr, K. Madsen, and J. Sondergaard. Space mapping: the state of the art. *IEEE Trans. Microw. Theory Tech.*, 52(1):337 – 361, Jan. 2004.

[5] J. W. Bandler, Q. S. Cheng, N. K. Nikolova, and M. A. Ismail. Implicit space mapping optimization exploiting preassigned parameters. *IEEE Trans. Microw. Theory Tech.*, 52(1):378 – 385, Jan. 2004.

[6] R. J. Cameron. Advanced coupling matrix synthesis techniques for microwave filters. *IEEE Trans. Microw. Theory Tech.*, 51(1):1 – 10, Jan. 2003.

[7] B. Gustavsen and A. Semlyen. Rational approximation of frequency domain responses by vector fitting. *IEEE Trans. Power Delivery*, 14(3):1052 –1061, Jul. 1999.

[8] A. Jedrzejewski, N. Leszczynska, L. Szydlowski, and M. Mrozowski. Zero-pole approach to computer aided design of in-line SIW filters with transmission zeros. *Progress In Electromagnetics Research*, 131:517 – 533, 2012.

[9] K. Kottapalli, T. K. Sarkar, Y. Hua, E. K. Miller, and G. J. Burke. Accurate computation of wide-band response of electromagnetic systems utilizing narrow-band information. *Microwave Theory and Techniques, IEEE Transactions on*, 39(4):682–687, 1991.

[10] P. Kozakowski and M. Mrozowski. Automated CAD of coupled resonator filters. *IEEE Microw. Wireless Compon. Lett.*, 12(12):470 –472, Dec. 2002.

[11] S. Koziel. Shape-preserving response prediction for microwave design optimization. *Microwave Theory and Techniques, IEEE Transactions on*, 58(11):2829–2837, 2010.

[12] S. Koziel, Q. S. Cheng, and J. W. Bandler. Space mapping. *Microwave Magazine, IEEE*, 9(6):105 –122, Dec. 2008.

[13] A. Lamecki, L. Balewski, and M. Mrozowski. An efficient framework for fast computer aided design of microwave circuits based on the higher-order 3D finite-element method. *Radioengineering*, 23(4), Dec 2014.

[14] L. Szydlowski, N. Leszczynska, and M. Mrozowski. Generalized Chebyshev bandpass filters with frequency-dependent couplings based on stubs. *Microwave Theory and Techniques, IEEE Transactions on*, 61(10):3601–3612, Oct 2013.

[15] L. Szydlowski, N. Leszczynska, and M. Mrozowski. A novel synthesis technique for microwave bandpass filters with frequency-dependent couplings. *Progress In Electromagnetics Research*, 137:35 – 50, 2013.

Chapter 5

Fast Full-Wave Multilevel Zero-Pole Optimization of Microwave Filters

Based on the publication:

N. Leszczynska, A. Lamecki, M. Mrozowski, *"Fast Full-Wave Multilevel Zero-Pole Optimization of Microwave Filters,"* published in IEEE Microwave and Wireless Components Letters, Vol. 26, No. 11, pp. 867 - 869, 2016.

A new concept is proposed for the full-wave computer-aided design of microwave filters. The method consists of two stages and operates on the zeros and poles of the transfer function and their derivatives. These quantities are evaluated from the response computed by a full-wave electromagnetic solver with two levels of accuracy. The two stages make use of different models that are optimized using a low-accuracy electromagnetic solver. The design involves one coarse-level optimization in the first stage and a few iterations in the second stage, each requiring a single computation of a high-accuracy response. The effectiveness of the proposed technique is demonstrated with two examples, in which design closure was achieved with just three evaluations of the high-accuracy full-wave solutions irrespective of the quality of the initial design.

5.1 Introduction

Design by optimization of microwave filters based entirely on full-wave electromagnetic simulations is a challenging computational problem. First of all, each iteration takes a long time and, even more importantly, the iterative optimization process often fails to converge if the starting point is not close to the final solution. To overcome this, several approaches have been proposed. In the zero-pole technique [4], the frequency response of an electromagnetic system, as computed by a full-wave solver, is fitted to

a rational function, and the optimization process tries to match the zeros and poles of the extracted function with the zeros and poles of an ideal filter found using circuit synthesis. Another possibility is to extract the coupling matrix from the simulations and to use it as a basis for the goal function. Finally, multifidelity or surrogate-based optimization (SBO) can be performed. In the multifidelity technique [5], a sequence of optimization problems with increasing fidelities for the electromagnetic model is solved, with the result of the optimization using lower-fidelity models serving as a starting point for the higher-fidelity computations. If a surrogate model is not available, a coarse-discretized model of different fidelity levels is utilized [5, 11]. Surrogate-based optimization is often combined with space mapping [1, 11] and enhanced with information on derivatives in order to increase the effectiveness of the optimization process [3, 5, 6, 9, 10]. To ensure convergence from poor starting points, a zero-pole cost function was proposed in [9] in both the surrogate optimization and parameter-extraction procedures. Other authors [5, 10] advocate response features in the definition of the goal function geared towards filter optimization. For instance, in [10], two sets of features are utilized—frequency parameters (reflection zeros) and ripple-height parameters. However, the feature-space approach to filter design fails if the starting point is computationally bad, in the sense that the initial point has the wrong number of feature frequencies [10].

In this chapter, we propose a new two-stage technique based on the concept of multilevel optimization using information on zeros and poles, and their derivatives, computed from full-wave simulations of various accuracies. Compared to the response-features approach [5, 10], our algorithm allows for the design of a much broader class of filters (eg. filters with complex transmission zeros) and converges in strikingly few iterations, even for very complex structures and for starting points that pose a challenge for the feature-space technique advocated for filters [10]. Compared to other multilevel and space mapping approaches [3, 5, 6, 10] our technique uses a different cost function and involves two stages with different models used at each stage. The derivatives of the fine model are needed only in the second stage. The parameters of models for both stages are evaluated from the frequency response computed by a FEM solver.

5.2 Theory

We use the zero-pole framework [4, 9]. The goal is to find a minimum, within the assumed design space, of $c = (\boldsymbol{\lambda}(\boldsymbol{x}) - \boldsymbol{\lambda}^r)^H(\boldsymbol{\lambda}(\boldsymbol{x}) - \boldsymbol{\lambda}^r)$, where $\boldsymbol{\lambda}(\boldsymbol{x})$ is a vector of zeros and poles extracted from a computed transmission and reflection response, $\boldsymbol{x}$ is a vector of design variables, and $\boldsymbol{\lambda}^r$ is a vector of reference zeros and poles. The reference values for the zeros and poles are found analytically, while the zeros and poles are extracted from the simulated response. In both cases the zeros and poles are denoted in the lowpass prototype domain [2]. Let us define $\mathbf{g} = \lambda(\boldsymbol{x}) - \lambda^r$; for a region close to $\boldsymbol{x}_0$, the cost function can be approximated as

$$c(\boldsymbol{x}_0 + \Delta\mathbf{x}) \approx \Delta\boldsymbol{\lambda}^H\Delta\boldsymbol{\lambda} + 2\mathbf{g}^H\Delta\boldsymbol{\lambda} + \mathbf{g}^H\mathbf{g}. \tag{5.1}$$

Here, $\Delta\boldsymbol{\lambda} = \mathbf{J}\Delta\mathbf{x}$ and $\Delta\mathbf{x}$ is the perturbation of the design variables around $\mathbf{x}_0$, while $\mathbf{J}$ is a Jacobian with elements evaluated at $\mathbf{x}_0$. With the above definition, the minimum of

the cost function over the entire design space can be found by successively solving a local problem using the trust region technique.

$$h(\Delta\mathbf{x}) = \Delta\mathbf{x}^T\mathbf{J}^H\mathbf{J}\Delta\mathbf{x} + 2\mathbf{g}^H\mathbf{J}\Delta\mathbf{x} + \mathbf{g}^H\mathbf{g}. \tag{5.2}$$

To this end, in the proposed technique, two (or more) levels of accuracy are utilized: a fine level, denoted by f, and a coarse level, denoted by the index c. The output data at these levels for fine and coarse models are $\boldsymbol{\lambda}^f$, $\mathbf{J}^f$, and $\boldsymbol{\lambda}^c$, $\mathbf{J}^c$, respectively. Our goal is to minimize the fine model. Since the evaluation of the high-accuracy model is expensive, we will use a surrogate of (5.2) at the fine level that can be constructed using the quantities computed at the coarse level. We assume that the derivatives at the fine level are available at a point $\boldsymbol{x}_0$.

Our algorithm is composed of two stages. In the first stage, to find a surrogate model, we compute and compare the results obtained from both levels of accuracy and automatically calculate the average frequency shift (s) between the corresponding zeros and poles in the coarse and fine models. To this end, the difference between the imaginary part of each coarse-model zero and pole and the corresponding fine-model zero and pole (denoted in the lowpass prototype domain) is computed, and s is set to the mean value. Next, we add this shift (which is an imaginary constant expressed in rad/s) to the zeros and poles of the coarse-model response. The optimization is then performed using form (5.2) with the frequency-shifted coarse level data and the trust region method. At this stage we do not use the derivatives of the high-fidelity model. Once the solution for the first surrogate model has been found at $\boldsymbol{x}_0$, we pass to the second stage. Here, we use a different surrogate model. We begin by calculating the coarse and fine solution and the Jacobians of both models at $\boldsymbol{x}_0$. The fine-level data $\boldsymbol{\lambda}^f$ and $\mathbf{J}^f$ are approximated around a point $\boldsymbol{x}_0$ using the following expressions:

$$\boldsymbol{\lambda}^f(\boldsymbol{x}) \approx \boldsymbol{\lambda}^c(\boldsymbol{x}) + \mathbf{d} + \boldsymbol{E}(\boldsymbol{x} - \boldsymbol{x}_0) \tag{5.3}$$

where $\mathbf{E} = \mathbf{J}^f(\boldsymbol{x}_0) - \mathbf{J}^c(\boldsymbol{x}_0)$, $\mathbf{d} = \boldsymbol{\lambda}^f(\boldsymbol{x}_0) - \boldsymbol{\lambda}^c(\boldsymbol{x}_0)$. We assume that the Jacobians at the two levels are related by

$$\mathbf{J}^f(\boldsymbol{x}) \approx \mathbf{J}^c(\boldsymbol{x}) + \mathbf{E}. \tag{5.4}$$

We use the approximate relationship between the vectors $\boldsymbol{\lambda}$ and the Jacobians at the two levels of accuracy to modify the quadratic form (5.2) by inserting $\mathbf{g} = \boldsymbol{\lambda}^c + \mathbf{d} + \mathbf{E}\Delta\mathbf{x} - \boldsymbol{\lambda}^r$ and $\mathbf{J} = \mathbf{J}^c + \mathbf{E}$. This yields

$$h_s(\Delta\mathbf{x}) = \Delta\mathbf{x}^T(\mathbf{J}^{cH}\mathbf{J}^c + 2\mathbf{E}^H\mathbf{J}^c + \mathbf{E}^H\mathbf{E})\Delta\mathbf{x} + 2\mathbf{g}^H(\mathbf{J}^c + \mathbf{E})\Delta\mathbf{x} + \mathbf{g}^H\mathbf{g}. \tag{5.5}$$

We have obtained a surrogate of (5.2) at the fine level, but since this involves only the Jacobian and the zeros and poles evaluated at the coarse level, it can be minimized relatively cheaply. This new form is used to find the minimum over the entire design space by the trust region technique with the zeros and poles and their derivatives evaluated quickly at the low fidelity level. Once this optimization converges, $\mathbf{d}$ and $\mathbf{E}$ are updated (a new surrogate is built with a single evaluation of the fine model) and a new iteration begins. While in principle, the second stage of our algorithm resembles the sensitivity-enhanced space mapping proposed in [6], we work only on the output data without time

consuming parameter extraction. In this respect, the second stage of our technique is similar to manifold mapping [3] rather to the procedure considered in [6], except that the relationship for the Jacobians and the response is assumed to take a different form.

5.3 Results

5.3.1 Inline Filter

To show the efficiency of the proposed algorithm, we compare our results for the same filter design problem with those obtained by cognition space-mapping optimization [10]. In our case, the filter is optimized with a FEM solver [7]. The solver employs higher-order curvilinear finite elements and fast frequency sweep. The response computed with the first-order and second-order basis functions and derivatives are accessible for processing in Matlab via an API, and we used as the data for the coarse and fine levels. A typical difference between model responses is shown in Fig. 5.1. One complete simulation takes 1 minute and 6 minutes at the first level and the second level, respectively. In both cases, the runtime includes derivative computation. The runtime for the fine level is identical to the runtime for high-accuracy computations reported in [10], and so direct comparison of CPU times between our method and the one proposed in [10] is possible. The filter is a fourth-order Chebyshev bandpass filter centered at 11 GHz, with a bandwidth of 300 MHz and a return loss level equal to 23.4 dB. The design parameters are the heights of the posts located at the center of each cavity and each coupling window $x = [h_1\ h_2\ h_3\ hc_1\ hc_2]^T$.

We tested our technique for three different starting points: the first two are the same as in [10] and the last is chosen so that not all frequency features (reflection zeros) are visible.

The first initial design solution is $x = [3.3\ 4.389\ 3.991\ 3.28\ 2.914]^T$, with value in millimeters. At first, we calculate the difference between the imaginary parts of zeros and poles of the coarse and fine model responses for the starting point. In this case, the shift s is equal to 0.487 rad/s. Next, we add calculated difference to coarse model

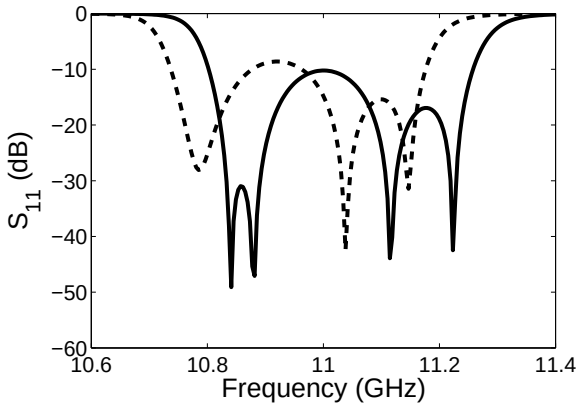

FIGURE 5.1: Responses of the low-fidelity (- - -) and the high-fidelity (—) models for the first starting point.

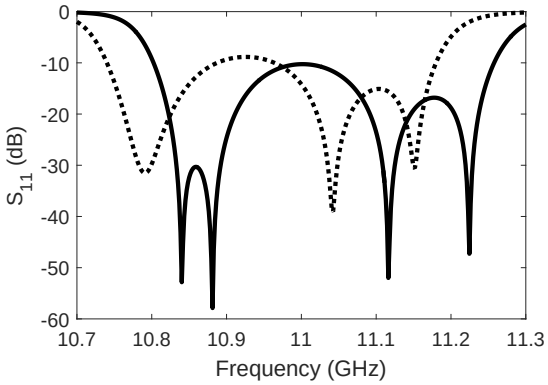

(a) Responses of the low-fidelity (- - -) and the high-fidelity (—) model before shift.

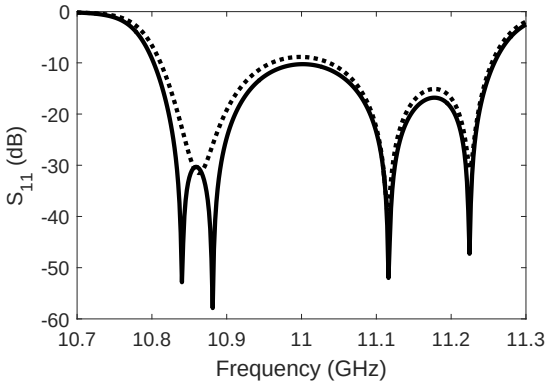

(b) Responses of the low-fidelity (- - -) and the high-fidelity (—) model after shift.

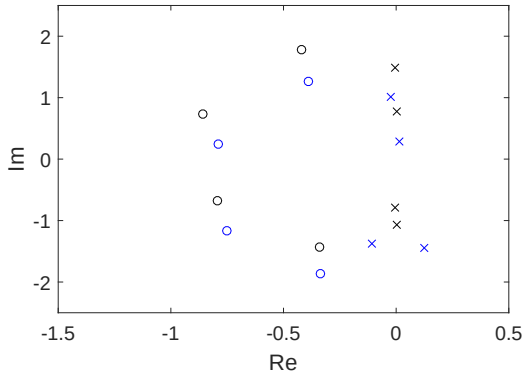

(c) Locations of zeros (x) and poles (o) of the low-fidelity (blue) and the high-fidelity model (black) before shift.

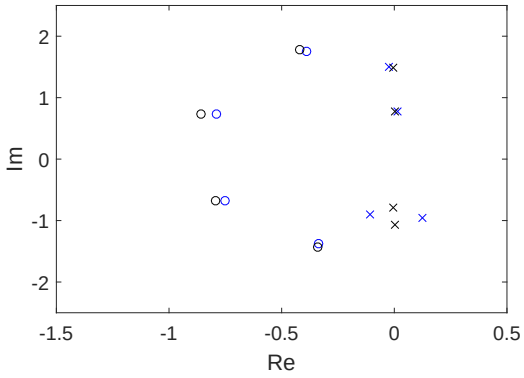

(d) Locations of zeros (x) and poles (o) of the low-fidelity (blue) and the high-fidelity model (black) after shift.

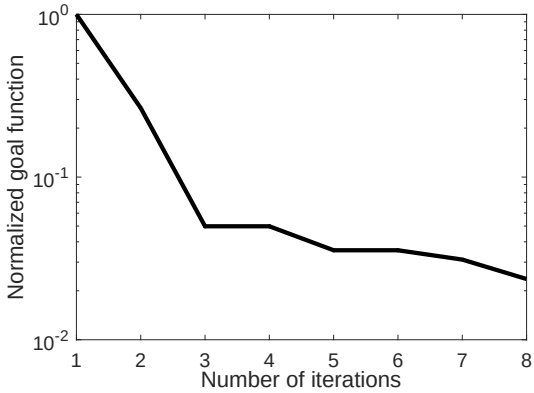

(e) Convergence of the low-fidelity model at the first stage.

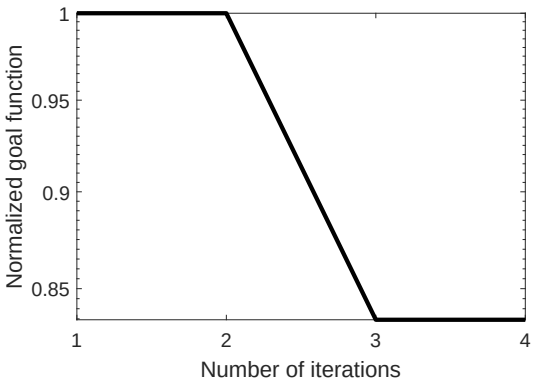

(f) Convergence of the low-fidelity model at the second stage.

FIGURE 5.2: Results for the first starting point.

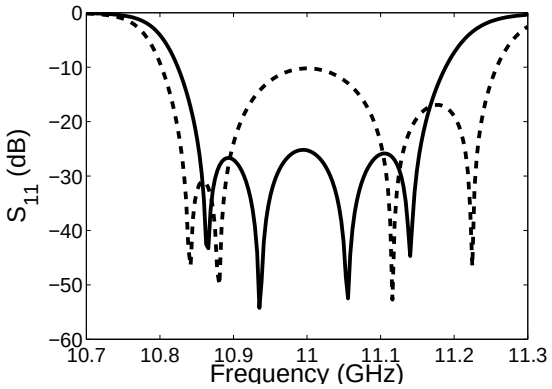

(a) Initial (- - -) and final (—) responses of the high-fidelity model.

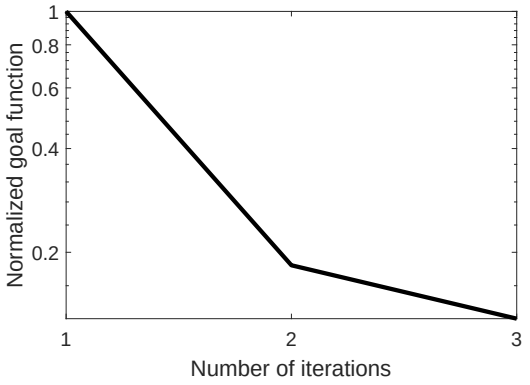

(b) Convergence of the filter's high-fidelity model through optimization process.

FIGURE 5.3: Results of EM model at the first starting point.

imaginary part of zeros and poles. As a result, the response of the low-fidelity model is the same range of frequency as high-fidelity model Fig.5.2b, it is also seen from the position of zeros and poles at imaginary axis at Fig. 5.2d. By performing the proposed preconditioning process we are able to save iterations in optimization for moving the characteristic in the frequency scope. Then, the numerical tunnig of low-fidelity model can be performed. Twelve evaluation of the low-fidelity model (eight at the first stage and four at the second one) were needed to reach the final solution. Normalized goal function values are presented in convergence plots Fig. 5.2e and Fig. 5.2f. As can be seen, the value of goal function change rapidly at the beginning of the first stage. To obtain results that satisfy the specifications, only three simulations of the high-fidelity model were needed (just one iteration in stage two). The results of optimization and convergence for the full-wave model is presented in Fig. 5.3. The total optimization time was 30 minutes, which is a better result than that reported in [10]. In that case, eight simulations of the fine model were required (seven iterations), and the whole process took 62 minutes, which is twice as long as for our method. The final solution is $x^* = [3.4642\ 4.1739\ 3.6561\ 3.2639\ 2.9596]^T$. The final design is presented in Fig. 5.3a.

The second starting point, again taken from [10], is $x = [3.020\ 4.680\ 4.314\ 3.480\ 3.028]^T$, with all values in millimeters. In this example the difference between imaginary parts of zeros and poles is found to be 0.5249 rad/s. The results of shifting the low-fidelity model in the frequency and imaginary domain are shown at Fig. 5.4b and Fig. 5.4d, respectively. In this case, again, just one iteration at stage two was needed to reach the design specification. In total, three simulations of the fine model were performed (both stages) and thirteen simulations of the low-fidelity model—including nine evaluations at the first stage and four at the second (Fig.5.4e and Fig.5.4f). The final result was obtained in 31 minutes, which again is a better result than that obtained in [10], which needed 15 fine-model simulations and 106 minutes. The final design is $x^* = [3.4874\ 4.2038\ 3.6975\ 3.2563\ 2.9565]^T$ and its characteristics with convergence profile are shown in Fig. 5.5.

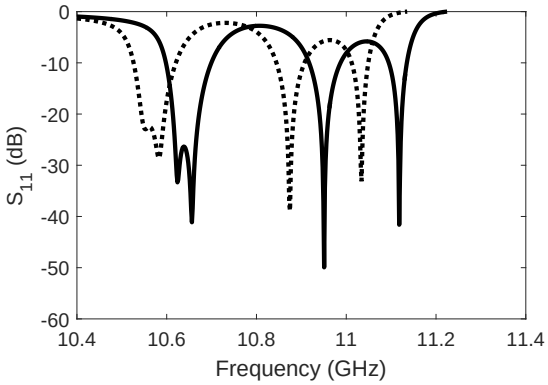

(a) Responses of the low-fidelity (- - -) and the high-fidelity (—) model before shift.

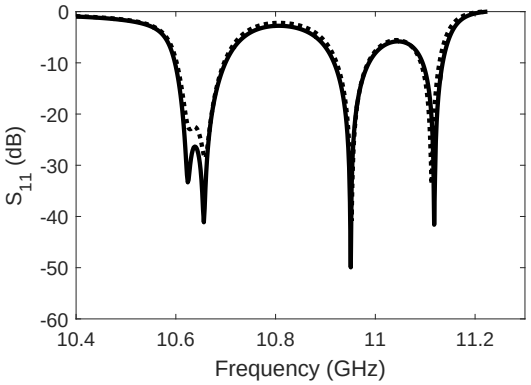

(b) Responses of the low-fidelity (- - -) and the high-fidelity (—) model after shift.

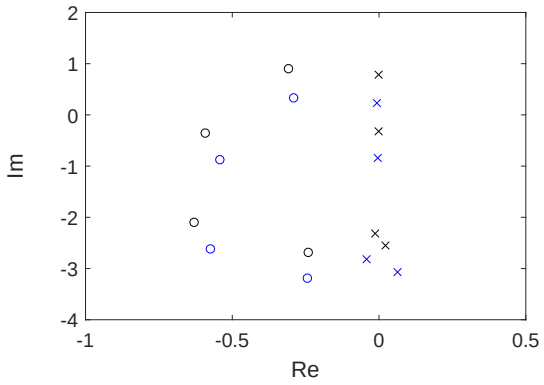

(c) Locations of zeros (x) and poles (o) of the low-fidelity (blue) and the high-fidelity model (black) before shift.

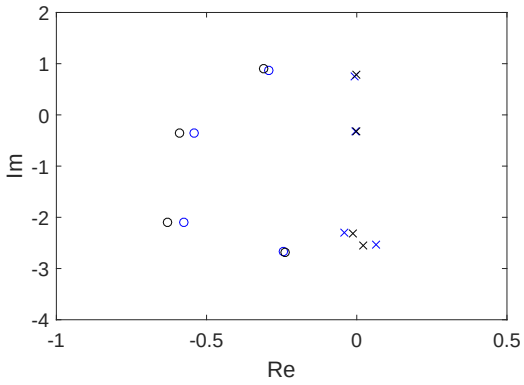

(d) Locations of zeros (x) and poles (o) of the low-fidelity (blue) and the high-fidelity model (black) after shift.

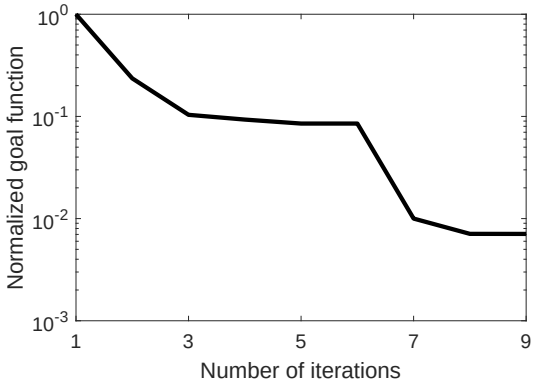

(e) Convergence of the low-fidelity model at the first stage.

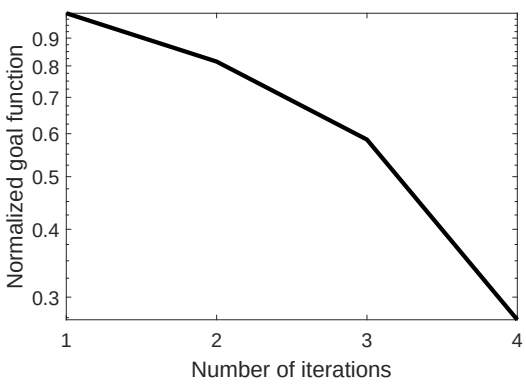

(f) Convergence of the low-fidelity model at the second stage.

FIGURE 5.4: Results for the second starting point.

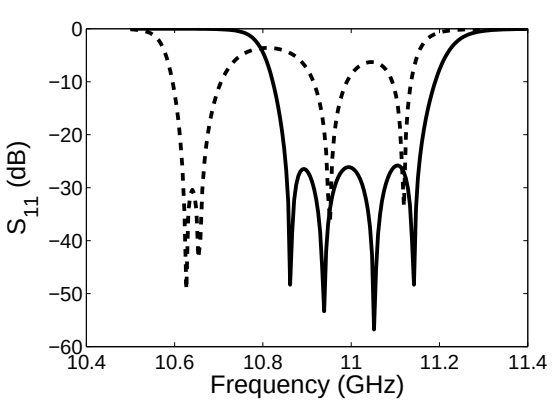

(a) Initial (- - -) and final (—) responses of the high-fidelity model.

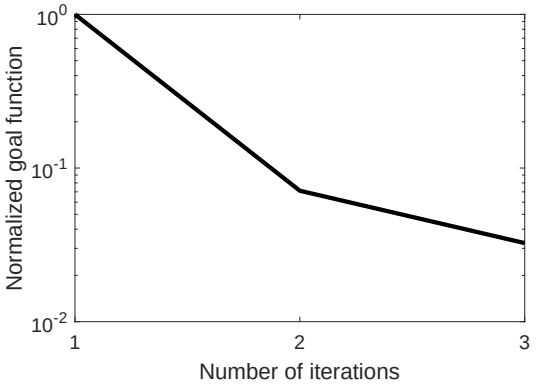

(b) Convergence of the filter's high-fidelity model through optimization process.

FIGURE 5.5: Results of EM model at the second starting point.

The final initial point was chosen at random within the range of possible dimensions of the given topology: $x = [3.0\ 4.2\ 4.9\ 3.7\ 3.5]^T$, with all values in mm. In this example the difference between imaginary parts of zeros and poles is found to be 0.47 rad/s. In this case, only two reflection zeros are visible in Fig. 5.6a, and for this reason, such a starting point would be deemed inadequate for the feature-space approach proposed in [10] or [5]. However, even for these challenging initial values, only three simulations of the fine model were needed in our method Fig. 5.7 (one iteration at the second stage). In this case, twenty four simulations of the coarse model were needed to minimize the surrogate form, with seventeen and seven at the first and the second stage (Fig.5.6e and Fig.5.6f), respectively. The whole process took 42 minutes. The final design vector is $x^* = [3.4239\ 4.1459\ 3.6383\ 3.2717\ 2.9584]^T$.

5.3.2 Linear Phase Filter

The final example, a fifth-order linear-phase filter [8], is very challenging. It involves as many as 15 design variables and the filter has four transmission zeros - a complex pair and two imaginary ones. Because of complex transmission zeros it is impossible to design this structure using the response features considered in [10]. A difference between model responses is presented in Fig. 5.8. The responses at the starting point for the coarse and fine level are shown in Fig.5.10a, together with the final high-fidelity response. It is clearly seen that the initial design is very far from the final one and that no response features can be identified from the initial response. Furthermore, the frequency scaling for aligning the coarse and fine response at the starting point using the traditional approach [6] would not be possible. With the proposed two-stage multilevel technique we determined the shift $s = 0.47$ rad/s for the first stage automatically (Fig.5.9a, Fig.5.9b and Fig.5.9c, Fig.5.9d). The total number of the coarse model simulations was twenty-four, five iteration were needed in first stage and eighteen in the second one Fig.5.9e and Fig.5.9f. The entire

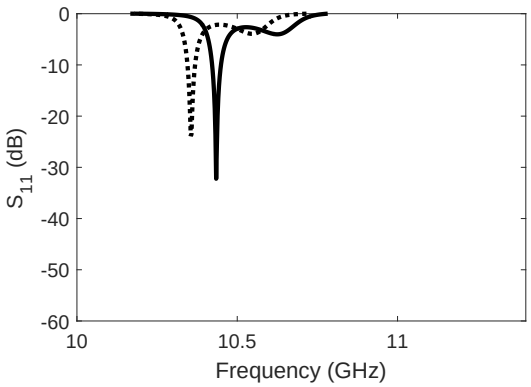

(a) Responses of the low-fidelity (- - -) and the high-fidelity (—) model before shift.

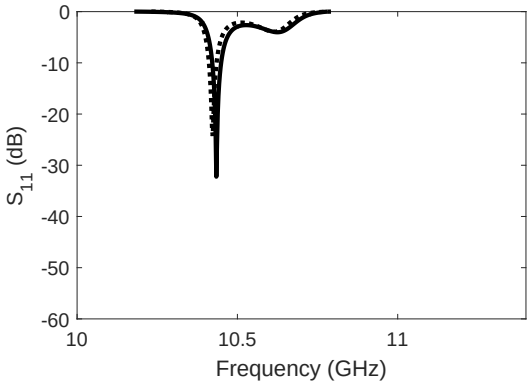

(b) Responses of the low-fidelity (- - -) and the high-fidelity (—) model after shift.

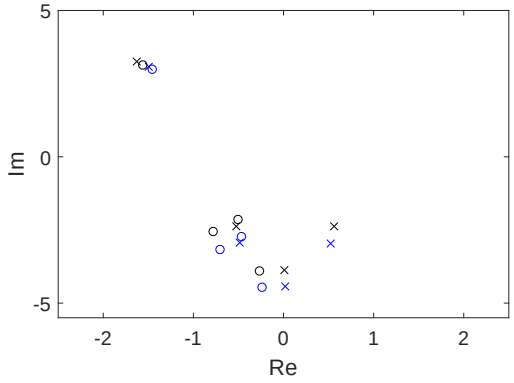

(c) Locations of zeros (x) and poles (o) of the low-fidelity (blue) and the high-fidelity model (black) before shift.

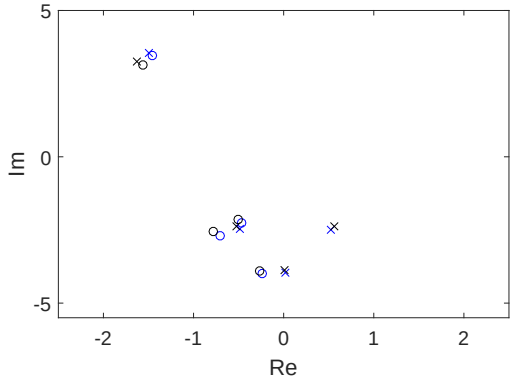

(d) Locations of zeros (x) and poles (o) of the low-fidelity (blue) and the high-fidelity model (black) after shift.

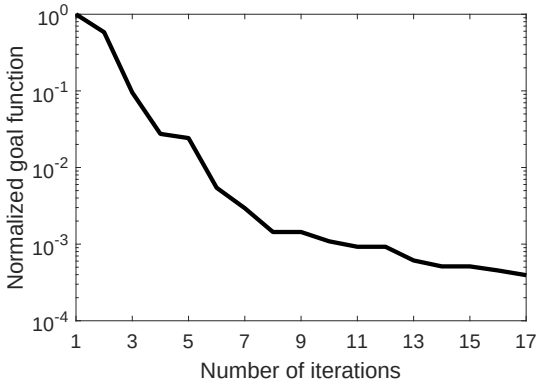

(e) Convergence of the low-fidelity model at the first stage.

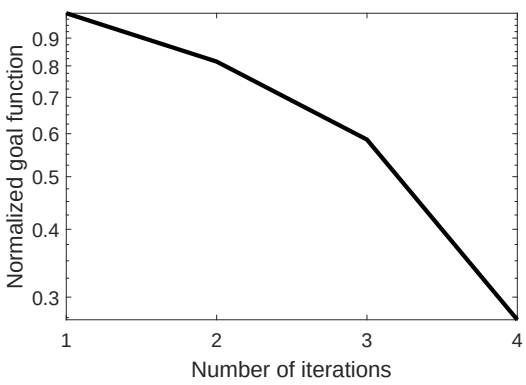

(f) Convergence of the low-fidelity model at the second stage.

FIGURE 5.6: Results for the third starting point.

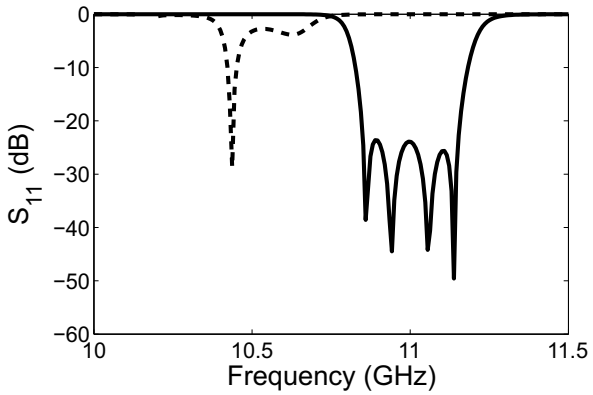

(a) Initial (- - -) and final (—) responses of the high-fidelity model.

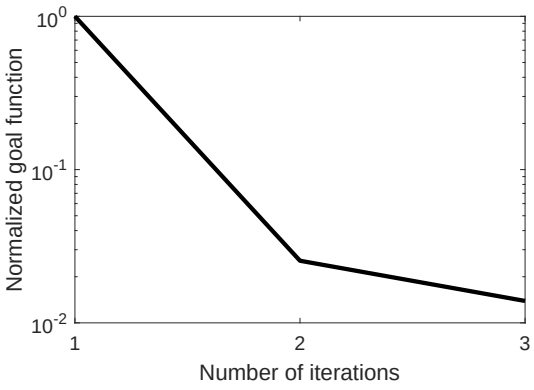

(b) Convergence of the filter's high-fidelity response through optimization process.

FIGURE 5.7: Results of EM model at the third starting point.

process converged again in just one iteration at the second stage Fig.5.10.

In all examples, we needed only one iteration at the second stage to reach the design specification, and both stages involved just three high-fidelity model evaluations (the derivatives at the fine level were computed only once). Note that the minimum number of high-accuracy model evaluations in any surrogate-based optimization method that converges in one iteration is two —the first for the initial solution and the second for verification. In addition, high-accuracy sensitivities have to be computed at least once. With our algorithm, for all benchmark problems, we needed three evaluation of the fine model and one evaluations of sensitivities, which means that the design closure was achieve with just one fine-model simulation more than this absolute minimum. This extra simulation comes from the first stage of our algorithm but it does not require fine model sensitivities. As can be seen from the tests, our method converges remarkably well, even if a bad

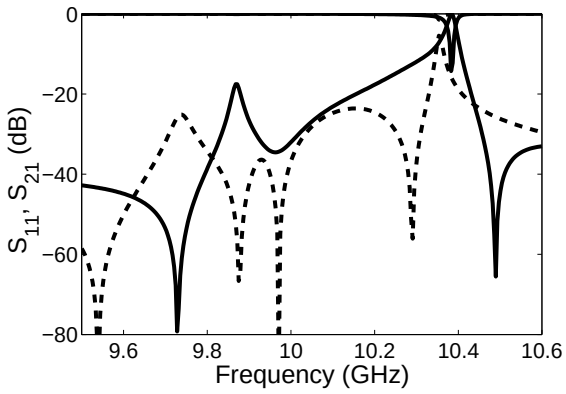

FIGURE 5.8: Low-fidelity (- - -) and high-fidelity (—) models at the starting point for the linear-phase filter with two complex and two imaginary transmission zeros [8].

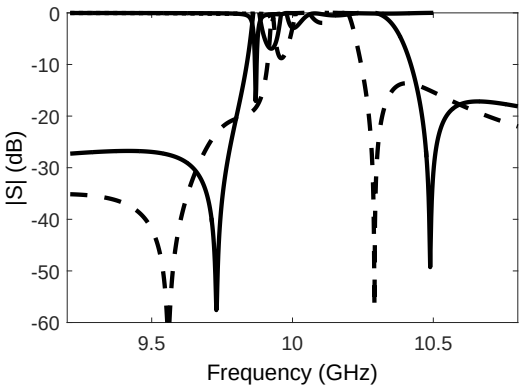

(a) Responses of the low-fidelity (- - -) and the high-fidelity (—) model before shift.

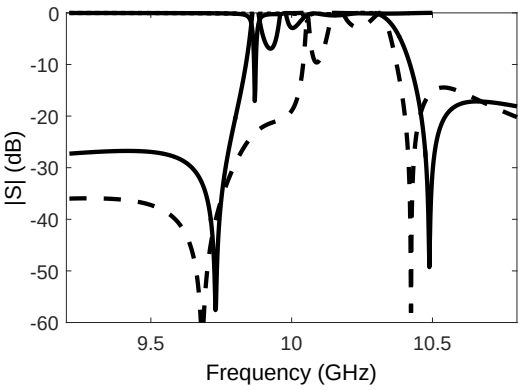

(b) Responses of the low-fidelity (- - -) and the high-fidelity (—) model after shift.

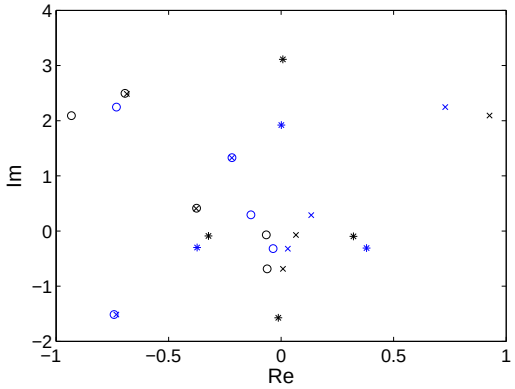

(c) Locations of zeros (x) and poles (o) of the low-fidelity (blue) and the high-fidelity model (black) before shift.

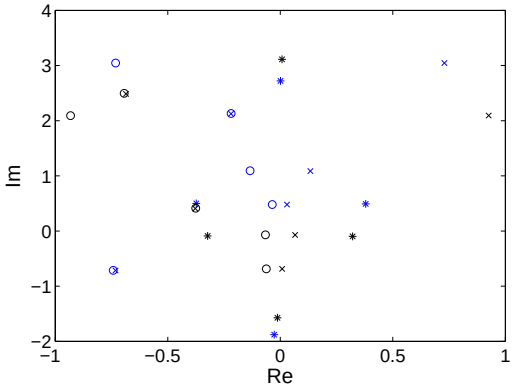

(d) Locations of zeros (x) and poles (o) of the low-fidelity (blue) and the high-fidelity model (black) after shift.

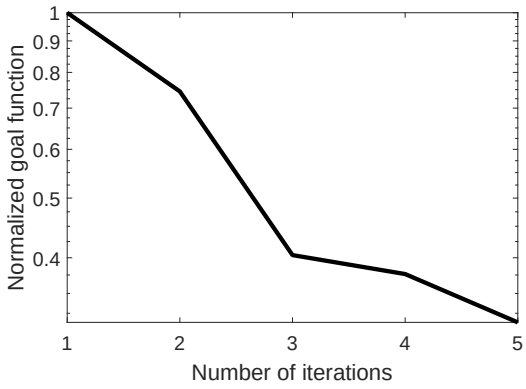

(e) Convergence of the low-fidelity model of linear phase filter at the first stage.

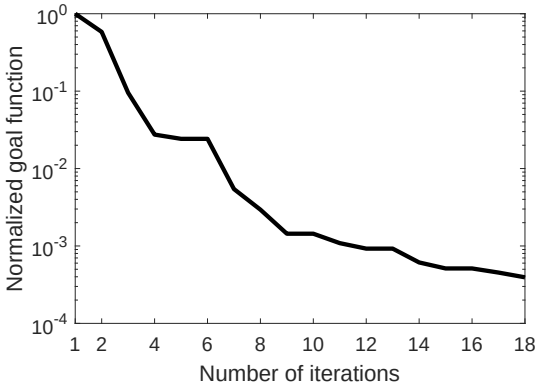

(f) Convergence of the low-fidelity model of linear phase filter at the second stage.

FIGURE 5.9: Results of both models.

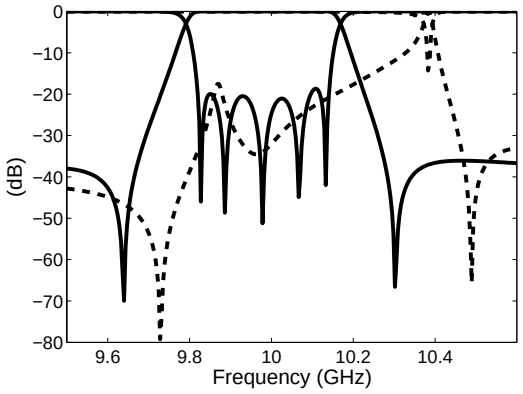

(a) Initial (- - -) and final (—) responses of the high-fidelity model of linear phase filter.

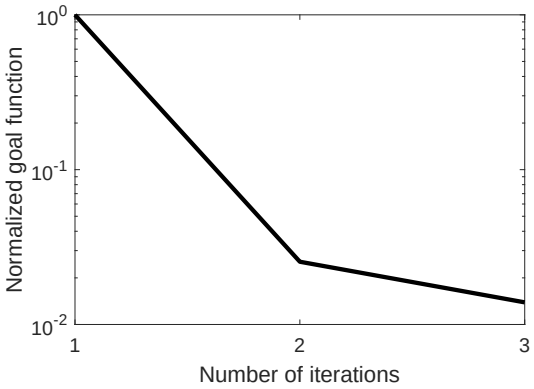

(b) Convergence of the high-fidelity model of the linear phase filter through optimization process.

FIGURE 5.10: Results of EM model.

starting point is chosen and the number of reflection zeros at the initial response is not equal to the filter order or the filter to be designed has complex (nonvisible) transmission zeros.

5.4 Summary

We have presented a concept for the design and optimization of microwave filters involving a zero-pole goal function at two levels of accuracy. The technique comprises two stages, in each of which a different analytical model linking the two levels is used. The new approach converges very quickly even if the starting point is far from the desired response.

Acknowledgment

This work was supported by the Polish National Science Center under contract UMO-2012/07/B/ST7/01241.

References

[1] J. Bandler, Q. Cheng, S. Dakroury, A. Mohamed, M. Bakr, K. Madsen, and J. Sondergaard. Space mapping: the state of the art. *IEEE Trans. Microw. Theory Tech.*, 52(1):337–361, Jan 2004.

[2] R. J. Cameron. General coupling matrix synthesis methods for chebyshev filtering functions. *IEEE Transactions on Microwave Theory and Techniques*, 47(4):433–442, Apr 1999.

[3] D. Echeverría and P. Hemker. Manifold mapping: a two-level optimization technique. *Comput. Vis. Sci.*, 11(4-6):193–206, 2008.

[4] P. Kozakowski and M. Mrozowski. Automated CAD of coupled resonator filters. *IEEE Microw. Wireless Compon. Lett.*, 12(12):470 –472, Dec. 2002.

[5] S. Koziel and J. W. Bandler. Fast EM-driven design optimization of microwave filters using adjoint sensitivity and response features. In *IEEE MTT-S Int. Microw. Symp. Dig*, pages 1–3, May 2015.

[6] S. Koziel, S. Ogurtsov, J. Bandler, and Q. Cheng. Reliable space-mapping optimization integrated with EM-based adjoint sensitivities. *IEEE Trans. Microw. Theory Tech.*, 61(10):3493–3502, Oct 2013.

[7] A. Lamecki, L. Balewski, and M. Mrozowski. An efficient framework for fast computer aided design of microwave circuits based on the higher-order 3D finite-element method. *Radioengineering*, 23(4), Dec 2014.

[8] N. Leszczynska, L. Szydlowski, and M. Mrozowski. Automated design of linear phase filters. In *Microwaves, Radar, and Wireless Communication (MIKON), 2014 20th International Conference on*, pages 1–4, June 2014.

[9] N. Leszczynska, L. Szydlowski, and M. Mrozowski. Zero-pole space mapping for CAD of filters. *IEEE Microw. Wireless Compon. Lett.*, 24(9):581–583, Sept 2014.

[10] C. Zhang, F. Feng, V.-M.-R. Gongal-Reddy, Q. J. Zhang, and J. Bandler. Cognition-driven formulation of space mapping for equal-ripple optimization of microwave filters. *IEEE Trans. Microw. Theory Tech.*, 63(7):2154–2165, July 2015.

[11] C. Zhang, F. Feng, and Q.-J. Zhang. EM optimization using coarse and fine mesh space mapping. In *Proc. Asia–Pacific Microw. Conf., Seoul, Korea*, pages 824–826, Nov 2013.

Chapter 6

Low-cost Residue-Pole-Zero Surrogate Models for Microwave Filters

Based on the publications:

N. Leszczynska, I. Couckuyt, T. Dhaene, M. Mrozowski, *"Low-cost Surrogate Models for Microwave Filters,"* published in IEEE Microwave and Wireless Components Letters, Vol. 26, No. 12, pp. 969 - 971, 2016.

N. Leszczynska, S. Ulaganathan, A. Lamecki, T. Dhaene, M. Mrozowski, *"Kriging Models for Microwave Filters,"* published in proceedings of IEEE MTT-S International Conference on Numerical Electromagnetic and Multiphysics Modeling and Optimization (NEMO), Beijing, pp. 1-2., 2016.

A novel low-cost kriging-based multivariable parametric macromodeling technique for microwave filters is presented. Earlier, kriging has been used to model the scattering parameters. Here, kriging is used to model both the residues and poles of a microwave filter's reflection coefficient, and the zeros of the transmission coefficient. The proposed residue-pole-zero (RPZ) technique is demonstrated to efficiently model microwave filters. The resulting scalable low-cost RPZ surrogate models can efficiently be used to design and optimize microwave filters for various design specifications.

6.1 Introduction

Design of microwave filters based on the full-wave electromagnetic solvers often requires a large number of computationally intensive and time-consuming simulations. To expedite the design process surrogate models whose response approximates the behaviour of a complex system can be used in lieu of electromagnetic analysis. This approach is

especially attractive for design-by-optimization. However, surrogate based optimization (SBO) makes sense only if the model is sufficiently accurate and cheap to build. Unfortunately, when the number of design variables increases, the cost of model construction often increases exponentially. For this reason it is essential to investigate techniques that are capable of evaluating the coefficients on multivariate models with as few electromagnetic simulations as possible.

A good problem formulation is a crucial aspect often overlooked in surrogate modeling. Often the values of the device's response at selected frequency points are considered [10, 11, 13]. For microwave circuits this implies creating a surrogate model of scattering parameters. This obvious choice does not have to be a good one. In [10, 11], so-called response feature points are utilized for modeling a scattering response. This method has been shown to give good results in the modeling of the amplitude of the transmission coefficient, provided the consistency of the feature points is maintained across a training set. Recently, several approaches based on the parametrization of rational models have been presented [3, 4]. In [4], interpolation of so-called root macromodels with sequential sampling is presented. In [3], neural networks are trained to learn the relationship between residues and poles of the rational model approximating scattering matrix and the geometrical parameters. In this approach, relatively many full-wave response samples were needed to build a precise surrogate model. Moreover, this technique was demonstrated for models involving a narrow variation of geometrical parameters and, hence, the resulting model is only accurate for a specified frequency interval and cannot be used for a new design with a different center frequency and bandwidth.

In this chapter, we present a new technique for low-cost surrogate modeling and design of microwave filters. Instead of using interpolated root macromodels or artificial networks advocated in [3, 4], a hierarchical approach based on vector fitting and a kriging interpolant [1] is employed to find the relationship between the residues and poles of filter's reflection coefficient as well as transmission zeros, all extracted from the full-wave frequency response, and geometrical parameters. This choice of the quantities to be modeled (RPZ) and the interpolation technique (kriging) yields high quality broadband surrogate models that are valid over a wide range of filter dimensions, and yet cheap to build. This is the main contribution of this chapter. The robustness and effectiveness of the proposed RPZ kriging methodology is demonstrated by modeling a microwave filter with pseudoelliptic characteristics. The cost of setting up the RPZ kriging model involving as many as eight parameters is just 30 full-wave simulations. The quality of the high-dimensional RPZ kriging model is verified for six designs of pseudoelliptic filters with different center frequency and bandwidths.

6.2 Theory

6.2.1 Surrogate model representation

Our model is the rational representation of the filter characteristics, as a function of the geometrical parameters. The reflection coefficient is represented in the residue-pole form (6.1), while its transmission coefficient is presented using the zero-pole (6.2) formulation, where $s = j\omega$. Both, S_{11} and S_{21} have common poles (p_i).

$$S_{11}(s) = \sum_{i=1}^{N} \frac{r_i}{s - p_i}, \qquad (6.1) \qquad S_{21}(s) = \frac{\prod_{i=1}^{N_z}(s - z_i)}{\prod_{i=1}^{N}(s - p_i)}. \qquad (6.2)$$

We would like to point out that using a different representation for S_{11} (residue-pole) and S_{21} (zero-pole) is essential for obtaining compact models. This can be explained as follows. The reflection response consists of N complex conjugate pairs of residues (r_i) and N complex conjugate pairs of poles (p_i), where N is the filter order. However, the number of transmission zeros (z_i) in the circuit is equal to N_z, which in most practical cases is lower than N. As a result, the RPZ surrogate model of an Nth order filter with N_z transmission zeros has $4N$ plus $2N_z$ scalable variables compared to $6N$ scalable parameters needed when the RP representation is used for both S_{11} and S_{21} (real and imaginary parts of residues, poles and zeros are modelled separately). In fact, $4N$ plus $2N_z$ independent surrogate models are created.

The computations of all data needed for model construction proceed as follows. First, the residues, poles and zeros for each sample are identified using an efficient Vector Fitting technique (VF) [6] based on the scattering parameters computed with a full-wave simulator. At the beginning of VF interpolation, the function order is set to $2N$ (VF yields a conjugate pair of each residue, pole or zero). To achieve good accuracy of the interpolation, the VF algorithm is invoked adaptively and the order of the function is increased as the interpolation becomes more accurate. As a result the final order of the VF model could be higher than needed for modeling the filter. The rational model of the reflection response in the vicinity of the passband is of order N. So, when VF stops, all insignificant poles (and corresponding residues) can be removed. The same holds for the transmission zeros. Firstly, all residues, zeros and poles with negative imaginary parts are discarded. Next, from the remaining values, the relevant residues, zeros and poles extracted from the simulated response are identified by matching them to the corresponding residues, poles and zeros of the ideal transfer function obtained from circuit synthesis [9]. After that process, the number of poles and the corresponding residues is equal to N, while the number of transmission zeros is N_z. Next, the kriging interpolation is used to create the surrogate model over the geometrical design parameters. For each training sample N residues, N poles and N_z zeros are modeled.

6.2.2 Kriging

Kriging is a well-known interpolation technique [2, 8]. Assume a set of n samples, $X = \{\mathbf{x}_1, \ldots, \mathbf{x}_n\}^T$ in d dimensions and $\mathbf{y}$ the associated function values, where $(\cdot)^T$ is the transpose of a vector or matrix.

The aim is to construct an interpolant for the given samples X and associated function values. In this work the kriging interpolant with a constant mean function α is used,

$$\hat{y}(\mathbf{x}^*) = \alpha + r(\mathbf{x}^*) \cdot \Psi^{-1} \cdot (\mathbf{y} - \alpha\mathbf{1}), \qquad (6.3)$$

where $\mathbf{1}$ is a column vector of ones. The coefficients α are determined using generalized least squares.

$r(\mathbf{x}^*) = (\psi(\mathbf{x}^*, \mathbf{x}_1), \ldots, \psi(\mathbf{x}^*, \mathbf{x}_n))$ is an $1 \times n$ vector of correlations between the test point $\mathbf{x}^*$ and the samples X. The $n \times n$ correlation matrix Ψ is,

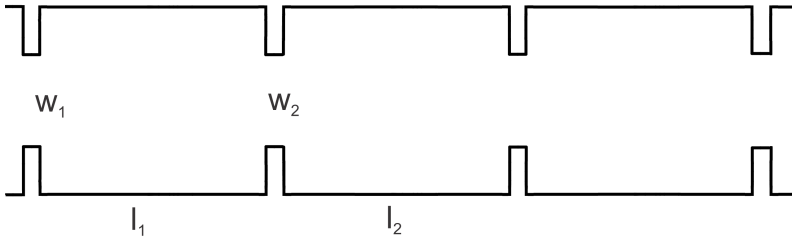

FIGURE 6.1: Geometry of an inline bandpass filter

$$\Psi = \begin{pmatrix} \psi(\mathbf{x}_1, \mathbf{x}_1) & \dots & \psi(\mathbf{x}_1, \mathbf{x}_n) \\ \vdots & \ddots & \vdots \\ \psi(\mathbf{x}_n, \mathbf{x}_1) & \dots & \psi(\mathbf{x}_n, \mathbf{x}_n) \end{pmatrix},$$

where $\psi(\cdot, \cdot)$ is the correlation function. $\psi(\cdot, \cdot)$ is parametrized by a set of hyperparameters θ, which are identified by Maximum Likelihood Estimation (MLE). Specifically, the (negative) concentrated ln-likelihood is minimized to find the optimal hyperparameters θ,

$$-\ln(\mathcal{L}_{marginal}) = -\frac{n}{2}\ln\sigma^2 - \frac{1}{2}\ln(|\Psi|) \tag{6.4}$$

where the signal variance $\sigma^2 = \frac{1}{n}(\mathbf{y} - \mathbf{1}\alpha)^T\Psi^{-1}(\mathbf{y} - \mathbf{1}\alpha)$. $|.|$ denotes the determinant of a matrix. The computational complexity is governed by the inverse of the correlation matrix Ψ which is $O(n^3)$ in the number of samples using Cholesky decomposition.

The popular Gaussian correlation functions assumes the underlying response surface to be infinite differentiable, which is unrealistical for many engineering problems. Hence, in this work we adopt the Matérn correlation function with $\nu = 5/2$ as it is twice differentiable [14],

$$\psi(\mathbf{x}, \mathbf{x}')_{\nu=5/2} = \left(1 + \sqrt{5}l + \frac{5l^2}{3}\right)\exp\left(-\sqrt{5}l\right),$$

with $l = \sqrt{\sum_{i=1}^{d}\theta_i(x_i - x_i')^2}$.

6.3 Numerical Example

6.3.1 In-line filter surrogate model

As an example we study a third-order inline bandpass filter. The filter is parametrized using 4 geometrical variables (Fig. 6.1): which are the lengths of the resonators and the widths of the irises windows: $\mathbf{x} = [l_1, l_2, w_1, w_2]^T$ (all dimensions in millimetres). The variable interval for surrogate model is set to [15 16.5 10.5 6.5] - [17 18.5 12.5 9.0]. The filter is designed in the WR90 waveguide standard, its width is 22.86 mm and its height is 10.16 mm.

In this example, two types of surrogate models have been constructed. One model is based on the residues and the poles and the other is developed using the scattering

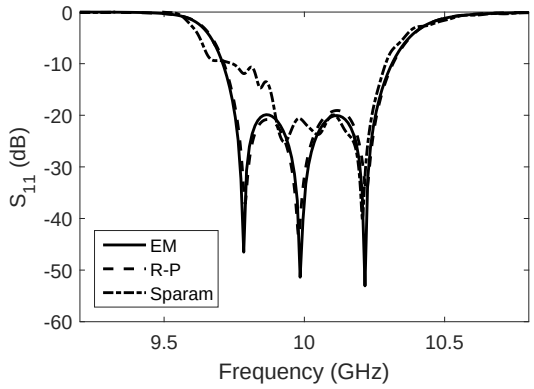

(a) Number of samples $nt = 25$

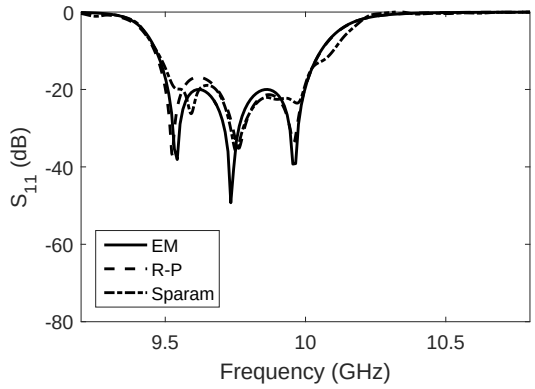

(b) Number of samples $nt = 25$

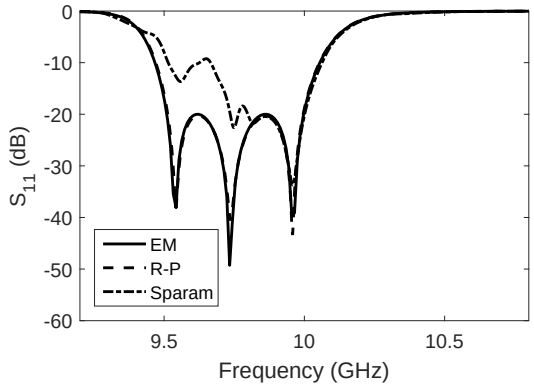

(c) Number of samples $nt = 50$

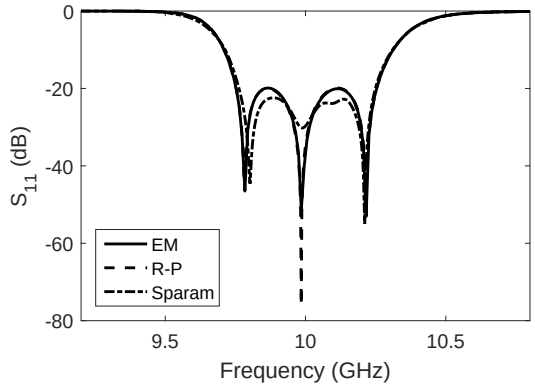

(d) Number of samples $nt = 50$

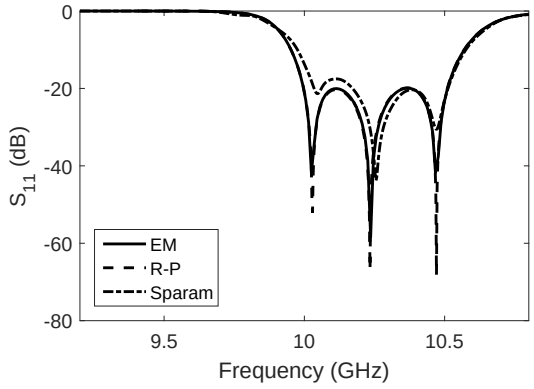

(e) Number of samples $nt = 100$

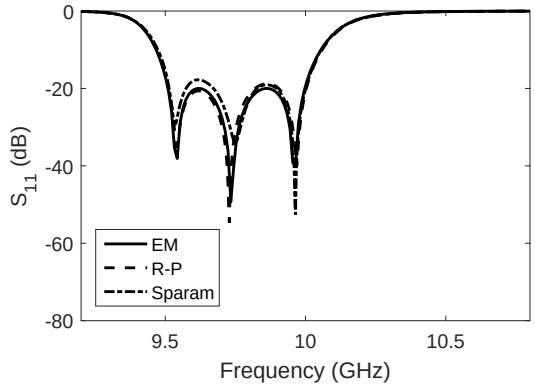

(f) Number of samples $nt = 100$

FIGURE 6.2: Comparison between residue-pole surrogate model (R-P) and scattering parameters surrogate models (Sparam) and corresponding full-wave (EM) model responses.

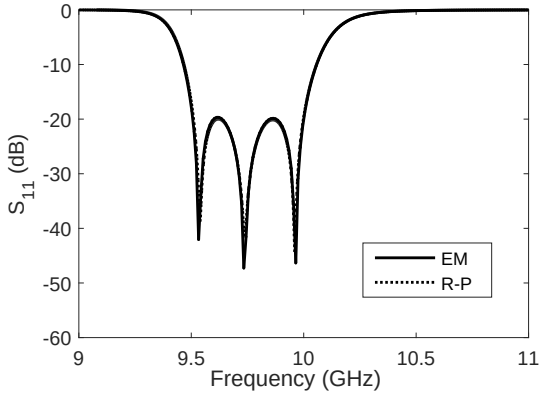

(a) $f_0 = 9.75$ GHz, $fbw = 0.05$

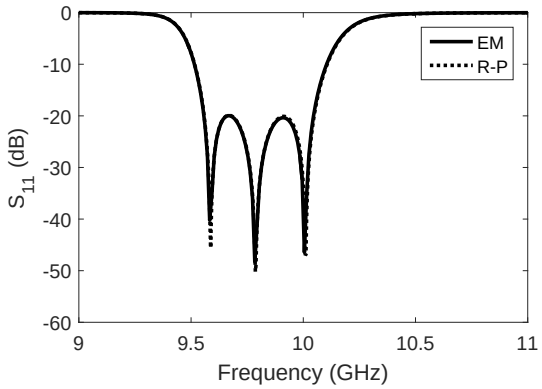

(b) $f_0 = 9.8$ GHz, $fbw = 0.05$

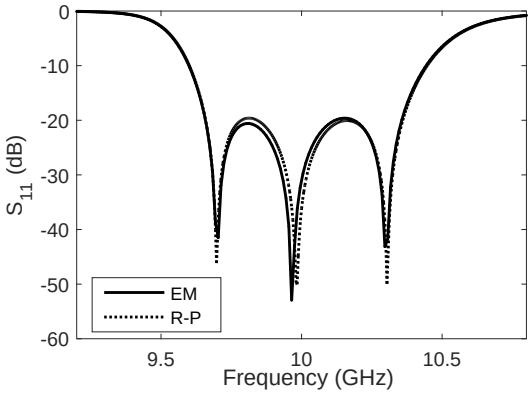

(c) $f_0 = 10$ GHz, $fbw = 0.07$

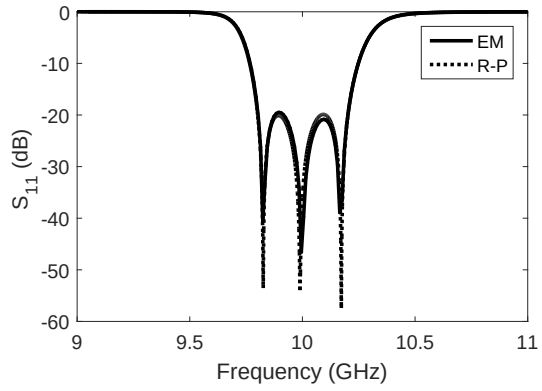

(d) $f_0 = 10$ GHz, $fbw = 0.04$

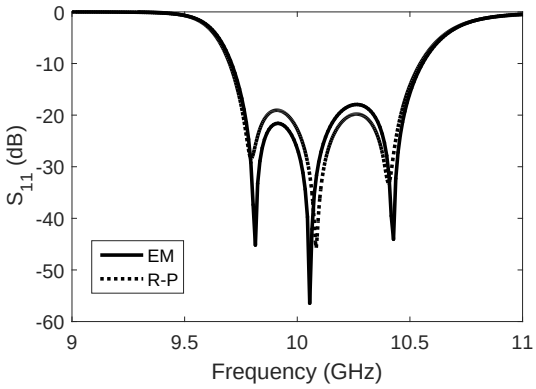

(e) $f_0 = 10.1$ GHz, $fbw = 0.07$

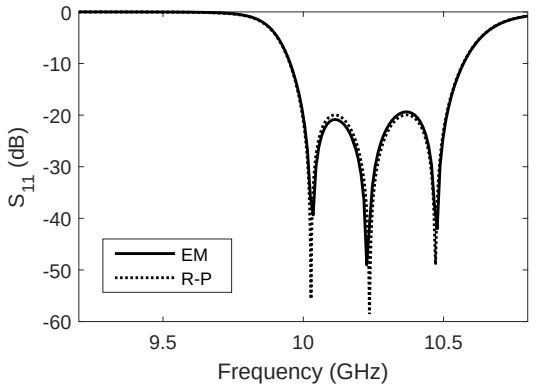

(f) $f_0 = 10.25$ GHz, $fbw = 0.05$

FIGURE 6.3: Comparison between optimization results and EM responses of a R-P models with nt=50 and various filter specifications.

TABLE 6.1: Accuracy of Residue-Pole (R-P) and S-parameters formulation

Number of training (nt) samples	Formulation	NRMSE
25	R-P	0.2679
	S-param	0.8892
50	R-P	0.0094
	S-param	0.4706
100	R-P	0.0067
	S-param	0.2883

parameters. Surrogate models built from the scattering parameters are modeled in the frequency range 9-11 GHz with 50 frequency points, so 100 kriging models are constructed (the real and the imaginary part is modeled separately). Three complex residues and poles (N=3) of the reflection coefficient of the microwave filter are modeled over the frequency range [9-11] GHz. The real and imaginary part of each residue and pole are modeled separately so the total number of (outputs) models is 12. The residues and poles are obtained by applying the vector fitting technique [6] to the response calculated with a full-wave solver.

The surrogate models are built using kriging interpolation with 25, 50 and 100 training samples (25,50 and 100 electromagnetic simulations) Fig. 6.2. The normalized Root Mean Square Error (NRMSE) is used to verify the accuracy of the surrogate models (Tab. 6.1).

To verify the accuracy of the model we designed-by-optimization filters for a few specifications Fig. 6.3 using R-P kriging models, built from 50 training samples. Then, we compared the surrogate-based filter response with the electromagnetic solver response evaluated at the corresponding optimal solution. The optimization was performed using a cost function based on the location of zeros and poles of the filter's transfer and reflection function [9, 12]. As can be seen, the residue-pole surrogate models are in good agreement with the full-wave solver response and give better results than kriging models based on the scattering parameters.

6.3.2 Open-loop surrogate model

The example is a third-order open-loop bandpass filter in a triplet configuration [7]. The filter is parametrized using 8 geometrical parameters (Fig. 6.4), which are the lengths of the resonators, the spacings between them, the positions of the feed lines, and the width of the resonators, so $\mathbf{x} = [l_1\ l_2\ d_1\ d_2\ s_1\ s_2\ t\ w]^T$ (all dimensions in mm). The variable interval for construction the surrogate RPZ model is set to [19 6 0.8 0.8 0.5 1.6 3.0 1.2] – [21 9 1.25 1.25 1.0 2.0 4.2 1.8]. The width of feed lines set to 1 mm, respectively. The dielectric constant is equal to 10.8, and the substrate height is 1.27 millimetres.

Three complex residues and poles (N=3) of the reflection coefficient and one complex transmission zero (N_z=1) of the microwave filter are modeled over the frequency range [0.8-1.15] GHz. The total number of independent surrogate models (scalable parameters) is 14, since the real and imaginary parts are modeled separately. The residues, zero and

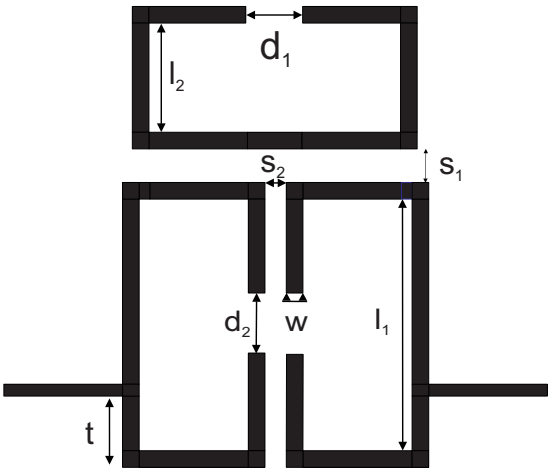

FIGURE 6.4: Geometry of an open-loop bandpass filter

poles are obtained by applying the VF algorithm (with subsequent processing described above). The EM response is obtained from the full-wave solver Momentum.

The kriging model is built using a research platform for surrogate modeling, the SUrrogate MOdeling (SUMO) toolbox [5]. The total budget of training samples is only 30 electromagnetic simulations in the 8D design space, arranged in a (maxi-min) Latin Hypercube Design using the translational propagation algorithm. The model accuracy is verified using 5-fold cross-validation, resulting in a mean root relative squared error of 0.1661 (the coefficient of determination, R^2 is 0.97).

For comparison we have applied kriging to model the magnitude of reflection S_{11} and transmission S_{21} coefficient and to create a model based on real and imaginary part of S_{11} and S_{21}. We used the same training set. The mean root relative squared error 1.3966 and 0.6744 was obtained for the first and the second kriging model, respectively. The

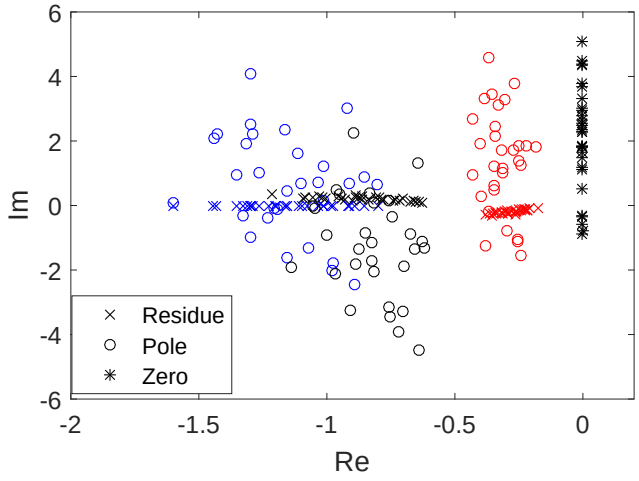

FIGURE 6.5: The distribution of the residues (x), poles (o) and zeros (*) for all training samples.

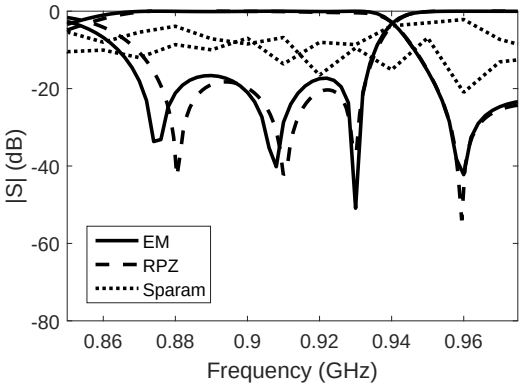

(a) $f_0 = 0.9$ GHz, $f_z = 0.96$ GHz, $fbw = 0.06$

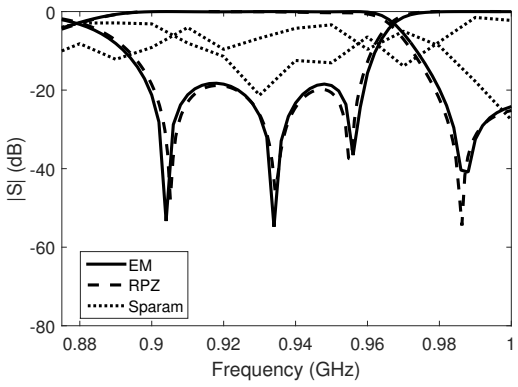

(b) $f_0 = 0.925$ GHz, $f_z = 0.986$ GHz, $fbw = 0.04$

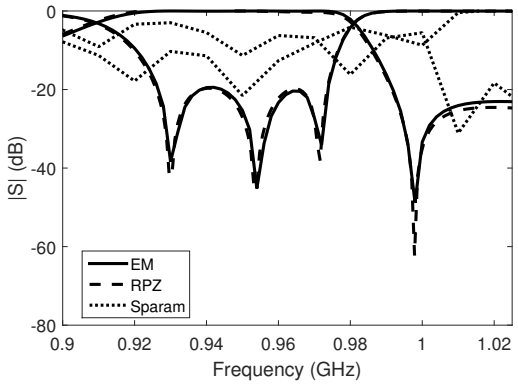

(c) $f_0 = 0.95$ GHz, $f_z = 0.998$ GHz, $fbw = 0.05$

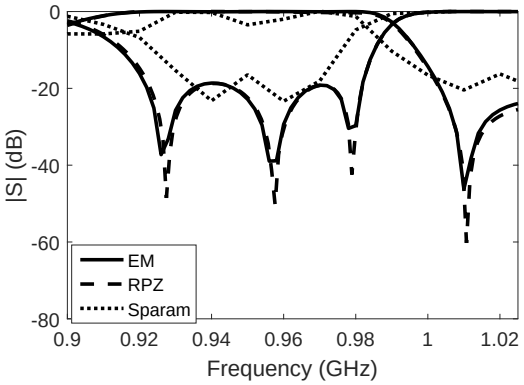

(d) $f_0 = 0.95$ GHz, $f_z = 1.01$ GHz, $fbw = 0.06$

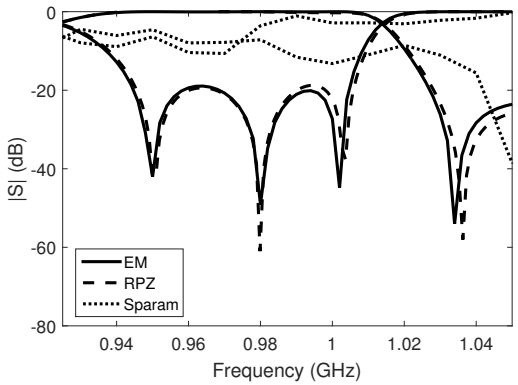

(e) $f_0 = 0.975$ GHz, $f_z = 1.034$ GHz, $fbw = 0.06$

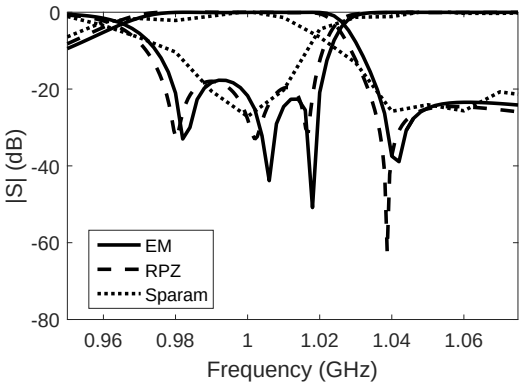

(f) $f_0 = 1.0$ GHz, $f_z = 1.04$ GHz, $fbw = 0.04$

FIGURE 6.6: Comparison between residue-pole-zero surrogate model (RPZ) and scattering parameters surrogate models (Sparam) and corresponding full-wave (EM) model responses.

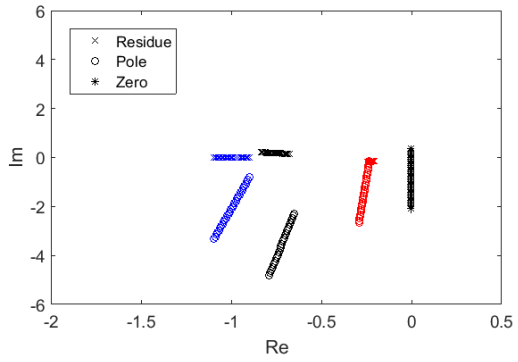

(a) First geometrical parameters varying.

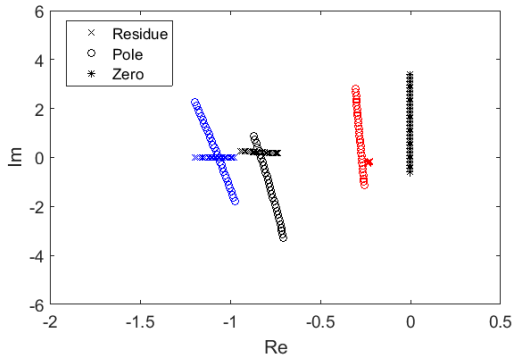

(b) Second geometrical parameters varying.

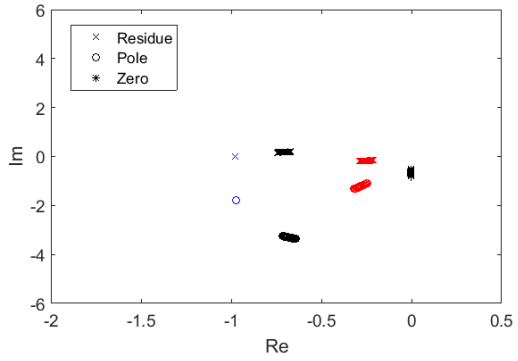

(c) Third geometrical parameters varying.

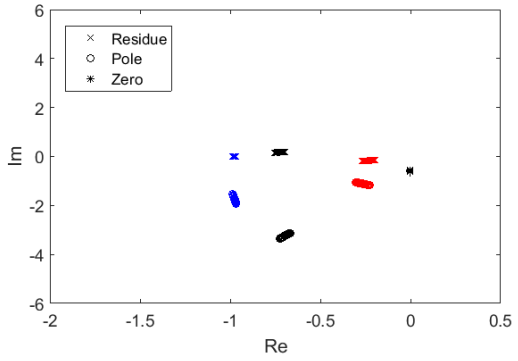

(d) Fourth geometrical parameters varying.

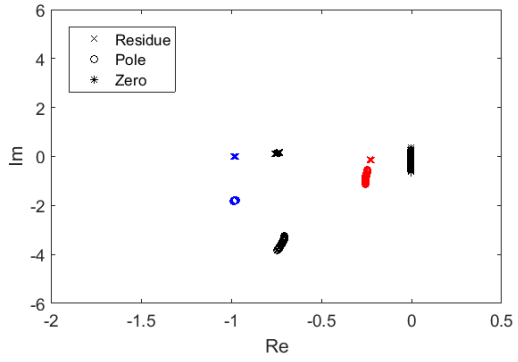

(e) Fifth geometrical parameters varying.

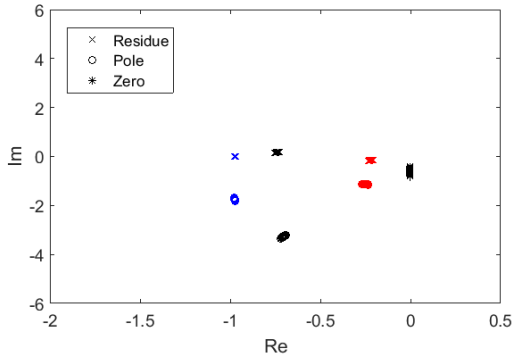

(f) Sixth geometrical parameters varying.

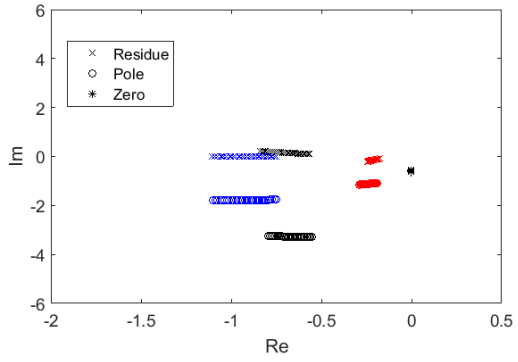

(g) Seventh geometrical parameters varying.

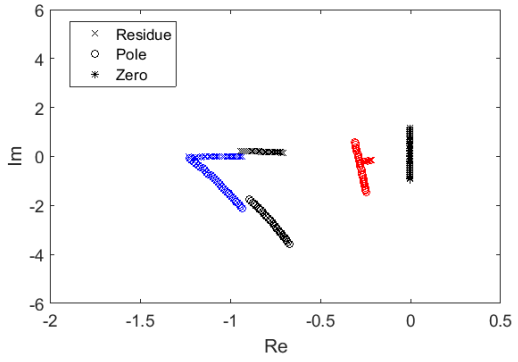

(h) Eighth geometrical parameters varying.

FIGURE 6.7: The distribution of the residues (x), poles (o) and zeros (*).

comparison between RPZ models and real, imaginary scattering parameters surrogate models (Sparam) is presented in Fig. 6.6.

The distribution of the residues (x), poles (o) and zero (*) for all samples used to create the model is presented in Fig. 6.5. Residues and the corresponding poles are denoted in one color. We have tree poles in our filter, so we have three groups of residues and poles described by red, blue and black colors. As can be seen the transmission zero moves only on the imaginary axis. The distribution for a single training point is also shown in the Fig. 6.7. The pictures presented show that the trajectories behave quite regularly. That is why the modeling of residues, poles and zeros is a better idea than creating a model based on scattering parameters.

To verify the accuracy of the model we designed-by-optimization six different filters using the scalable RPZ kriging model and compared the surrogate-based filter response with the electromagnetic solver response evaluated at the corresponding optimal solution. Optimization was performed using a cost function based on the location of zeros and poles of filter's transfer and reflection function [9]. To this end, residues predicted by the constructed RPZ kriging surrogate model are converted to reflection zeros.

The designs on which the RPZ surrogate model was tested involved a variety of specifications, including the center frequency (f_0) over the range 0.9-1.0 GHz, the fractional bandwidth (fbw) in the following interval 0.04-0.06 and different positions of transmission zeros (f_z). The return loss level in all cases is set to 20 dB. The comparison between the optimized response of the surrogate model and the full-wave characteristics is presented in Fig. 6.8 a-f. It is seen that in all cases the RPZ surrogate models and EM simulations responses are in good agreement.

6.4 Summary

This work introduces a novel approach for parametric modeling of microwave filters using kriging functions. A mixed residue-pole-zero (RPZ) representation of a filter's transfer and reflection coefficient has been proposed for kriging-based modeling of a pseudoelliptic microwave bandpass filter. The RPZ model was constructed for a high dimensional design space for a wide range of geometrical parameters with using only 30 training samples. The accuracy of the presented method has been verified by design and optimization of six different bandpass filters. Despite the high number of geometric parameters (8), a very low number of computational expansive samples can be used to build surrogate models.

Acknowledgment

This work was supported by the Polish National Science Center under contract UMO-2012/07/B/ST7/01241.

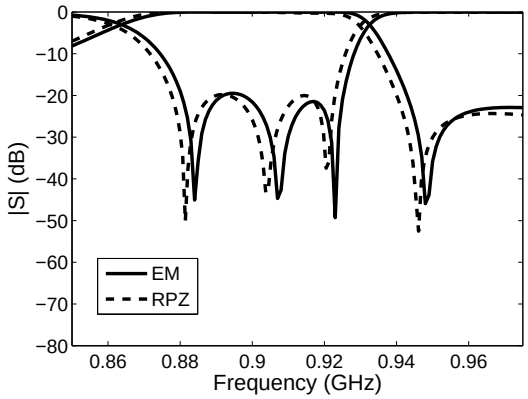

(a) $f_0 = 0.9$ GHz, $f_z = 0.948$ GHz, $fbw = 0.05$

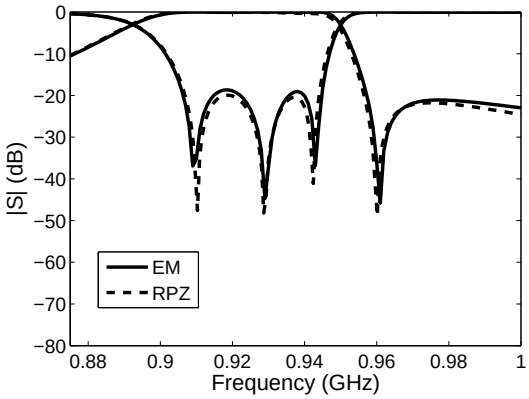

(b) $f_0 = 0.925$ GHz, $f_z = 0.96$ GHz, $fbw = 0.04$

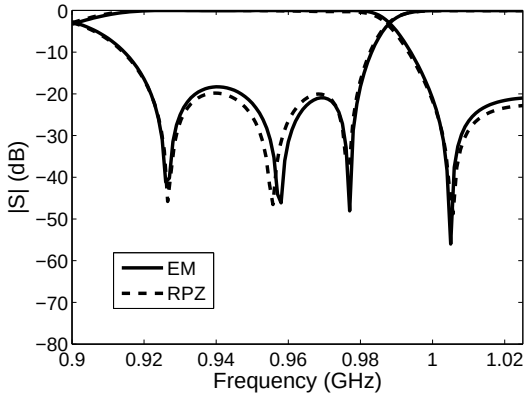

(c) $f_0 = 0.95$ GHz, $f_z = 1.005$ GHz, $fbw = 0.06$

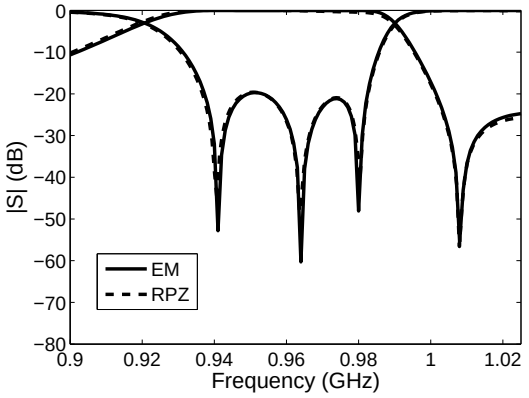

(d) $f_0 = 0.96$ GHz, $f_z = 1.008$ GHz, $fbw = 0.045$

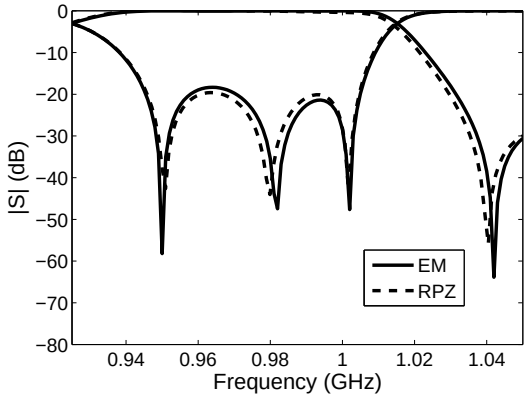

(e) $f_0 = 0.975$ GHz, $f_z = 1.042$ GHz, $fbw = 0.06$

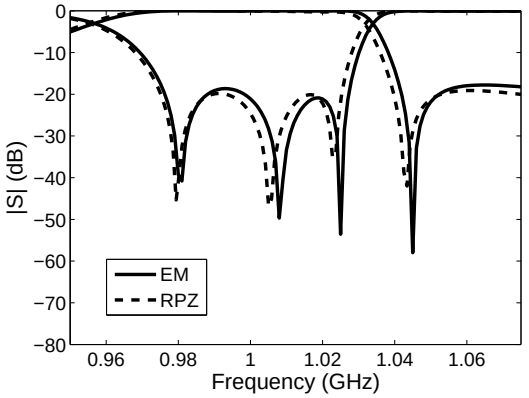

(f) $f_0 = 1.0$ GHz, $f_z = 1.045$ GHz, $fbw = 0.05$

FIGURE 6.8: Comparison between surrogate model (RPZ) optimization results and corresponding full-wave (EM) model responses.

References

[1] I. Couckuyt, F. Declercq, T. Dhaene, H. Rogier, and L. Knockaert. Surrogate-based infill optimization applied to electromagnetic problems. *International Journal of RF and Microwave Computer-Aided Engineering*, 20(5):492–501, 2010.

[2] I. Couckuyt, T. Dhaene, and P. Demeester. ooDACE toolbox: A flexible object-oriented kriging implementation. *Journal of Machine Learning Research*, (15):3183–3186, 2014.

[3] F. Feng, C. Zhang, J. Ma, and Q.-J. Zhang. Parametric modeling of EM behavior of microwave components using combined neural networks and pole-residue-based transfer functions. *Microwave Theory and Techniques, IEEE Transactions on*, 64(1):60–77, Jan 2016.

[4] F. Ferranti, T. Dhaene, and L. Knockaert. Compact and passive parametric macromodeling using reference macromodels and positive interpolation operators. *Components, Packaging and Manufacturing Technology, IEEE Transactions on*, 2(12):2080–2088, Dec 2012.

[5] D. Gorissen, K. Crombecq, I. Couckuyt, P. Demeester, and T. Dhaene. A surrogate modeling and adaptive sampling toolbox for computer based design. *Journal of Machine Learning Research*, (11):2051–2055, 2010.

[6] B. Gustavsen and A. Semlyen. Rational approximation of frequency domain responses by vector fitting. *IEEE Trans. Power Del.*, 14(3):1052 –1061, Jul. 1999.

[7] M. L. J-S. Hong. *Microstrip Filters for RF/Microwave Application*. John Wiley and Sons, 2001.

[8] J. Kleijnen. *Design and Analysis of Simulation Experiments*. John Wiley and Sons, 2008.

[9] P. Kozakowski and M. Mrozowski. Automated CAD of coupled resonator filters. *IEEE Microw. Wireless Compon. Lett.*, 12(12):470 –472, Dec. 2002.

[10] S. Koziel and J. W. Bandler. Reliable microwave modeling by means of variable-fidelity response features. *IEEE Transactions on Microwave Theory and Techniques*, 63(12):4247–4254, Dec 2015.

[11] S. Koziel, Q. S. Cheng, and J. W. Bandler. Feature-based surrogates for low-cost microwave modelling and optimisation. *IET Microwaves, Antennas Propagation*, 9(15):1706–1712, 2015.

[12] A. Lamecki, L. Balewski, and M. Mrozowski. An efficient framework for fast computer aided design of microwave circuits based on the higher-order 3d finite-element method. *Radioengineering*, 23(4):971, 2014.

[13] A. Lamecki, P. Kozakowski, and M. Mrozowski. Efficient implementation of the Cauchy method for automated CAD-model construction. *Microwave and Wireless Components Letters, IEEE*, 13(7):268–270, 2003.

[14] M. Stein. *Interpolation of Spatial Data: Some Theory for Kriging*. Springer-Verlag, 1999.

Chapter 7

Zero-Pole Electromagnetic Optimization

Based on the publication:

N. Leszczynska, A. Lamecki, M. Mrozowski, *"Zero-Pole Electromagnetic Optimization,"* published in IEEE Microwave and Wireless Components Letters, Vol. 27, No. 4, pp. 317 - 319, 2017.

A fast technique for the full-wave optimization of transmission or reflection properties of general linear time-invariant high-frequency components is proposed. The method is based on the zeros and poles of the rational function representing the scattering parameters of the device being designed and is an extension of technique formerly used for optimization of microwave filters. First, the design of a component is carried out using classical circuit-based techniques, and zeros and poles are extracted from the frequency characteristics of this design. These zeros and poles serve as reference values in the second stage, where the optimization of the structure is performed using a full-wave electromagnetic solver. The full-wave frequency response is converted to the zero-pole form and an optimizer attempts to match these zeros and poles with the reference values. The performance of the proposed technique is demonstrated with three examples: a patch antenna, an impedance transformer, and a branchline coupler. Fast convergence was observed for all examples, regardless of the quality of the starting point.

7.1 Introduction

From the circuit-theory point of view, passive microwave circuits are linear time-invariant (LTI) systems whose circuit properties are described by a scattering matrix. The techniques for designing such circuits are mature [1, 12], but they assume that transmission lines are ideal and do not take into account many field effects, such as dispersion, parasitic coupling and radiation, higher-order modes, conductor and dielectric loss, etc. This implies that the final design needs to be optimized based on simulations carried out with

electromagnetic (EM) solvers, which require large computational resources and are time-consuming.

In order to assure that the design meets the desired specifications, a final tuning consisting of a minimization process with a cost function that reflects the design requirements is employed. The optimization process can involve various cost functions. Most often, functions based on the scattering parameters, computed at many frequency points, are utilized [2] to ensure the desired reflection or transmission properties. However, while this choice is quite typical for microwave circuits, the convergence of the optimization is quite slow. Since full-wave electromagnetic EM simulation is the most time-consuming step in the circuit design process, the challenge is to reduce the number of EM simulations required. One possibility is to use a space-mapping concept or surrogate-based optimization, but acceleration can be also achieved on the full-wave simulation level by modifying the cost function. Recently, a cost function based on the so-called response features has been proposed for microwave passive circuit optimization [6, 7]. However, the feature response approach fails if the starting point is computationally bad, in the sense that the initial point has the wrong number of feature frequencies. Moreover, phase characteristics cannot be tuned using response features [7].

In this chapter, we address the problem of the full-wave optimization of transmission and reflection properties of electromagnetic systems, and to this end we take advantage of the fact that passive circuits are LTI systems whose characteristics can be described by a scattering matrix, which is a matrix-valued rational function. In the optimization procedure, we postulate using a cost function based on the locations of the zeros and poles of the rational function approximating scattering parameters, rather than the samples of the frequency response. This definition of the cost function, combined with a gradient-optimization technique, was proposed in [5], and has been shown to give very good results in full-wave filter design [4, 8–11]. The method can be applied to filters with real and complex transmission zeros. It converges very fast and requires a very few high accuracy full-wave solves, especially when used with space mapping [9, 11] or multilevel optimization techniques [10]. The extension of the zero-pole technique to other types of circuits is not obvious, since the reference zeros and poles have to be known. In the case of filters, the rational function character of the filter transmission and reflection characteristics is one of the design assumptions, so the reference zeros and poles are computed from the circuit synthesis. For other types of circuits, the synthesis procedure does not directly lead to a rational function, so the reference zeros and poles have to be found in some other way. We propose that the location of the reference zeros and poles be computed from the simulated response of a distributed element circuit model composed of sections of ideal transmission lines, or a simplified lumped element circuit model of a component, or both. The simplified circuit model is synthesized using the classic method or is quickly optimized using fast circuit simulators. The zeros and poles extracted from the optimized response of the circuit model are then used as references to perform a numerical tuning of the actual complex design using an electromagnetic solver. Compared to the traditional approach based directly on electrical parameters, the zero-pole representation of the cost function is more compact and allows for optimization both of magnitude and phase characteristics.

7.2 Theory

The state-space system representation is a relevant way of modeling and analyzing circuits with N-port networks. Such networks can be characterized in the frequency domain by a matrix-valued transfer function. In the case of microwave circuits, the scattering matrix circuit description is commonly used. All matrix elements share the same set of poles, while the zeros define the transmission or reflection zeros.

In our approach, we consider microwave structures as an LTI system whose transmission or reflection properties are represented as rational functions. We propose to extend the application of a goal function based on the zeros and poles from the optimization of filters [4, 5, 8, 11] to general LTI networks. In general, with this concept, the goal function is expressed in terms of the difference between the current location of the zeros Z_i and poles P_i of the scattering parameters obtained from the simulated response, and the reference zeros Z_i^{ref} and poles P_i^{ref}.

$$C = \sum_{i=1}^{N} |Z_i - Z_i^{ref}|^2 + \sum_{i=1}^{M} |P_i - P_i^{ref}|^2 \tag{7.1}$$

where M is the number of poles and N is number of zeros of scattering coefficients [4, 5, 8–11].

Our algorithm has two stages. In the first stage, we determine the reference positions of the zeros and poles. To this end, we construct an equivalent circuit or a low-fidelity model of the structure applying traditional design techniques using ideal components. Next, if required, the equivalent circuit is tuned to meet the design specifications. During the tuning classic optimization schemes can be used, since the evaluation of the goal function is cheap. The reference zeros and poles are then computed from the optimal solution of the equivalent (idealized) circuit. In the second stage, the actual structure is optimized to obtain the desired characteristics. Zeros and poles are extracted from the response calculated with a full-wave electromagnetic simulator and compared with the reference zeros and poles. The design variables are varied until the cost function (7.1) reaches a minimum.

The zeros and poles, in both stages, are identified from the scattering parameters using the vector fitting (VF) technique [3]. The vector fitting algorithm operates until a good fitting between the interpolation and the simulated response is achieved. If VF yields a model of an order higher than required, this model is truncated to fit the order of the reference circuit by discarding roots which are far from the frequency band under consideration.

7.3 Numerical examples

7.3.1 Patch antenna

The first example is a simple inset-fed patch antenna (Fig. 7.1) implemented in ADS Momentum. It has four geometrical variables: the length (l) and width (w) of the patch and the length (l_x) and width (w_x) of the inset feed. All the geometrical variables are

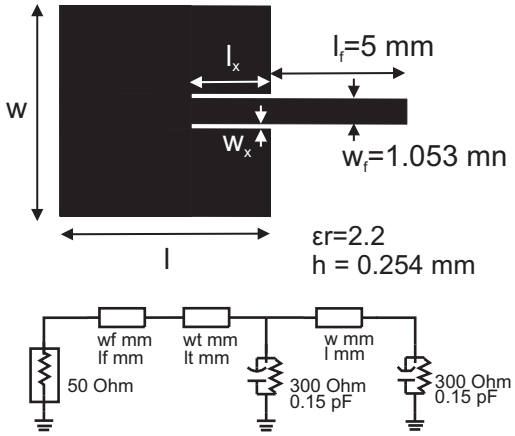

FIGURE 7.1: Geometry of a patch antenna.

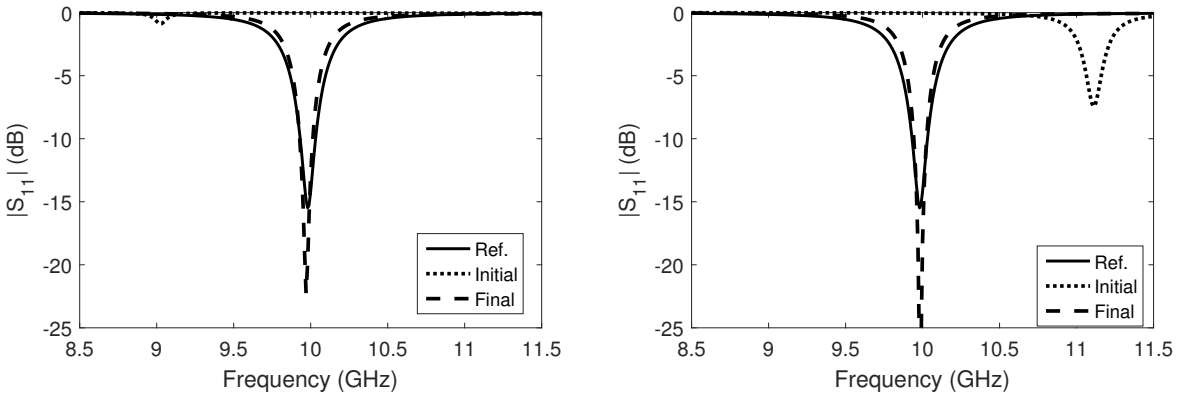

(a) First starting point.

(b) Second starting point.

FIGURE 7.2: Geometry of a patch antenna and its equivalent circuit with EM responses of the patch antenna at different starting points and final solutions.

used in the optimization routine, $\mathbf{x} = [w\ l\ w_x\ l_x]^T$ mm. The relative permittivity of the substrate is equal to 2.2 and its height is 0.254 mm. Our goal is to match this antenna at 10 GHz.

The equivalent circuit is implemented in ADS - a circuit simulator. As can be seen, the model consists of three microstrip lines corresponding to the patch, an impedance transformer, the feed line ($w_f = 1.053$ mm, $l_f = 5$ mm), and two parallel resistor and capacitor pairs. Different configurations for the feed are utilized for the equivalent circuit and the optimized antenna. The equivalent circuit involves an impedance transformer, denoted as a microstrip line, of width w_t and length l_t, while in the the optimized antenna, the inset feed is used. Despite this, the simplified model provides a good reference. The parameters of the low-fidelity model were calculated using analytical equations [1] and tuned to match at 10 GHz. The antenna model response can be represented with one complex reflection zero and one complex reflection pole. The reference zero (-0.0299 +

9.9818i)·10^9 and pole (-0.1784 + 9.9822i)·10^9 are targets for the full-wave optimization of the actual physical structure, carried out in Momentum, and the geometry is varied until the zero and pole extracted from the full-wave response match the desired values.

We have tested our technique for two different starting points chosen at random within the possible dimensions. The initial design solutions are $x_1 = [11.0\ 11.0\ 0.2\ 5.0]^T$, and $x_2 = [11.0\ 9.0\ 0.7\ 3.0]^T$, with values in millimeters. We deliberately did not take the dimensions from the equivalent circuit as starting points, in order to demonstrate the robustness and correctness of our method. Note that the response for both starting points is very far from the goal. Despite this, to obtain results that satisfy the specification, six iterations were needed for the first starting point and only three for the second case. The final design is $x_1^* = [14.548\ 9.984\ 0.118\ 3.089]^T$ and $x_2^* = [12.650\ 10.065\ 0.595\ 2.922]^T$ (mm). As can be seen, the optimized characteristics coincide with the reference response (Fig. 7.2).

7.3.2 Impedance transformer

The second example is a five-section impedance transformer which matches 150 Ω to 50 Ω in the frequency range 5-15 GHz (Fig. 7.3a). The circuit involves ten design parameters—namely, the widths and lengths of each section, $\mathbf{x} = [l_1\ l_2\ l_3\ l_4\ l_5\ w_1\ w_2\ w_3\ w_4\ w_5]^T$ mm. The substrate parameters are as follows $\epsilon_r = 3.5$ and $h = 0.508$ mm. The matching transformer is simulated in the ADS Momentum solver.

The reference values, five complex zeros $[0.0000+5.3045i,\ 0.0001+7.2709i,\ -0.0005+9.9997i,\ 0.0006+12.7289i,\ 0.0003+14.6952i]\cdot 10^9$ and five complex poles $[-3.5205+3.0077i,\ -4.3874+6.7618i,\ -4.5664+10.0049i,\ -4.2480+13.1997i,\ -3.7030+16.3723i]\cdot 10^9$ needed for the second step, are extracted from the simulated response of an equivalent circuit. The reference model consists of TEM transmission lines described by the characteristic impedance, the electrical lengths (in all cases set to 90 degrees) and the reference frequency of 10 GHz. The values of the characteristic impedance for each section are set

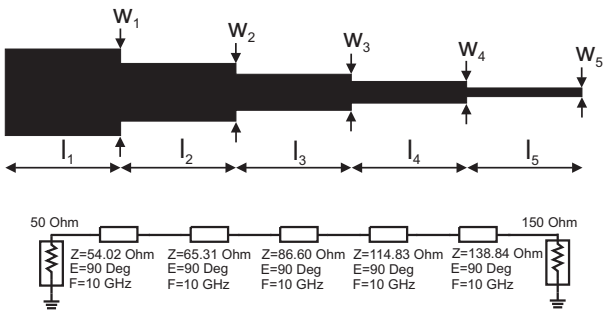

(a) Geometry of an impedance transformer and its equivalent circuit.

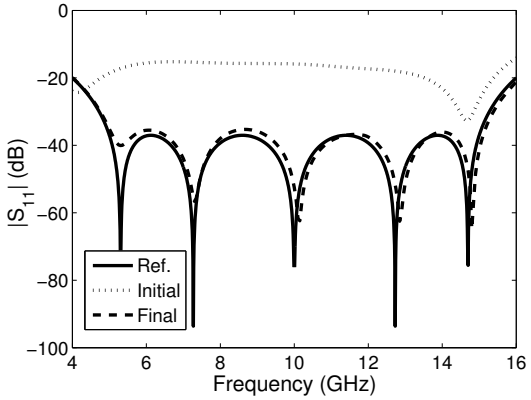

(b) Third starting point.

FIGURE 7.3: Geometry and EM response of the impedance transformer at different starting points and final solutions.

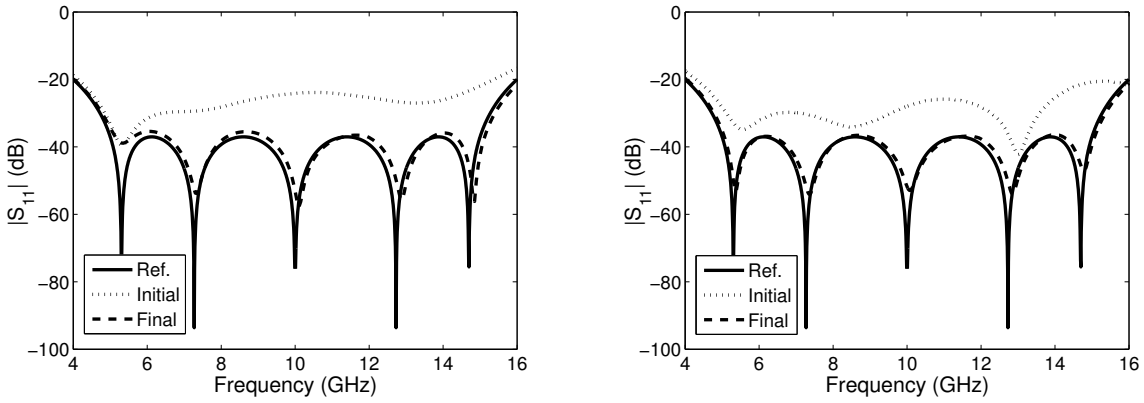

(a) First starting point. (b) Second starting point.

FIGURE 7.4: EM responses of the impedance transformer at different starting points and final solutions.

to $Z = [54.02\ 65.31\ 86.60\ 114.83\ 138.84]^T\ \Omega$. In this case, the equivalent circuit does not have to be tuned, as the required values can be found from analytical formulas [12].

In order to verify the correctness of our approach, we have tested it with three starting solutions far from the desired characteristics (again, we did not synthesize the microstrip lines deliberately). The initial design vector values are $x_1 = [4.6\ 4.57\ 4.67\ 5.55\ 4.95\ 1.00\ 0.641\ 0.312\ 0.235\ 0.09]^T$, $x_2 = [4.5\ 4.3\ 5.0\ 4.55\ 4.6\ 1\ 0.75\ 0.4\ 0.2\ 0.1]^T$ and $x_3 = [4.7\ 4.0\ 4.2\ 4.2\ 5.2\ 0.97\ 0.67\ 0.39\ 0.2\ 0.1]^T$ (mm). The optimal solutions, found after 9, 6, and 7 iterations for the first, second, and third starting points respectively are as follows ($x_1^* = [4.513\ 4.514\ 4.608\ 4.708\ 4.855\ 0.996\ 0.699\ 0.389\ 0.196\ 0.108]^T$, $x_2^* = [4.521\ 4.516\ 4.597\ 4.699\ 4.842\ 0.991\ 0.689\ 0.381\ 0.192\ 0.107]^T$ and $x_3^* = [4.562\ 4.513\ 4.602\ 4.673\ 4.824\ 1.017\ 0.735\ 0.418\ 0.208\ 0.111]^T$ mm). The final solutions are presented in Fig. 7.4. For all the initial responses, the final results meet the specifications.

7.3.3 Branchline coupler

The last example is a miniaturized three-section branchline microstrip coupler, shown in Fig. 7.5, optimized with InventSIM, an FEM solver [8]. The design space for the coupler involves as many as sixteen design variables $\mathbf{x} = [w_1\ w_2\ w_3\ w_4\ l_1\ l_2\ l_3\ l_4\ l_5\ l_6\ l_7\ l_8\ l_9\ l_{10}\ l_{11}\ l_{12}]^T$ mm. The length of each segment in a section is optimized. The relative permittivity is $\epsilon_r = 2.2$ and the substrate height is $h = 1.5748$ mm. Our goal in this case was not to minimize the size of the circuit, but to achieve, for the modified circuit layout, the characteristics of a classic, easy to synthesize, hybrid quadrature coupler despite the modified circuit layout.

The equivalent circuit is composed of ideal transmission lines as shown in Fig.7.5 ($Z = [30.02\ 36.02\ 133.03\ 84.00]^T\ \Omega$), the electrical lengths (90 degrees), and the reference frequency (1 GHz). The electrical design was carried out using a standard procedure [12]. The reference circuit response consists of three complex zeros $[-0.0079+0.6432i,\ 0.0074+1.0005i,\ -0.0084+1.3567i] \cdot 10^9$ and three complex poles $[-0.1106+0.5708i,\ -0.3452+$

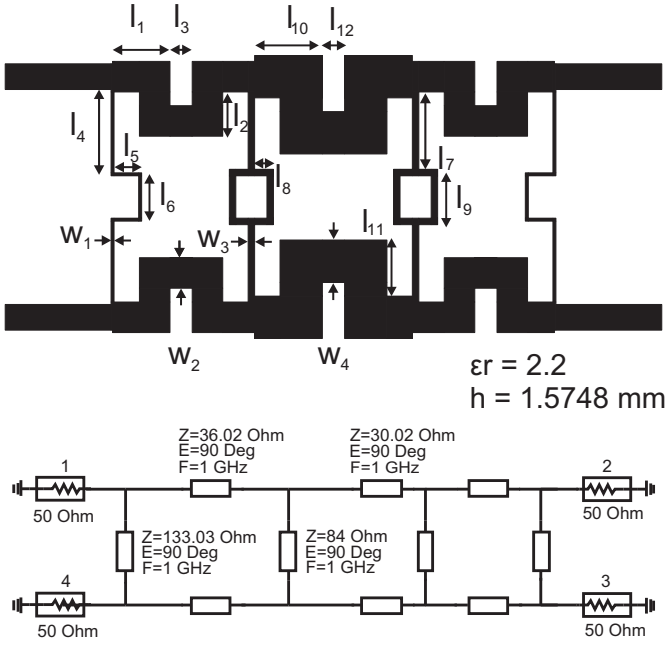

FIGURE 7.5: Geometry of a branchline coupler and a simplified circuit model at the center frequency 1GHz.

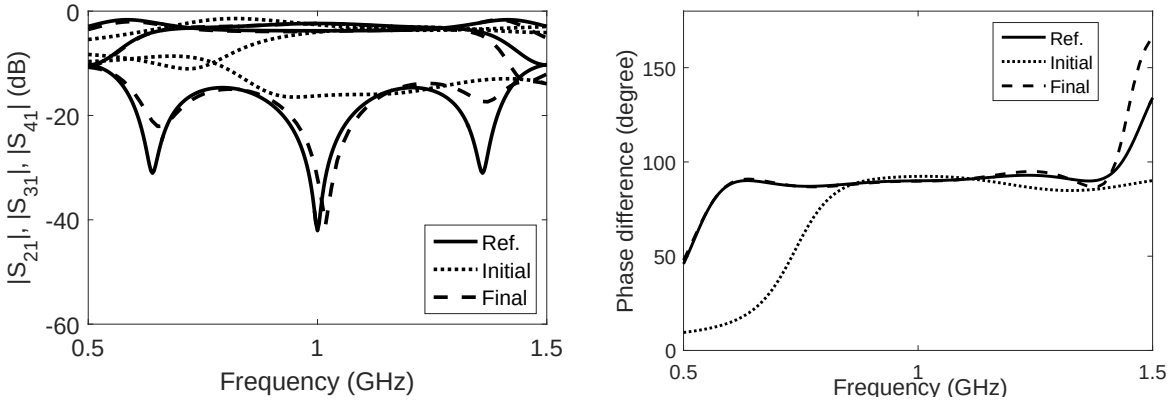

FIGURE 7.6: EM responses of the branchline coupler at the first starting point with a final solution and phase difference between transmission and coupled ports.

$1.0256i,\ -0.1096 + 1.4350i] \cdot 10^9$.

In this case, we also verified our technique using two distinct starting points $x_1 = [0.5\ 7\ 2\ 8\ 7\ 3\ 4\ 14\ 7\ 8\ 12\ 8\ 6\ 9\ 2\ 5]^T$, $x_2 = [1\ 5\ 2\ 8\ 9\ 4\ 5\ 13\ 5\ 6\ 13\ 5\ 6\ 9\ 4\ 5]^T$ (mm).

The optimal designs were found after 10 and 9 iterations for the first and second starting points, respectively. The final design is $x_1^* = [0.5597\ 7.2139\ 1.6976\ 10.8122\ 7.8832\ 3.9643\ 4.8654\ 18.7616\ 9.0922\ 9.0974\ 16.6813\ 9.6799\ 7.4851\ 9.8569\ 2.1137\ 7.9306]^T$, $x_2^* = [0.3950\ 5.9644\ 0.9871\ 8.1494\ 7.9520\ 7.0988\ 6.2000\ 18.2520\ 6.7427\ 6.5135\ 17.0333\ 9.7500\ 6.7000\ 7.2333\ 7.3031\ 6.2000]^T$ (mm). As can be seen, all the solutions found by the technique meet the

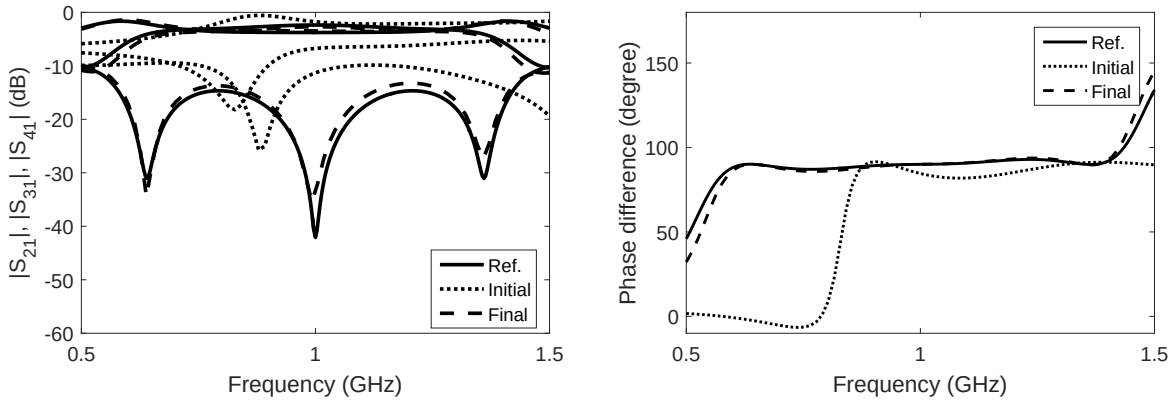

FIGURE 7.7: EM responses of the branchline coupler at the second starting point with a final solution and phase difference between transmission and coupled ports.

design specifications (Fig. 7.6, Fig. 7.7). We noted earlier that, compared to classic approaches and feature-based optimization [7], the zero-pole technique allows the simultaneous optimization of magnitude and phase characteristics to match the properties of the ideal circuit. In the frequency band under consideration, for both starting points the achieved phase difference is equal to 90 degrees, which is the desired result.

7.4 Summary

We have presented a new concept for the design and optimization of a wide class of LTI microwave components by utilizing a goal function based on the positions of the zeros and poles of the rational approximation of the scattering parameters, rather than the samples of the frequency response. The proposed method has been verified by optimizing two types of circuits. The method can be further improved by using space-mapping or multilevel techniques considered in chapters 4 and 5 and in publications [10, 11].

Acknowledgment

This work was supported by the Polish National Science Centre under contract UMO-2012/07/B/ST7/01241.

References

[1] C. E. Balanis. *Antenna Theory.* John Wiley and Sons, 1997.

[2] Y.-C. Chiang and C.-Y. Chen. Design of a wide-band lumped-element 3-dB quadrature coupler. *IEEE Trans. Microw. Theory Tech.*, 49(3):476–479, Mar 2001.

[3] B. Gustavsen and A. Semlyen. Rational approximation of frequency domain responses by vector fitting. *IEEE Trans. Power Del.*, 14(3):1052 –1061, Jul. 1999.

[4] A. Jedrzejewski, N. Leszczynska, L. Szydlowski, and M. Mrozowski. Zero-pole approach to computer aided design of in-line SIW filters with transmission zeros. *Progress Electromag. Res.*, 131:517 – 533, 2012.

[5] P. Kozakowski and M. Mrozowski. Automated CAD of coupled resonator filters. *IEEE Microw. Wireless Compon. Lett.*, 12(12):470 –472, Dec. 2002.

[6] S. Koziel. Fast simulation-driven antenna design using response-feature surrogates. *International Journal of RF and Microwave Computer-Aided Engineering*, 25(5):394–402, 2015.

[7] S. Koziel and A. Bekasiewicz. Fast simulation-driven feature-based design optimization of compact dual-band microstrip branch-line coupler. *International Journal of RF and Microwave Computer-Aided Engineering*, 26(1):13–20, 2016.

[8] A. Lamecki, L. Balewski, and M. Mrozowski. An efficient framework for fast computer aided design of microwave circuits based on the higher-order 3D finite-element method. *Radioengineering*, 23(4), Dec 2014.

[9] N. Leszczynska, M. Klinkosz, and M. Mrozowski. Substrate-integrated waveguide (SIW) filter design using space mapping. In *2016 21st International Conference on Microwave, Radar and Wireless Communications (MIKON)*, pages 1–4, May 2016.

[10] N. Leszczynska, A. Lamecki, and M. Mrozowski. Fast full-wave multilevel zero-pole optimization of microwave filters. *IEEE Microw. and Wireless Componen. Lett.*, 26(11):867–869, Nov 2016.

[11] N. Leszczynska, L. Szydlowski, and M. Mrozowski. Zero-pole space mapping for CAD of filters. *IEEE Microw. Wireless Compon. Lett.*, 24(9):581–583, Sept 2014.

[12] D. M. Pozar. *Microwave Engeering.* John Wiley and Sons, 2012.

Chapter 8

Conclusions

This thesis has discussed optimisation strategies for the design of microwave passive structures including filters, couplers, antennas and impedance transformers, and the construction of various surrogate models used to speed up the design process. Direct and hybrid optimisation methodologies including space mapping and multilevel algorithms have been proposed. Various surrogate models at different levels of fidelity have been used to design microwave components. The models considered have included equivalent circuits, coarsely discretized models and parametrised kriging models. All optimisation strategies outlined in this thesis have used a goal function based on the locations of zeros and poles of a rational approximation of the circuit scattering response combined with SBO techniques.

While CAD methodologies have been extensively researched over the last two decades, the author believes that this thesis makes significant contributions to this field. The advantages of the proposed methodology can be seen by considering the following shortcomings of the most popular methods proposed to date. Known optimisation and modelling methods have been successfully applied to the design of non-complicated circuits, most often the number of design parameters being less than ten [1, 5, 7, 10–13]. What is more, in the examples presented in literature, the initial solutions are close to the desired ones [3, 6, 11, 13]. The cost functions consist of samples of amplitude characteristics [1, 4, 8, 13], most often including only the transmission coefficient [2, 5, 7, 9, 10]. In this thesis, it has been shown that the proposed strategies are applicable to much more complex problems, with more than ten design variables, and the proposed methods converge even when the initial solution is far from the design specification. What is more, both magnitude and phase characteristics are tuned in the optimisation loop.

The main results of this work can be summarised as follows:

- The design goal for all problems has been expressed using a zero-pole representation instead of a conventional cost function based on the frequency response evaluated at many frequency points.

- A new space-mapping technique tailored to the CAD of microwave filters has been developed. The filter to be designed has been represented by a rational filtering function, whose zeros and poles determine the properties of the device. To quickly align the coarse and fine models and speed up the direct optimisation of the coarse

model, matching is performed of the zeros and poles of a rational function extracted from scattering parameters, rather than frequency responses. Both magnitude and phase characteristics can by tuned using this methodology.

- Multilevel CAD methods have been proposed for use with the information on the more accurate approximation of zeros and poles (and their derivatives with respect to design parameters) of high frequency systems obtained from time-consuming simulations based on physical principles.

- New schemes have been developed allowing extraction of both the zeros and poles of the transfer function with various levels of accuracy and computation of the gradient of individual zeros and poles at each level with a negligible cost.

- The optimisation strategy employing the analytical relationship between the transfer function based on matching of zeros and poles with respect to design variables has been extended for the optimisation of passive circuit structures such as couplers, antennas and impedance transformers.

- A low-cost kriging-based multivariable parametric macro-modelling technique has been developed for microwave filters. This new method exploits a rational representation of filter response that, together with kriging interpolation, allows the creation of surrogate models. Numerical tests and comparison with alternative techniques have shown that the method creates models whose outputs are closer to the EM characteristics obtained for the same set of variables than those of models based on scattering parameters.

The effectiveness and robustness of the presented methodologies are illustrated with examples including filters with Chebyshev and pseudo-elliptic characteristics as well as other structures such as a coupler, an antenna and an impedance transformer. All of the examples presented involve many design variables.

The results presented in this thesis could be implemented in commercial tools as optimisation procedures with the proposed surrogate models to speed up the design cycle.

Recommendations for future work are as follows:

- Development of other optimisation techniques for decreasing the number of EM simulations run in the design of various microwave components

- Extension of the multilevel and space-mapping zero-pole modelling technique to other passive structures like couplers, antennas and power dividers

- Enhancement of the interpolation process in the modelling, with the inclusion of derivative information, in order to decrease the number of samples used to create the model and improve its accuracy.

To conclude, the techniques proposed in this thesis are applicable to a wide spectrum of simulation problems that occur in high-frequency circuit design. The methods presented reduce the design time.

References

[1] O. Glubokov and S. Koziel. EM-driven tuning of substrate integrated waveguide filters exploiting feature-space surrogates. In *2014 IEEE MTT-S International Microwave Symposium (IMS2014)*, pages 1–3, June 2014.

[2] S. Koziel and J. W. Bandler. Accurate modeling of microwave structures using variable-fidelity response features. In *2015 IEEE MTT-S International Microwave Symposium*, pages 1–3, May 2015.

[3] S. Koziel and J. W. Bandler. Fast EM-driven design optimization of microwave filters using adjoint sensitivity and response features. In *IEEE MTT-S Int. Microw. Symp. Dig*, pages 1–3, May 2015.

[4] S. Koziel and J. W. Bandler. Rapid yield estimation and optimization of microwave structures exploiting feature-based statistical analysis. *IEEE Transactions on Microwave Theory and Techniques*, 63(1):107–114, Jan 2015.

[5] S. Koziel and J. W. Bandler. Reliable microwave modeling by means of variable-fidelity response features. *IEEE Transactions on Microwave Theory and Techniques*, 63(12):4247–4254, Dec 2015.

[6] S. Koziel, J. W. Bandler, and Q. S. Cheng. Constrained parameter extraction for microwave design optimisation using implicit space mapping. *IET Microwaves, Antennas Propagation*, 5(10):1156–1163, July 2011.

[7] S. Koziel, J. W. Bandler, and Q. S. Cheng. Low-cost feature-based modeling of microwave structures. In *2014 IEEE MTT-S International Microwave Symposium (IMS2014)*, pages 1–3, June 2014.

[8] S. Koziel and A. Bekasiewicz. Fast simulation-driven feature-based design optimization of compact dual-band microstrip branch-line coupler. *International Journal of RF and Microwave Computer-Aided Engineering*, 26(1):13–20, 2016.

[9] S. Koziel, Q. S. Cheng, and J. W. Bandler. Feature-based surrogates for low-cost microwave modelling and optimisation. *IET Microwaves, Antennas Propagation*, 9(15):1706–1712, 2015.

[10] S. Koziel and L. Leifsson. Generalised shape-preserving response prediction for accurate modelling of microwave structures. *IET Microwaves, Antennas Propagation*, 6(12):1332–1339, September 2012.

[11] S. Koziel, S. Ogurtsov, J. W. Bandler, and Q. S. Cheng. Reliable space-mapping optimization integrated with em-based adjoint sensitivities. *IEEE Transactions on Microwave Theory and Techniques*, 61(10):3493–3502, Oct 2013.

[12] S. Koziel, S. Ogurtsov, Q. S. Cheng, and J. W. Bandler. Rapid electromagnetic-based microwave design optimisation exploiting shape-preserving response prediction and adjoint sensitivities. *IET Microwaves, Antennas Propagation*, 8(10):775–781, July 2014.

[13] C. Zhang, F. Feng, V.-M.-R. Gongal-Reddy, Q. J. Zhang, and J. Bandler. Cognition-driven formulation of space mapping for equal-ripple optimization of microwave filters. *IEEE Trans. Microw. Theory Tech.*, 63(7):2154–2165, July 2015.

Acknowledgments

I would like to thank my supervisor, prof. Mrozowski, for his expert guidance and supervision but especially I would like to thank him for constant support, help, patience and faith in me during my work on this thesis.

I would like to thank my colleagues from the department for the time spent together.

Publications

The research results obtained during this PhD research have been published as journal articles and presented at a series of international conferences. The thesis shows the results that were reported only in selected publications. The following list provides a complete list of the papers published during my PhD research. Publication Automated Design of Linear Phase Filters received the European Microwave Association First prize at the 20th Microwave and Radar Week in 2014, while the publication Design of Substrate Integrated Waveguide Filter Using Implicit Space Mapping Technique received the AP/AES/MTT Joint Chapter, Poland Section IEEE award for the best young scientist presentation at the 19th International Conference on Microwaves, Radar and Wireless Communications in 2012. To date papers have been cited 40 times (ISI WOS - no self-citations) and resulted in H index equal 5.

Publications in international journals

1. A. Jedrzejewski, **N. Leszczynska**, L. Szydlowski, and M. Mrozowski, *Zero-pole approach to computer aided design of in-line SIW filters with transmission zeros.* Published in Progress In Electromagnetics Research, Vol. 131, pp. 517-533, 2012.

2. L. Szydlowski, **N. Leszczynska**, A. Lamecki and M. Mrozowski, *A Substrate Integrated Waveguide (SIW) Bandpass Filter in A Box Configuration With Frequency-Dependent Coupling.* Published in IEEE Microwave and Wireless Components Letters, vol. 22, no. 11, pp. 556-558, Nov. 2012.

3. **N. Leszczynska**, L. Szydlowski, and M. Mrozowski, *A novel synthesis technique for microwave bandpass filters with frequency-dependent couplings.* Published in Progress In Electromagnetics Research, Vol. 137, pp. 35-50, 2013.

4. L. Szydlowski, **N. Leszczynska** and M. Mrozowski, *Generalized Chebyshev Bandpass Filters With Frequency-Dependent Couplings Based on Stubs.* Published in IEEE Transactions on Microwave Theory and Techniques, vol. 61, no. 10, pp. 3601-3612, Oct. 2013.

5. L. Szydlowski, **N. Leszczynska** and M. Mrozowski, *A Linear Phase Filter in*

Quadruplet Topology With Frequency-Dependent Couplings. Published in IEEE Microwave and Wireless Components Letters, vol. 24, no. 1, pp. 32-34, Jan. 2014.

6. L. Szydlowski, **N. Leszczynska** and M. Mrozowski, *Dimensional Synthesis of Coupled-Resonator Pseudoelliptic Microwave Bandpass Filters With Constant and Dispersive Couplings*. Published in IEEE Transactions on Microwave Theory and Techniques, vol. 62, no. 8, pp. 1634-1646, Aug. 2014.

7. **N. Leszczynska**, L. Szydlowski and M. Mrozowski, *Zero-Pole Space Mapping for CAD of Filters*. Published in IEEE Microwave and Wireless Components Letters, vol. 24, no. 9, pp. 581-583, Sept. 2014.

8. **N. Leszczynska**, A. Lamecki and M. Mrozowski, *Fast Full-Wave Multilevel Zero-Pole Optimization of Microwave Filters*. Published in IEEE Microwave and Wireless Components Letters, vol. 26, no. 11, pp. 867-869, Nov. 2016.

9. **N. Leszczynska**, I. Couckuyt, T. Dhaene and M. Mrozowski, *Low-Cost Surrogate Models for Microwave Filters*. Published in IEEE Microwave and Wireless Components Letters, vol. 26, no. 12, pp. 969-971, Dec. 2016.

10. **N. Leszczynska**, A. Lamecki and M. Mrozowski, *Zero-Pole Electromagnetic Optimization*. Published in IEEE Microwave and Wireless Components Letters, vol. 27, no. 4, pp. 317 - 319, Apr. 2017.

Publications in international conferences

1. **N. Leszczynska**, L. Szydlowski and J. Podwalski, *Design of substrate integrated waveguide filters using implicit space mapping technique*. Published in proceedings of the 19th International Conference on Microwaves, Radar & Wireless Communications, Warsaw, 2012, pp. 315-318.

2. **N. Leszczynska**, L. Szydlowski and M. Mrozowski, *Automated design of linear phase filters*. Published in proceedings of the 20th International Conference on Microwaves, Radar and Wireless Communications (MIKON), Gdansk, 2014, pp. 1-4.

3. **N. Leszczynska**, M. Klinkosz and M. Mrozowski, *Substrate-integrated waveguide (SIW) filter design using space mapping*. Published in proceedings of the 21st International Conference on Microwave, Radar and Wireless Communications (MIKON), Krakow, 2016, pp. 1-4.

4. **N. Leszczynska**, S. Ulaganathan, A. Lamecki, T. Dhaene and M. Mrozowski, *Kriging models for microwave filters*. Published in proceedings of the IEEE MTT-S International Conference on Numerical Electromagnetic and Multiphysics Modeling and Optimization (NEMO), Beijing, 2016, pp. 1-2.

Abstracts in international conferences

1. **N. Leszczynska**, A. Lamecki, and M. Mrozowski, *Optimization of General Microwave Passive Circuits Based on Zero-pole Technique*. Published in book of abstracts of the Progress In Electromagnetics Research Symposium Abstracts, Prague, Czech Republic, July 6-9, 2015.

2. **N. Leszczynska**, S. Ulaganathan, A. Lamecki, T. Dhaene, and M. Mrozowski, *Kriging and Gradient Enhanced Kriging Surrogate Models For Zero-Pole Optimization of Microwave Filters*. Published in book of abstracts of the European Congress on Computational Methods in Applied Sciences and Engineering, ECCOMAS Congress 2016, 5 - 10 June 2016 Crete Island, Greece.